# Development and validation of a three dimensional wave-current interaction formulation

Nguyen, T.D.

**DOI**
10.4233/uuid:2804b274-ee21-4257-a052-a46408899c1f

**Publication date**
2022

**Document Version**
Final published version

**Citation (APA)**
Nguyen, T. D. (2022). *Development and validation of a three dimensional wave-current interaction formulation*. [Dissertation (TU Delft), Delft University of Technology]. UNESCO-IHE Institute for Water Education. https://doi.org/10.4233/uuid:2804b274-ee21-4257-a052-a46408899c1f

**Important note**
To cite this publication, please use the final published version (if applicable).
Please check the document version above.

# Development and Validation of a Three Dimensional Wave – Current Interaction Formulation

Duoc Tan Nguyen

# DEVELOPMENT AND VALIDATION OF A THREE DIMENSIONAL WAVE – CURRENT INTERACTION FORMULATION

Duoc Tan Nguyen

# DEVELOPMENT AND VALIDATION OF A THREE DIMENSIONAL WAVE – CURRENT INTERACTION FORMULATION

DISSERTATION

Submitted in fulfillment of the requirements of
the Board for Doctorates of Delft University of Technology
and
of the Academic Board of the IHE Delft
Institute for Water Education
for
the Degree of DOCTOR
to be defended in public on
Friday, 10 June 2022, at 10:00 hours
in Delft, the Netherlands

by

Duoc Tan NGUYEN
Master of Science in Oceanography, Vietnam National University, Hanoi
born in Hai Phong, Vietnam

This dissertation has been approved by the promotors:
Prof.dr.ir. J.A. Roelvink and Prof.dr.ir. A.J.H.M. Reniers

Composition of the doctoral committee:

| | |
|---|---|
| Rector Magnificus TU Delft | Chairman |
| Rector IHE Delft | Vice-Chairman |
| Prof.dr.ir. J.A. Roelvink | TU Delft/IHE Delft, promotor |
| Prof.dr.ir. A.J.H.M. Reniers | TU Delft, promotor |
| | |
| Independent members: | |
| Prof.dr.ir. S.G.J. Aarninkhof | TU Delft |
| Prof.dr. J. Monbaliu | Ku Leuven, Belgium |
| Prof.dr. A.-C. Bennis | Université de Caen Normandie, France |
| Dr. J. Groeneweg | Deltares |
| Prof.dr.ir. W.S.J. Uijttewaal | TU Delft, reserve member |
| | |
| Other committee member: | |
| Dr. N.G. Jacobsen | Vattenfall, Denmark |

*This research was conducted under the auspices of the Graduate School for Socio-Economic and Natural Sciences of the Environment (SENSE)*



Published by IHE Delft Institute for Water Education
www.un-ihe.org
ISBN 978-90-73445-42-0

Dedicated to my beloved family

# ACKNOWLEDGMENTS

It was started in October 2012 since I contacted Professor J.A. Roelvink and asked him for an opportunity to become a Ph.D. fellow at UN-IHE/Delft University of Technology. He asked me to come to the Netherlands in a framework of a special program. I worked closely with him for three months. Before finishing that period, I felt very happy when he accepted me as his Ph.D. fellow. I started doing my Ph.D. research in March of 2014. Under his supervision, I got much of his support not only in my study but also in my life. He spent a lot of time guiding my research, reading my papers and dissertation, and giving many valuable comments. In the deepest of my heart, I appreciate his help and would like to express all my love and great thanks to him. I learned from him not only knowledge but also his personality.

I would like to give my special thanks to Dr. Niels Jacobsen, who spent a lot of time on my work. Through the meeting and email contact, he gave me much detailed and useful advice for my research. I would like to express my sincere thanks to Professor A.J.H.M. Reniers, who spent much time reading my thesis and paper, and give me many useful suggestions.

In the time of living and studying in the Netherlands, I have many good friends. They made my life so colorful and happy. Many thanks to Lan, my high school friend, who help me a lot in the time I stayed in the Netherlands. Thanks to all my friends from IHE Delft including Hieu, Trang, Lan, Thanh, Ha, Nguyen as well as friends from T.U Delft including Thao, Hung, Nghi, Tung, and many other friends that I do not have enough space to mention here. We had funny and happy times when playing the sport, having delicious parties, and traveling around together. I also would like to send my thanks to all other IHE Delft friends. We had a great time and enjoy many common activities together.

Especially, I would like to express my love to all members of my family. This dissertation is dedicated to you with all my love.

Duoc Tan Nguyen

# SUMMARY

This study aims at developing a new set of equations of mean motion in the presence of surface waves, which is practically applicable from deep water to the coastal zone, estuaries, and outflow areas. The Generalized Lagrangian Mean method is employed to derive a set of Quasi-Eulerian mean three-dimensional equations of motion, where effects of surface waves are included through source terms. The obtained equations are expressed to the second-order of wave amplitude. Whereas the classical Eulerian-mean equations of motion are only applicable below the wave trough, the new set of equations is valid until the mean water surface even in the presence of finite-amplitude surface waves. Both conservative and non-conservative waves are under consideration, especially in the presence of a strong ambient current. A concept of three-dimensional wave radiation stress is introduced to express the effects of surface waves on the currents. It is an extension of the classical radiation stress concept. Especially, the relationship between three-dimensional wave radiation stress and vortex force representations is investigated in detail in conditions of both conservative and nonconservative waves. Through that relationship, comparisons between the new set of equations and other sets of equations implemented in recent well-known numerical models are given. It is useful for selecting a suitable numerical ocean model to simulate the mean current in a specific condition of waves combined with currents.

A two-dimensional numerical model (2DV model) is developed to validate the new set of equations of motion. The model passes the test of steady monochromatic waves propagating on a slope without dissipation (adiabatic condition). This is a primary test for equations of mean motion with a known analytical solution. In addition to this, experimental data for the interaction between random waves and currents in both non-breaking and breaking waves are employed to validate the 2DV model. As shown by this successful implementation and validation, the implementation of the new set of equations in any 3D model code is straightforward and may be expected to provide consistent results from deep water to the surfzone, in both conditions of weak and strong ambient currents.

# SAMENVATTING

Deze studie heeft tot doel een nieuwe reeks vergelijkingen van gemiddelde beweging in aanwezigheid van oppervlaktegolven te ontwikkelen, die praktisch toepasbaar is van diep water tot de kustzone, estuaria en uitstroomgebieden. De gegeneraliseerde Lagrangiaanse gemiddelde methode wordt gebruikt om een reeks quasi-Euleriaanse gemiddelde driedimensionale bewegingsvergelijkingen af te leiden, waarbij effecten van oppervlaktegolven worden opgenomen via brontermen. De verkregen vergelijkingen worden uitgedrukt in de tweede orde van golfamplitude. Terwijl de klassieke Euleriaanse gemiddelde bewegingsvergelijkingen alleen van toepassing zijn onder het golfdal, is de nieuwe reeks vergelijkingen geldig tot het gemiddelde wateroppervlak, zelfs in de aanwezigheid van oppervlaktegolven met eindige amplitude. Zowel conservatieve als niet-conservatieve golven worden overwogen, vooral in de aanwezigheid van een sterke omgevingsstroom. Een concept van driedimensionale golfstralingsspanning wordt geïntroduceerd om de effecten van oppervlaktegolven op de stromingen uit te drukken. Het is een uitbreiding van het klassieke concept van stralingsstress. Vooral de relatie tussen driedimensionale golfstralingsspanning en vortexkrachtrepresentaties wordt in detail onderzocht in omstandigheden van zowel conservatieve als niet-conservatieve golven. Door die relatie worden vergelijkingen gegeven tussen de nieuwe reeks vergelijkingen en andere reeksen vergelijkingen die in recente bekende numerieke modellen zijn geïmplementeerd. Het is nuttig voor het selecteren van een geschikt numeriek oceaanmodel om de gemiddelde stroming in een specifieke toestand van golven in combinatie met stromingen te simuleren.

Een tweedimensionaal numeriek model (2DV-model) is ontwikkeld om de nieuwe reeks bewegingsvergelijkingen te valideren. Het model doorstaat de test van stabiele monochromatische golven die zich voortplanten op een helling zonder dissipatie (adiabatische toestand). Dit is een primaire test voor vergelijkingen van gemiddelde beweging met een bekende analytische oplossing. Daarnaast worden experimentele gegevens voor de interactie tussen willekeurige golven en stromen in zowel niet-brekende als brekende golven gebruikt om het 2DV-model te valideren. Zoals blijkt uit deze succesvolle implementatie en validatie, is de implementatie van de nieuwe reeks vergelijkingen in elke 3D-modelcode eenvoudig en kan worden verwacht dat deze consistente resultaten oplevert van diep water tot de surfzone, zowel in omstandigheden van zwakke als sterke omgevingsstromingen.

# CONTENTS

**Acknowledgments** ..... **vii**
**Summary** ..... **viii**
**Samenvatting** ..... **ix**
**Contents** ..... **xi**
**1 INTRODUCTION** ..... **1**
1.1 General introduction to the study ..... 2
1.2 Research questions and objectives of this study ..... 3
1.2.1 Research questions ..... 3
1.2.2 Objectives of this study ..... 3
1.2.3 Literature review ..... 4
1.2.4 The outline of this dissertation ..... 7
**2 DERIVATION OF THE QUASI-EULERIAN MEAN EQUATIONS OF MOTION** ..... **9**
2.1 Definition of Quasi-Eulerian mean quantity ..... 10
2.1.1 Overview of Generalized Lagrangian Mean method ..... 10
2.1.2 Definition of Quasi-Eulerian mean quantity ..... 11
2.2 Derivation of Quasi-Eulerian mean momentum equation ..... 12
2.3 Derivation of the Quasi-Eulerian mean mass conservation equation ..... 19
**3 THREE-DIMENSIONAL WAVE RADIATION STRESS AND VORTEX FORCE REPRESENTATIONS** ..... **21**
3.1 Introduction ..... 22
3.2 Three-dimensional wave radiation stress representation ..... 23
3.2.1 Conservative part of the normal component of the wave radiation stress in weak ambient current ..... 24
3.2.2 Conservative part of the normal component of the wave radiation stress in a strong ambient current ..... 25
3.2.3 Decay-related part of normal components of the wave radiation stress ..... 26
3.3 Vortex force representation ..... 27
3.4 Relationship between wave radiation stress and vortex force representations 27
3.4.1 Conservative waves ..... 29
3.4.2 Non-conservative waves ..... 31
3.5 Conclusions ..... 32
**4 EQUATIONS OF MOTION IN THE HYDROSTATIC ASSUMPTION** ..... **33**
4.1 Quasi-Eulerian mean equations of motion ..... 34

4.1.1 Momentum equation of motion ..... 34
4.1.2 Depth-integrated continuity equation ..... 35
4.2 Generalized Lagrangian Mean equations of motion ..... 36
4.2.1 Momentum equation of motion ..... 36
4.2.2 Mass conservation equation of motion ..... 37
4.3 Equations of mean motion in vortex force representation ..... 38
**5 APPLICATIONS ..... 39**
5.1 Model implementation ..... 40
5.1.1 Wave energy balance equation ..... 41
5.1.2 The 2DV governing equations ..... 45
5.1.3 Vertical distribution of wave-induced forcing ..... 46
5.2 Numerical approximation ..... 48
5.3 Adiabatic test ..... 48
5.3.1 Bathymetry ..... 49
5.3.2 Boundary conditions ..... 49
5.3.3 Numerical results ..... 49
5.4 Mean currents in the presence of non-breaking waves ..... 51
5.4.1 Input parameters ..... 51
5.4.2 Boundary conditions ..... 53
5.4.3 The numerical results ..... 54
5.5 Breaking waves propagating in a wave flume ..... 61
5.5.1 Bathymetry and the wave properties at the boundary ..... 61
5.5.2 Boundary conditions ..... 62
5.5.3 Model validation ..... 63
5.6 Breaking waves propagating in a large-scale facility ..... 68
5.6.1 Laboratory setup ..... 68
5.6.2 Boundary conditions ..... 69
5.6.3 Numerical results and discussion ..... 70
5.7 Discussion ..... 75
**6 COMPARISONS WITH OTHER SETS OF EQUATIONS OF MEAN MOTION ..... 77**
6.1 Comparison with equations of motion of Walstra *et al.* (2001) ..... 78
6.2 Comparison with equations of motion of Bennis *et al.* (2011) ..... 81
6.3 Comparison with equations of motion of Kumar *et al.* (2012) ..... 83
6.4 Conclusions ..... 86
**7 CONCLUSIONS ..... 87**
7.1 Conclusions ..... 88
7.2 Answer to research questions ..... 89
**References ..... 91**

**List of acronyms** ..... **95**
**List of Tables** ..... **96**
**List of Figures** ..... **97**
**About the author** ..... **99**

# 1

# INTRODUCTION

## 1.1 GENERAL INTRODUCTION TO THE STUDY

In the ocean, the surface waves do not travel on a quiescent water surface but travel on the currents. Due to the effects of currents, the wave field is modified by processes such as diffraction, dissipation, refraction, or deformation. The surface waves also modify the oceanic currents, particularly in the near-shore and coastal oceans. The surface gravity waves generate the Stokes drift, which affects the sea state and ocean circulation (Longuet-Higgins and Stewart, 1960). In many cases, the interaction between waves and currents plays a significant role that we cannot ignore in processes such as contaminant and sediment transport, Langmuir currents, long-shore currents, rip currents, and wave set-down and setup. The requirements for improving the accuracy of coastal and ocean forecasts are increasing due to the increase in human activities on the ocean. Two methods are usually applied to simulate ocean currents. They are the Eulerian mean and the Generalized Lagrangian Mean (GLM) methods.

In the Eulerian mean method, the mean flow properties are obtained by a time-averaged technique. However, the difference in temporal and spatial scales between surface gravity waves and currents is extremely large. Then, the use of a direct numerical simulation approach is impractical. To solve this problem, a multi-scale asymptotic theory was proposed by McWilliams *et al.* (2004). Equations for the evolution of mean current were obtained in the presence of surface gravity waves. Their equations are valid in conditions of coastal water outside the surfzone. In the presence of finite-amplitude waves, the region between wave trough and wave crest is not always filled by the fluid but by the air during part of the wave period. Then, the use of the Eulerian mean method in this region poses a problem due to a large difference in density between the fluid and the air.

Another approach is using the GLM method introduced by Andrews and McIntyre (1978). This method is capable of properly separating air and water between the wave crest and the wave trough leading to the physical interpretation of definitions of mean properties from the wave trough to the mean water level. The problem with this method is that the wave properties are expressed implicitly through disturbance quantities, which represent departures from conservative motion. In practice, it is necessary to have an explicit approximation of wave action or wave momentum from wave kinetics.

In this study, equations of mean motion are developed based on the GLM method. These equations are written in terms of Quasi-Eulerian velocity which is defined as GLM velocity minus Stokes drift. The new equations are valid from offshore to coastal areas. In the case of infinitesimal and conservative waves, the new equations reduce to the well-known classical Eulerian mean equations of motion. The new equations are validated and calibrated with various sets of experimental data including adiabatic test, non-breaking random waves propagating on a strong ambient current in a wave flume (Klopman, 1994), breaking random waves propagating over a barred profile in a wave flume (Boers, 2005), and breaking random waves propagating in a large-scale laboratory facility (Hamilton

and Ebersole, 2001). These works were published in a recent paper by Nguyen *et al.* (2021a).

The effect of waves on the mean current is expressed explicitly in terms of three-dimensional (3D) wave radiation stress representation. Moreover, the relationship between 3D wave radiation stress and vortex force representations is proven mathematically. Besides, comparisons between the new set of equations of mean motion and other sets of equations implemented in recent well-known numerical models are given. It is useful for selecting a suitable numerical ocean model to simulate the mean current in specific conditions of waves combined with currents. These works are presented in Nguyen *et al.* (2021b).

## 1.2 RESEARCH QUESTIONS AND OBJECTIVES OF THIS STUDY

### 1.2.1 Research questions

This study aims to answer the following questions:

1) How to simulate three-dimensional mean currents from the deep ocean to the coastal, estuary, and outflow areas in the presence of finite-amplitude nonconservative waves?

2) How to express the effects of surface waves on three-dimensional mean currents, especially under the condition of non-conservative waves and strong ambient currents?

3) Is there any relationship between vortex force and radiation stress representations?

### 1.2.2 Objectives of this study

1) Develop a practical set of three-dimensional equations of mean motion which is valid from the bottom to the mean surface even in the presence of finite-amplitude non-conservative surface waves. The new set of equations should be suitable for applications from the deep water to the coastal, estuaries, and outflow areas.

2) Study the wave-induced forcing on the mean current and the relationship between 3D wave radiation stress and vortex force representations.

3) Develop a two-dimensional numerical model (2DV model) to validate the new set of equations of mean motion. The following experiments are employed:

- Adiabatic test: a monochromatic wave propagates on a slope without dissipation.

- The experiment of Klopman (1994): random non-breaking waves propagate on a strong ambient current in a wave flume.

- The experiment of Boers (2005): random breaking waves propagate in a wave flume.

- The experiment of Hamilton and Ebersole (2001): random breaking waves propagate in a Large-Scale Sediment Transport Facility (LSTF).

4) Compare the new set of equations with other sets of equations implemented in well-known numerical ocean models.

### 1.2.3 Literature review

The interaction between waves and currents has been the subject of much research in recent decades. There are two representations of wave-averaged effects on the currents called “radiation stress” and “vortex force”. The concept of “radiation stress: was first introduced by Longuet-Higgins and Stewart (1960) to explain the transfer of wave energy to a uniform current. This concept was used by Longuet-Higgins and Stewart (1962) to study the changes in the mean surface level and the currents caused by gravity waves. The radiation stress concept has been successful in explaining phenomena such as wave “set-up”, “surf beats”, the steepening of the surface waves on adverse currents (Longuet-Higgins and Stewart, 1964), and the generation of long-shore currents by oblique incident waves (Bowen, 1969; Longuet-Higgins, 1970; Thornton, 1970). However, since “radiation stress” introduced by Longuet-Higgins and Stewart (1960) is a two-dimensional horizontal tensor it is only practical for two-dimensional, depth-averaged models. In reality, the current is depth-dependent, so the vertical structure of the radiation stress should be specified.

Some scientists attempted to apply the “radiation stress” concept in three-dimensional models. Xie *et al.* (2001) applied the radiation stress as a depth uniform body force in the Princeton Ocean Model (POM), even though the radiation stress is caused by depth-varying wave velocity and hydrodynamic pressure. Therefore, their assumption for the vertical structure of radiation stress is not accurate. Xia *et al.* (2004) considered the vertical structure of radiation stress; however, the three-dimensional radiation stress formulation was derived from two-dimensional radiation stress.

The second representation of the wave and current interaction is expressed in terms of the vortex force. This representation was first developed by Craik and Leibovich (1976) in the work of constructing a realistic theoretical model of steady Langmuir circulations. Their research focused on the near-surface layer to explain the generation of Langmuir currents as a result of the interaction between surface waves and wind-driven circulation through the action of a vortex force. Leibovich (1977) extended this theory to allow vertical density stratification and slow time variation. McWilliams and Restrepo (1999) developed a perturbation theory to obtain wave-averaged equations of motion. Their theory is based on the assumption of small wave slope and deep water. McWilliams *et al.* (2004) developed a system of mean equations of motion based on an asymptotic theory to account for the interaction of waves and currents. In this, the effects of waves on the current are expressed in terms of the vortex force formalism. However, the equations of McWilliams *et al.* (2004) are only valid when the ratio of mean current to the wave orbital velocity is a small quantity, and are only applicable outside the breaking zone. Newberger and Allen (2007) developed a three-dimensional, hydrostatic model for surf zone

applications, with applicability to linear waves interacting with a depth-uniform mean current. They divided the effect of waves on the mean currents into surface and body forces. The surface force represents the wave dissipation, and the body force represents the gradient of the Bernoulli head and vortex-force. Equations of McWilliams *et al.* (2004) were used by Uchiyama *et al.* (2010) for surf zone applications. In this, the non-conservative forcing by breaking waves, roller waves, bottom and surface streaming and wave-enhanced mixing are added through empirical formulas. Their equations were implemented in the COAWST (coupled ocean-atmosphere-wave-sediment transport) modeling system by Kumar *et al.* (2012) with some modifications for empirical formulas of wave-induced forcing.

The relationship between "radiation stress" and "vortex force" representations was studied by Lane *et al.* (2007). In this, the asymptotic assumption proposed by McWilliams *et al.* (2004) was used to look for the similarities and discrepancies between these two representations. They proved that these two representations are equivalent. However, their work was restricted to non-dissipative waves only. All the theories mentioned above are expressed in an Eulerian-mean framework, though when finite-amplitude waves are present, the region between the wave trough and wave crest is not always filled by the fluid but by the air during part of the wave period. This poses a problem due to a large difference in density between the fluid and the air.

In the work of Mellor (2003) and Mellor (2008), a wave-following sigma-coordinate system was employed to couple the three-dimensional circulation models with wave models. The coupling included depth-dependent wave radiation stress terms. Their equations are inconsistent in the simple case of shoaling waves without energy dissipation (Ardhuin *et al.*, 2008). Recently, Mellor (2015) and Mellor (2016) derived prognostic equations for Eulerian mean flow on sigma coordinates. The three-dimensional momentum equations were inferred from the vertically integrated momentum equations by adding a term for which vertical integration is zero. Similar to the work of Xia *et al.* (2004), the inference of three-dimensional momentum equations from two-dimensional momentum equations is not straightforward. This inconsistency was also pointed out by Ardhuin *et al.* (2017). Moreover, in the momentum equation of Mellor (2015) and Mellor (2016), there is a missing term related to the divergence of the vertical momentum flux (Ardhuin *et al.*, 2017).

The generalized Lagrangian mean (GLM) method was introduced by Andrews and McIntyre (1978), hereafter referred to as AM. The basic idea of this method is to average over disturbance positions of the fluid particle. Therefore, the GLM method is valid from the bottom to the mean water surface even in conditions of finite-amplitude waves. This method provides a powerful foundation for the analysis of the wave-current interaction and gives a physical interpretation of the interaction between waves and currents. Based on the GLM method, AM developed a set of equations of mean motion in a general condition of the wave-current interaction. Their set of equations is complete and depends

on thermodynamic properties such as entropy and enthalpy. However, the disturbance-related quantities, which include both wave-induced and turbulence-induced effects, are not explicitly represented through source terms. Their equations were employed by Leibovich (1980) to derive Langmuir circulation equations under the assumption that the waves are dominated by their irrotational part. The GLM equations of AM were simplified by Dingemans (1997) with the assumption of constant density, and removing all thermodynamic terms, yet leaving the disturbance quantities as implicit. Groeneweg (1999) used an alternative method to obtain GLM equations, where the Reynolds-averaged Navier–Stokes (RANS) equations were rewritten in terms of GLM quantities. The mean quantities in RANS equations are obtained by applying the Eulerian mean method; therefore, the set of equations of Groeneweg (1999) is not suitable for the region above the wave trough. His set of equations was implemented in the Delft3D-FLOW model by Walstra *et al.* (2001) with simplification for the wave-induced driving force. Ardhuin *et al.* (2008) developed a practical set of equations of mean motion based on the work of Dingemans (1997). Their equations are written in terms of Quasi-Eulerian mean velocity $\hat{u}_i$ defined by:

$$\hat{u}_i = \overline{u}_i^L - \mathbf{p}_i, \tag{1.1}$$

where, $\overline{u}_i^L$ is the $i^{th}$- component of GLM velocity and $\mathbf{p}_i$ is the $i^{th}$-component of pseudomomentum defined by:

$$\mathbf{p}_i = \overline{\frac{\partial \xi_j}{\partial x_i}\left\{u_j^l + \left(\Omega \times \xi\right)_j\right\}}, \tag{1.2}$$

where, $x_i$ is the ith-component of position x, $\xi$ is the disturbance displacement of the fluid particle, $u_j^{\,l}$ is the $j^{th}$-component of Lagrangian disturbance velocity, and $\Omega$ is the angular velocity of the Earth. In the equation (1.2) the summation convention for the indices is employed. This convention is also used throughout this work with the indices from 1 to 3.

Equations of mean motion by Ardhuin *et al.* (2008) are explicit in terms of the wave forcing and applicable outside the breaking zone; their equations provide qualitative results for surf zone applications (Ardhuin *et al.*, 2008). This is due to the fact that the Stokes drift only approximates to pseudomomentum when the waves are irrotational and the mean flow is of second-order of the disturbance amplitude (AM). Equations of Ardhuin *et al.* (2008) were employed by Bennis *et al.* (2011) for coastal applications with an addition of dissipative forcing terms (i.e. breaking wave and roller wave-induced forcing, wave-induced mixing, wave-induced bottom friction).

In this study, a set of equations of mean motion using the GLM method is developed. These equations are written in terms of Quasi-Eulerian velocity defined as GLM velocity minus Stokes drift. The new equations are valid from offshore to coastal areas. Outside

the surf zone and for non-dissipative waves, the new equations are identical to the equations of Ardhuin *et al.* (2008); for dissipative waves, there are subtle differences. In the case of infinitesimal and conservative waves, the new equations reduce to the well-known classical Eulerian mean equations of motion. The new set of equations is validated with an adiabatic test, non-breaking waves propagating on a strong ambient current in a wave flume, breaking waves propagating over a barred profile in a wave flume, and obliquely incident breaking waves in a large-scale sediment transport facility (LSTF).

### 1.2.4 The outline of this dissertation

This dissertation is organized as follows:

In Chapter 1, the general information and the need of carrying out this study are presented. The research questions, objectives, literature review, and the outline of this dissertation are given in the second part of this Chapter. The derivation of the new equations of motion is presented in detail in Chapter 2. In this, the momentum equation and continuity equation are expressed in terms of Quasi-Eulerian mean quantities. In Chapter 3, a concept of 3D wave radiation stress is introduced to express the mean effect of waves on 3D currents. The 3D wave radiation stress is specified in different conditions of waves combined with currents. Besides, the relationship between 3D wave radiation stress and vortex force representation is also proved mathematically. In Chapter 4, the Quasi-Eulerian mean equations of motion are simplified under the hydrostatic assumption of the mean flow. Equations of motion are expressed in terms of both Quasi-Eulerian mean and GLM velocities. In Chapter 5, various experimental data sets are employed to validate the new set of equations of mean motion. Four experiments were selected including steady monochromatic waves propagating on a slope without dissipation (adiabatic condition), random non-breaking waves propagating on a strong ambient current in a wave flume, random breaking waves propagating on a sloping bed, and random breaking waves propagating in a Large-Scale Sediment Transport (LSTF) facility. The comparison of the new equations of motion with recent well-known equations of the mean motion of fluid-particle is given in Chapter 6. The general conclusion of this study is given in Chapter 7.

# 2

# DERIVATION OF THE QUASI-EULERIAN MEAN EQUATIONS OF MOTION[1]

[1] This Chapter is based on the publication: Nguyen, D.T., Jacobsen, N.G., Roelvink, D., 2021a. Development and Validation of Quasi-Eulerian Mean Three-Dimensional Equations of Motion Using the Generalized Lagrangian Mean Method. Journal of Marine Science and Engineering 9, 76.

## 2.1 DEFINITION OF QUASI-EULERIAN MEAN QUANTITY

### 2.1.1 Overview of Generalized Lagrangian Mean method

The GLM method is an exact theory of nonlinear waves on a Lagrangian-mean flow proposed by AM. In the following, only some properties of the GLM operator are present. Full details of this method are given in the original paper of AM. The basic idea of the GLM method is to average over positions displaced by a certain disturbance. The GLM of any quantity $\varphi(\mathbf{x},t)$ is defined as:

$$\overline{\varphi}^L(\mathbf{x},t) = \overline{\varphi\{\mathbf{x}+\xi(\mathbf{x},t),t\}}, \tag{2.1}$$

where, operator $\overline{(\ )}$ expresses a time average over a wave period. The term on the right-hand side of equation (2.1) is a usual Eulerian mean operator. Where, the particle displacement is assumed a true disturbance quantity, i.e.:

$$\overline{\xi(\mathbf{x},t)} = 0. \tag{2.2}$$

The following notation was employed throughout this study:

$$\varphi\{\mathbf{x}+\xi(\mathbf{x},t),t\} = \varphi^{\xi}(\mathbf{x},t). \tag{2.3}$$

The Lagrangian disturbance quantity $\varphi^l$ is defined as the deviation of the real quantity $\varphi^{\xi}$ from the GLM quantity $\overline{\varphi}^L$, i.e.:

$$\varphi^l(\mathbf{x},t) = \varphi^{\xi}(\mathbf{x},t) - \overline{\varphi}^L(\mathbf{x},t). \tag{2.4}$$

If the quantity $\varphi$ is the velocity vector $\mathbf{u}$ then we have the following definition of the GLM velocity:

$$\overline{\mathbf{u}}^L(\mathbf{x},t) = \overline{\mathbf{u}^{\xi}(\mathbf{x},t)}. \tag{2.5}$$

The Lagrangian mean material derivative is defined as (AM):

$$\bar{D}^L = \partial/\partial t + \overline{\mathbf{u}}^L.\nabla, \tag{2.6}$$

where, $\nabla = \left(\frac{\partial}{\partial x}, \frac{\partial}{\partial y}, \frac{\partial}{\partial z}\right)$ is the gradient operator. From equation (2.4) the Lagrangian disturbance velocity vector is defined by:

$$\mathbf{u}^l(\mathbf{x},t) = \mathbf{u}^{\xi} - \overline{\mathbf{u}}^L. \tag{2.7}$$

As pointed out by AM, the disturbance velocity $\mathbf{u}^l$ is equal to the mean material rate of change of disturbance displacement $\xi$, i.e.:

$$\bar{D}^L\xi = \mathbf{u}^l. \tag{2.8}$$

Evidently, the Lagrangian disturbance velocity is also a true disturbance quantity, i.e.:

$$\overline{\mathbf{u}^l} = 0. \tag{2.9}$$

Equations (2.1), (2.2), (2.7), and (2.8) are the fundamental equations of the GLM theory.

## 2.1.2 Definition of Quasi-Eulerian mean quantity

In this part, the fluid is assumed incompressible ( $\rho = const$ ) and the dependence of hydrodynamic processes on thermo-dynamics terms is neglected (assumption A1). For small disturbance amplitude, using a Taylor expansion the value of the function $\varphi$ at the disturbance position $\Xi(\mathbf{x},t) = \mathbf{x} + \xi(\mathbf{x},t)$ is expressed by:

$$\varphi^{\xi}(\mathbf{x},t) = \varphi(\mathbf{x},t) + \xi_j \frac{\partial \varphi}{\partial x_j} + \frac{1}{2}\xi_j \xi_k \frac{\partial^2 \varphi}{\partial x_j \partial x_k} + O(\varepsilon^3), \tag{2.10}$$

where, Einstein summation convention is employed with $j$ and $k$ run from 1 to 3, $\varepsilon = |\xi|$ is a small parameter in the order of disturbance displacement amplitude. The first term on the right-hand side of equation (2.10) is the Quasi-Eulerian quantity. The second and the third terms on the right-hand side of equation (2.10) express the effect of disturbance motion on function $\varphi$ correct to the second order of $\varepsilon$ .

The Quasi-Eulerian mean quantity $\overline{\varphi}$ is defined by:

$$\overline{\varphi}(\mathbf{x},t) = \overline{\varphi}^L(\mathbf{x},t) - \overline{\varphi}^S(\mathbf{x},t), \tag{2.11}$$

where, $\overline{\varphi}^S$ is the Stokes correction of the Quasi-Eulerian mean quantity $\overline{\varphi}$ defined by (AM):

$$\overline{\varphi}^S(\mathbf{x},t) = \overline{\xi_j \frac{\partial \varphi'}{\partial x_j}} + \frac{1}{2}\overline{\xi_j \xi_k} \frac{\partial^2 \overline{\varphi}}{\partial x_j \partial x_k} + O(\varepsilon^3), \tag{2.12}$$

where, $\varphi'$ is the Quasi-Eulerian disturbance defined as the difference between the Quasi-Eulerian quantity $\varphi$ and the Quasi-Eulerian mean quantity $\overline{\varphi}$ :

$$\varphi' = \varphi - \overline{\varphi}. \tag{2.13}$$

Equations (2.11) and (2.12) show that the Quasi-Eulerian mean quantity is approximated to the second-order of the disturbance amplitude.

We assume that any Quasi-Eulerian disturbance can be decomposed into wave and turbulence components, such as:

$$\varphi' = \tilde{\varphi} + \varphi^t, \tag{2.14}$$

where, $\tilde{\varphi}$ and $\varphi^t$ are the wave and turbulent quantities, respectively. Moreover, the turbulent and wave quantities are assumed to be uncorrelated, i.e., for any $\varphi$ and $\psi$ we have:

$$\overline{\tilde{\varphi}\psi^t} = 0. \tag{2.15}$$

## 2.2 DERIVATION OF QUASI-EULERIAN MEAN MOMENTUM EQUATION

Let us start with the momentum equation for the total flow written in the Eulerian framework. The $i^{th}$ equation is expressed by:

$$\frac{\partial u_i}{\partial t} + u_j \frac{\partial u_i}{\partial x_j} + 2(\Omega \times \mathbf{u})_i + \frac{\partial \Phi}{\partial x_i} + \frac{1}{\rho}\frac{\partial p}{\partial x_i} + X_i = 0, \tag{2.16}$$

where, Einstein summation convention is applied with $j$ runs from 1 to 3, the angular velocity of the Earth $\Omega$ is assumed constant, $\Phi(\mathbf{x},t)$ is the potential of the gravitational force, $p$ is pressure, and $X$ is a function of non-wave dissipative forcing.

Evaluating equation (2.16) at disturbance position of the fluid particle $\Xi = \mathbf{x} + \xi$ to obtain:

$$\left(\frac{\partial u_i}{\partial t} + u_j \frac{\partial u_i}{\partial x_j}\right)^{\xi} + \left(2(\Omega \times \mathbf{u})_i\right)^{\xi} + \left(\frac{\partial \Phi}{\partial x_i}\right)^{\xi} + \left(\frac{1}{\rho}\frac{\partial p}{\partial x_i}\right)^{\xi} + \left(X_i\right)^{\xi} = 0. \tag{2.17}$$

Equation (2.17) is valid from the bottom to the free water surface. Assuming that the gravitational acceleration $g$ is constant, we have:

$$\frac{\partial \Phi}{\partial x_i} = \delta_{i3} g, \tag{2.18}$$

where, $\delta_{i3}$ is Kronecker delta function given by:

$$\delta_{i3} = \begin{cases} 1 & \text{if } i = 3 \\ 0 & \text{otherwise} \end{cases}. \tag{2.19}$$

The GLM momentum equation is obtained by averaging equation (2.17) over a wave period, i.e.:

$$\overline{\left(\frac{\partial u_i}{\partial t} + u_j \frac{\partial u_i}{\partial x_j}\right)^{\xi}} + \overline{\left(2(\Omega \times \mathbf{u})_i\right)^{\xi}} + \overline{\left(\frac{\partial \Phi}{\partial x_i}\right)^{\xi}} + \overline{\left(\frac{1}{\rho}\frac{\partial p}{\partial x_i}\right)^{\xi}} + \overline{\left(X_i\right)^{\xi}} = 0. \tag{2.20}$$

According to AM, the first term on the left-hand side of equation (2.20) can be rewritten as:

$$\overline{\left(\frac{\partial u_i}{\partial t}+u_j\frac{\partial u_i}{\partial x_j}\right)^{\xi}}=\bar{D}^L\bar{u}_i^L. \tag{2.21}$$

Since $\boldsymbol{\Omega}$ is constant then the second term on the left-hand side of equation (2.20) becomes:

$$\overline{\left(2(\Omega\times\mathbf{u})_i\right)^{\xi}}=2(\Omega\times\bar{\mathbf{u}}^L)_i. \tag{2.22}$$

From equation (2.18), the third term on the left-hand side of equation (2.20) is:

$$\overline{\left(\frac{\partial\Phi}{\partial x_i}\right)^{\xi}}=\overline{\left(\delta_{i3}g\right)^{\xi}}=\delta_{i3}g. \tag{2.23}$$

When $\nabla.\mathbf{u}'=0$ the divergence of disturbance displacement is of the second order of small disturbance amplitude (AM), i.e.:

$$\nabla.\xi=O(\varepsilon^2). \tag{2.24}$$

Using a Taylor expansion and equation (2.24) the pressure gradient term in equation (2.20) can be expressed as:

$$\frac{1}{\rho}\overline{\left(\frac{\partial p}{\partial x_i}\right)^{\xi}}=\frac{1}{\rho}\frac{\partial\bar{p}}{\partial x_i}+\frac{1}{\rho}\overline{\frac{\partial}{\partial x_j}\left(\xi_j\frac{\partial p'}{\partial x_i}\right)}+\frac{1}{2\rho}\overline{\xi_j\xi_k}\frac{\partial^3\bar{p}}{\partial x_i\partial x_j\partial x_k}+O(\varepsilon^3). \tag{2.25}$$

Inserting equations (2.21), (2.22) (2.23) and (2.25) into equation (2.20), we obtain the following momentum equation in the GLM framework, i.e.:

$$\begin{aligned}&\bar{D}^L\bar{u}_i^L+2\left(\Omega\times\bar{\mathbf{u}}^L\right)_i+\delta_{i3}g+\frac{1}{\rho}\frac{\partial\bar{p}}{\partial x_i}+\bar{X}_i^L=-\frac{1}{\rho}\overline{\frac{\partial}{\partial x_j}\left(\xi_j\frac{\partial p'}{\partial x_i}\right)}\\&-\frac{1}{2\rho}\overline{\xi_j\xi_k}\frac{\partial^3\bar{p}}{\partial x_i\partial x_j\partial x_k}+O(\varepsilon^3).\end{aligned} \tag{2.26}$$

In the above equation, both effects of waves and turbulence on the current are involved in the Quasi-Eulerian disturbance and GLM terms. For example, Quasi-Eulerian disturbance pressure $p'$ includes wave-induced pressure $\tilde{p}$ and turbulence-induced pressure $p^t$. However, there is no available theory to calculate such Quasi-Eulerian disturbance terms. Therefore, it is necessary to separate wave and turbulent terms from the Quasi-Eulerian disturbance. In the following, equation (2.26) is used to develop a Quasi-Eulerian mean momentum equation in the GLM framework. The goal of this exercise is that the wave-induced velocity, the turbulence, and the mean current velocity are separated.

For any quantity $\varphi$, AM obtained the following relationship between Lagrangian disturbance and Quasi-Eulerian disturbance:

$$\varphi^l = \varphi' + \xi_j \frac{\partial \overline{\varphi}}{\partial x_j} + O(\varepsilon^2). \tag{2.27}$$

Using equation (2.27) the first term in the right-hand side of equation (2.26) can be expressed as:

$$\frac{1}{\rho}\frac{\partial}{\partial x_j}\left(\overline{\xi_j \frac{\partial p'}{\partial x_i}}\right) = \frac{1}{\rho}\frac{\partial}{\partial x_j}\left[\overline{\xi_j \left(\frac{\partial p}{\partial x_i}\right)^l}\right] - \frac{1}{\rho}\frac{\partial}{\partial x_j}\left(\overline{\xi_j \xi_k}\frac{\partial^2 \overline{p}}{\partial x_k \partial x_i}\right) + O(\varepsilon^3). \tag{2.28}$$

Subtracting equation (2.26) from equation (2.17) to obtain the following equation for the evolution of disturbance motion:

$$\bar{D}^L u_i^l + \left(2(\Omega \times \mathbf{u})_i\right)^l + \left(\delta_{i3} g\right)^l + \left(X_i\right)^l + \left(\frac{1}{\rho}\frac{\partial p}{\partial x_i}\right)^l = 0. \tag{2.29}$$

Since the gravitational acceleration $g$ is assumed constant, the third term on the left-hand side of equation (2.29) is neglected. Multiply equation (2.29) with $\xi_j$ and then take the spatial derivative $\partial / \partial x_j$ to obtain:

$$\frac{1}{\rho}\frac{\partial}{\partial x_j}\left[\overline{\xi_j \left(\frac{\partial p}{\partial x_i}\right)^l}\right] = -\frac{\partial}{\partial x_j}\left(\overline{\xi_j \bar{D}^L u_i^l}\right) - \frac{\partial}{\partial x_j}\left(\overline{2\xi_j (\Omega \times \mathbf{u}^l)_i}\right) - \frac{\partial}{\partial x_j}\left(\overline{\xi_j X_i^l}\right). \tag{2.30}$$

The first term on the right-hand side of equation (2.30) is decomposed as:

$$\frac{\partial}{\partial x_j}\left(\overline{\xi_j \bar{D}^L u_i^l}\right) = \bar{D}^L\left(\overline{\xi_j \frac{\partial u_i^l}{\partial x_j}}\right) + \frac{\partial\left(\overline{\xi_j u_i^l}\right)}{\partial x_k}\frac{\partial \overline{u}_k^L}{\partial x_j} - \frac{\partial}{\partial x_j}\left(\overline{u_i^l \bar{D}^L \xi_j}\right) + O(\varepsilon^3). \tag{2.31}$$

From the definition of Lagrangian velocity disturbance (2.8) the second term on the right-hand side of equation (2.31) becomes:

$$\frac{\partial}{\partial x_j}\left(\overline{u_i^l \bar{D}^L \xi_j}\right) = \frac{\partial\left(\overline{u_i^l u_j^l}\right)}{\partial x_j}. \tag{2.32}$$

Substitute equations (2.32) and (2.31) into equation (2.30) we obtain:

$$\begin{aligned}\frac{1}{\rho}\frac{\partial}{\partial x_j}\left[\overline{\xi_j \left(\frac{\partial p}{\partial x_i}\right)^l}\right] &= -\bar{D}^L\left(\overline{\xi_j \frac{\partial u_i^l}{\partial x_j}}\right) - \frac{\partial\left(\overline{\xi_j u_i^l}\right)}{\partial x_k}\frac{\partial \overline{u}_k^L}{\partial x_j} + \frac{\partial\left(\overline{u_i^l u_j^l}\right)}{\partial x_j} \\ &- \frac{\partial}{\partial x_j}\left(\overline{2\xi_j (\Omega \times \mathbf{u}^l)_i}\right) - \frac{\partial}{\partial x_j}\left(\overline{\xi_j X_i^l}\right) + O(\varepsilon^3).\end{aligned} \tag{2.33}$$

In the following, all terms on the right-hand side of equation (2.33) are rewritten in terms of Quasi-Eulerian disturbance based on the relationship (2.27). The first term in the right-hand side of equation (2.33) can be expressed as:

$$\begin{aligned}\bar{D}^L\left(\overline{\xi_j\frac{\partial u_i^l}{\partial x_j}}\right)&=\bar{D}^L\left(\overline{\xi_j\frac{\partial u_i'}{\partial x_j}}\right)+\bar{D}^L\left[\frac{\partial}{\partial x_j}\left(\overline{\xi_j\xi_k}\frac{\partial\bar{u}_i}{\partial x_k}\right)\right]=\bar{D}^L\left(\overline{\xi_j\frac{\partial u_i'}{\partial x_j}}\right)\\&+\frac{\partial}{\partial x_j}\left[\bar{D}^L\left(\overline{\xi_j\xi_k}\frac{\partial\bar{u}_i}{\partial x_k}\right)\right]-\frac{\partial\overline{\xi_j\xi_k}}{\partial x_l}\frac{\partial\bar{u}_i}{\partial x_k}\frac{\partial\bar{u}_l}{\partial x_j}-\overline{\xi_j\xi_k}\frac{\partial\bar{u}_l}{\partial x_j}\frac{\partial^2\bar{u}_i}{\partial x_k\partial x_l}+O(\varepsilon^3).\end{aligned}\tag{2.34}$$

Similarly, the second term on the right-hand side of equation (2.33) becomes:

$$\begin{aligned}&\frac{\partial\left(\overline{\xi_j u_i^l}\right)}{\partial x_k}\frac{\partial\bar{u}_k^L}{\partial x_j}=\frac{\partial\left(\overline{\xi_j u_i'}\right)}{\partial x_k}\frac{\partial\bar{u}_k^L}{\partial x_j}+\frac{\partial\left(\overline{\xi_j\xi_l}\right)}{\partial x_k}\frac{\partial\bar{u}_i}{\partial x_l}\frac{\partial\bar{u}_k}{\partial x_j}+\overline{\xi_j\xi_l}\frac{\partial\bar{u}_k}{\partial x_j}\frac{\partial^2\bar{u}_i}{\partial x_k\partial x_l}\\&=\frac{\partial}{\partial x_k}\left(\overline{\xi_j u_i'}\frac{\partial\bar{u}_k}{\partial x_j}\right)+\frac{\partial\left(\overline{\xi_j\xi_l}\right)}{\partial x_k}\frac{\partial\bar{u}_i}{\partial x_l}\frac{\partial\bar{u}_k}{\partial x_j}+\overline{\xi_j\xi_l}\frac{\partial\bar{u}_k}{\partial x_j}\frac{\partial^2\bar{u}_i}{\partial x_k\partial x_l}+O(\varepsilon^3).\end{aligned}\tag{2.35}$$

The third term on the right-hand side of equation (2.33) is expressed by:

$$\frac{\partial\left(\overline{u_i^l u_j^l}\right)}{\partial x_j}=\frac{\partial\left(\overline{u_i'u_j'}\right)}{\partial x_j}+\frac{\partial}{\partial x_j}\left[\overline{u_i'\xi_l}\frac{\partial\bar{u}_j}{\partial x_l}+\overline{u_j'\xi_k}\frac{\partial\bar{u}_i}{\partial x_k}+\overline{\xi_k\xi_l}\frac{\partial\bar{u}_i}{\partial x_k}\frac{\partial\bar{u}_j}{\partial x_l}\right]+O(\varepsilon^3).\tag{2.36}$$

Similarly, the fourth term on the right-hand side of equation (2.33) is expressed in term of Quasi-Eulerian disturbance quantities as:

$$\begin{aligned}&\frac{\partial}{\partial x_j}\left(\overline{2\xi_j(\Omega\times\mathbf{u}^l)_i}\right)=2\varepsilon_{imn}\Omega_m\overline{\xi_j\frac{\partial u_n^l}{\partial x_j}}+O(\varepsilon^3)\\&=2\varepsilon_{imn}\Omega_m\overline{\xi_j\frac{\partial u_n'}{\partial x_j}}+\frac{\partial}{\partial x_j}\left(2\varepsilon_{imn}\Omega_m\overline{\xi_j\xi_k}\frac{\partial\bar{u}_n}{\partial x_k}\right)+O(\varepsilon^3),\end{aligned}\tag{2.37}$$

where, $\varepsilon_{imn}$ is the Levi-Civita symbol defined by:

$$\varepsilon_{imn}=\begin{cases}+1 & \text{if } (i,m,n) \text{ is an even permutation of (1,2,3)}\\ -1 & \text{if } (i,m,n) \text{ is an odd permutation of (1,2,3)}\\ 0 & \text{if any index is repeated}\end{cases}.\tag{2.38}$$

The fifth term on the right-hand side of equation (2.33) is expressed by:

$$\frac{\partial}{\partial x_j}\left(\overline{\xi_j X_i^l}\right)=\overline{\xi_j\frac{\partial X_i^l}{\partial x_j}}=\overline{\xi_j\frac{\partial X_i'}{\partial x_j}}+\frac{\partial}{\partial x_j}\left(\overline{\xi_j\xi_k}\frac{\partial\bar{X}_i}{\partial x_k}\right)+O(\varepsilon^3).\tag{2.39}$$

From equations (2.34)-(2.39) equation (2.33) can be expressed in terms of Quasi-Eulerian disturbance quantities as:

$$\begin{aligned}
&\frac{1}{\rho}\frac{\partial}{\partial x_j}\left[\overline{\xi_j\left(\frac{\partial p}{\partial x_i}\right)^l}\right]=\frac{\partial\left(\overline{u_i'u_j'}\right)}{\partial x_j}+\frac{\partial}{\partial x_j}\left[\overline{u_j'\xi_k}\frac{\partial\overline{u}_i}{\partial x_k}+\overline{\xi_k\xi_l}\frac{\partial\overline{u}_i}{\partial x_k}\frac{\partial\overline{u}_j}{\partial x_l}\right]\\
&-\bar{D}^L\left(\overline{\xi_j\frac{\partial u_i'}{\partial x_j}}\right)-\frac{\partial}{\partial x_j}\left[\bar{D}^L\left(\overline{\xi_j\xi_k}\frac{\partial\overline{u}_i}{\partial x_k}\right)\right]-2\varepsilon_{imn}\Omega_m\overline{\xi_j\frac{\partial u_n'}{\partial x_j}}\\
&-\frac{\partial}{\partial x_j}\left(2\varepsilon_{imn}\Omega_m\overline{\xi_j\xi_k}\frac{\partial\overline{u}_n}{\partial x_k}\right)-\overline{\xi_j\frac{\partial X_i'}{\partial x_j}}-\frac{\partial}{\partial x_j}\left(\overline{\xi_j\xi_k}\frac{\partial\overline{X}_i}{\partial x_k}\right)+O(\varepsilon^3).
\end{aligned}\tag{2.40}$$

Replacing equation (2.40) into equation (2.28) we obtain:

$$\begin{aligned}
&\frac{1}{\rho}\frac{\partial}{\partial x_j}\left(\overline{\xi_j\frac{\partial p'}{\partial x_i}}\right)=\frac{\partial\left(\overline{u_i'u_j'}\right)}{\partial x_j}-\bar{D}^L\left(\overline{\xi_j\frac{\partial u_i'}{\partial x_j}}\right)-2\varepsilon_{imn}\Omega_m\overline{\xi_j\frac{\partial u_n'}{\partial x_j}}-\overline{\xi_j\frac{\partial X_i'}{\partial x_j}}\\
&+\frac{\partial}{\partial x_j}\left[\overline{u_j'\xi_k}\frac{\partial\overline{u}_i}{\partial x_k}+\overline{\xi_k\xi_l}\frac{\partial\overline{u}_i}{\partial x_k}\frac{\partial\overline{u}_j}{\partial x_l}\right]-\frac{\partial}{\partial x_j}\left[\frac{\partial\overline{u}_i}{\partial x_k}\bar{D}^L\left(\overline{\xi_j\xi_k}\right)\right]-\frac{\partial}{\partial x_j}\left[\overline{\xi_j\xi_k}\bar{D}^L\left(\frac{\partial\overline{u}_i}{\partial x_k}\right)\right]\\
&-\frac{\partial}{\partial x_j}\left(2\varepsilon_{imn}\Omega_m\overline{\xi_j\xi_k}\frac{\partial\overline{u}_n}{\partial x_k}\right)-\frac{\partial}{\partial x_j}\left(\overline{\xi_j\xi_k}\frac{\partial\overline{X}_i}{\partial x_k}\right)-\frac{1}{\rho}\frac{\partial}{\partial x_j}\left(\overline{\xi_j\xi_k}\frac{\partial^2\overline{p}}{\partial x_k\partial x_i}\right)+O(\varepsilon^3).
\end{aligned}\tag{2.41}$$

From equation (2.8) and equation (2.27) the sixth term on the right-hand side of equation (2.41) can be expressed as:

$$\begin{aligned}
&\frac{\partial\overline{u}_i}{\partial x_k}\bar{D}^L\left(\overline{\xi_j\xi_k}\right)=\frac{\partial\overline{u}_i}{\partial x_k}\left[\overline{\xi_j\bar{D}^L\xi_k}+\overline{\xi_k\bar{D}^L\xi_j}\right]=\frac{\partial\overline{u}_i}{\partial x_k}\left(\overline{\xi_ju_k^l}+\overline{\xi_ku_j^l}\right)\\
&=\overline{\xi_ju_k'}\frac{\partial\overline{u}_i}{\partial x_k}+\overline{\xi_ku_j'}\frac{\partial\overline{u}_i}{\partial x_k}+\overline{\xi_j\xi_l}\frac{\partial\overline{u}_k}{\partial x_l}\frac{\partial\overline{u}_i}{\partial x_k}+\overline{\xi_k\xi_l}\frac{\partial\overline{u}_j}{\partial x_l}\frac{\partial\overline{u}_i}{\partial x_k}+O(\varepsilon^3).
\end{aligned}\tag{2.42}$$

Similarly, the seventh term on the right-hand side of equation (2.41) is expressed as:

$$\overline{\xi_j\xi_k}\bar{D}^L\left(\frac{\partial\overline{u}_i}{\partial x_k}\right)=\overline{\xi_j\xi_k}\frac{\partial}{\partial x_k}\left(\bar{D}^L\overline{u}_i\right)-\overline{\xi_j\xi_k}\frac{\partial\overline{u}_l^L}{\partial x_k}\frac{\partial\overline{u}_i}{\partial x_l}+O(\varepsilon^3).\tag{2.43}$$

Then, the total of the last four terms on the right-hand side of equation (2.41) is expressed by:

$$\begin{aligned}&\frac{\partial}{\partial x_j}\left[\overline{\xi_j\xi_k}\bar{D}^L\left(\frac{\partial \bar{u}_i}{\partial x_k}\right)+\left(2\varepsilon_{imn}\Omega_m\overline{\xi_j\xi_k}\frac{\partial \bar{u}_n}{\partial x_k}\right)+\left(\overline{\xi_j\xi_k}\frac{\partial \bar{X}_i}{\partial x_k}\right)+\frac{1}{\rho}\left(\overline{\xi_j\xi_k}\frac{\partial^2\bar{p}}{\partial x_k\partial x_i}\right)\right]\\&=\frac{\partial}{\partial x_j}\left[\overline{\xi_j\xi_k}\frac{\partial}{\partial x_k}\left(\bar{D}^L\bar{u}_i+2\left(\Omega\times\bar{\mathbf{u}}\right)_i+\delta_{i3}g+\bar{X}_i+\frac{1}{\rho}\frac{\partial\bar{p}}{\partial x_i}\right)\right]\\&-\frac{\partial}{\partial x_j}\left(\overline{\xi_j\xi_k}\frac{\partial\bar{u}_l}{\partial x_k}\frac{\partial\bar{u}_i}{\partial x_l}\right)+O(\varepsilon^3).\end{aligned}\tag{2.44}$$

Since $\bar{\varphi}^S=O(\varepsilon^2)$ then from equation (2.26) we have:

$$\bar{D}^L\bar{u}_i+2\left(\Omega\times\bar{\mathbf{u}}\right)_i+\delta_{i3}g+\bar{X}_i+\frac{1}{\rho}\frac{\partial\bar{p}}{\partial x_i}=O(\varepsilon^2).\tag{2.45}$$

Therefore, in the second-order of the accuracy of the small disturbance amplitude equation (2.44) can be rewritten as:

$$\begin{aligned}&\frac{\partial}{\partial x_j}\left[\overline{\xi_j\xi_k}\bar{D}^L\left(\frac{\partial \bar{u}_i}{\partial x_k}\right)+2\varepsilon_{imn}\Omega_m\left(\overline{\xi_j\xi_k}\frac{\partial \bar{u}_n}{\partial x_k}\right)+\left(\overline{\xi_j\xi_k}\frac{\partial \bar{X}_i}{\partial x_k}\right)+\frac{1}{\rho}\left(\overline{\xi_j\xi_k}\frac{\partial^2\bar{p}}{\partial x_k\partial x_i}\right)\right]\\&=-\frac{\partial}{\partial x_j}\left(\overline{\xi_j\xi_k}\frac{\partial\bar{u}_l}{\partial x_k}\frac{\partial\bar{u}_i}{\partial x_l}\right)+O(\varepsilon^3).\end{aligned}\tag{2.46}$$

From equations (2.42) and (2.46), the total of the last six terms on the right-hand side of equation (2.41) can be expressed by:

$$\begin{aligned}&\frac{\partial}{\partial x_j}\left[\overline{u_j'\xi_k}\frac{\partial\bar{u}_i}{\partial x_k}+\overline{\xi_k\xi_l}\frac{\partial\bar{u}_i}{\partial x_k}\frac{\partial\bar{u}_j}{\partial x_l}\right]-\frac{\partial}{\partial x_j}\left[\frac{\partial\bar{u}_i}{\partial x_k}\bar{D}^L\left(\overline{\xi_j\xi_k}\right)\right]-\frac{\partial}{\partial x_j}\left[\overline{\xi_j\xi_k}\bar{D}^L\left(\frac{\partial\bar{u}_i}{\partial x_k}\right)\right]\\&-\frac{\partial}{\partial x_j}\left[2\varepsilon_{imn}\Omega_m\left(\overline{\xi_j\xi_k}\frac{\partial\bar{u}_n}{\partial x_k}\right)\right]-\frac{\partial}{\partial x_j}\left[\left(\overline{\xi_j\xi_k}\frac{\partial\bar{X}_i}{\partial x_k}\right)\right]-\frac{\partial}{\partial x_j}\left[\frac{1}{\rho}\left(\overline{\xi_j\xi_k}\frac{\partial^2\bar{p}}{\partial x_k\partial x_i}\right)\right]\\&=-\frac{\partial}{\partial x_j}\left(\overline{\xi_ju_k'}\frac{\partial\bar{u}_i}{\partial x_k}\right)+O(\varepsilon^3).\end{aligned}\tag{2.47}$$

Substitute equation (2.47) into equation (2.41) to obtain the following relationship:

$$\begin{aligned}&\frac{1}{\rho}\frac{\partial}{\partial x_j}\left(\overline{\xi_j\frac{\partial p'}{\partial x_i}}\right)=\frac{\partial\left(\overline{u_i'u_j'}\right)}{\partial x_j}-\bar{D}^L\left(\overline{\xi_j\frac{\partial u_i'}{\partial x_j}}\right)-2\varepsilon_{imn}\Omega_m\overline{\xi_j\frac{\partial u_n'}{\partial x_j}}\\&-\overline{\xi_j\frac{\partial X_i'}{\partial x_j}}-\frac{\partial}{\partial x_j}\left[\overline{\xi_ju_k'}\frac{\partial\bar{u}_i}{\partial x_k}\right]+O(\varepsilon^3).\end{aligned}\tag{2.48}$$

Following the definition of Stokes correction (2.12) the second term on the right-hand side of equation (2.48) can be expressed as:

$$\bar{D}^L\left(\overline{\xi_j\frac{\partial u_i'}{\partial x_j}}\right)=\bar{D}^L\bar{u}_i^S-\bar{D}^L\left(\frac{1}{2}\overline{\xi_j\xi_k}\frac{\partial^2\bar{u}_i}{\partial x_j\partial x_k}\right)+O(\varepsilon^3), \tag{2.49}$$

where, $\bar{u}_i^S$ is the $i^{th}$- component of Stoke drift $\bar{\mathbf{u}}^S$.

Using equations (2.8) and (2.27) the second term in the right-hand side of equation (2.49) is expressed as:

$$\begin{aligned}
&\bar{D}^L\left(\frac{1}{2}\overline{\xi_j\xi_k}\frac{\partial^2\bar{u}_i}{\partial x_j\partial x_k}\right)=\frac{1}{2}\overline{\xi_j\xi_k}\bar{D}^L\left(\frac{\partial^2\bar{u}_i}{\partial x_j\partial x_k}\right)+\frac{1}{2}\frac{\partial^2\bar{u}_i}{\partial x_j\partial x_k}\bar{D}^L\left(\overline{\xi_j\xi_k}\right)\\
&=\frac{1}{2}\overline{\xi_j\xi_k}\left[\frac{\partial^2}{\partial x_j\partial x_k}\left(\bar{D}^L\bar{u}_i\right)-\frac{\partial^2\bar{u}_l}{\partial x_j\partial x_k}\frac{\partial\bar{u}_i}{\partial x_l}-\frac{\partial\bar{u}_l}{\partial x_k}\frac{\partial^2\bar{u}_i}{\partial x_j\partial x_l}-\frac{\partial\bar{u}_l}{\partial x_j}\frac{\partial^2\bar{u}_i}{\partial x_k\partial x_l}\right]\\
&+\frac{1}{2}\left(\overline{\xi_ju_k'}+\overline{\xi_j\xi_l}\frac{\partial\bar{u}_k}{\partial x_l}+\overline{\xi_ku_j'}+\overline{\xi_k\xi_l}\frac{\partial\bar{u}_j}{\partial x_l}\right)\frac{\partial^2\bar{u}_i}{\partial x_j\partial x_k}+O(\varepsilon^3)\\
&=\frac{1}{2}\overline{\xi_j\xi_k}\left[\frac{\partial^2}{\partial x_j\partial x_k}\left(\bar{D}^L\bar{u}_i\right)\right]-\frac{1}{2}\overline{\xi_j\xi_k}\frac{\partial^2\bar{u}_l}{\partial x_j\partial x_k}\frac{\partial\bar{u}_i}{\partial x_l}+\overline{\xi_ju_k'}\frac{\partial^2\bar{u}_i}{\partial x_j\partial x_k}+O(\varepsilon^3).
\end{aligned} \tag{2.50}$$

The last three terms on the right-hand side of equation (2.48) can be expressed, respectively, as:

$$2\varepsilon_{imn}\Omega_m\overline{\xi_j\frac{\partial u_n'}{\partial x_j}}=2\left(\Omega\times\bar{\mathbf{u}}^S\right)_i-2\varepsilon_{imn}\Omega_m\left(\frac{1}{2}\overline{\xi_j\xi_k}\frac{\partial^2\bar{u}_n}{\partial x_j\partial x_k}\right)+O(\varepsilon^3), \tag{2.51}$$

$$\overline{\xi_j\frac{\partial X_i'}{\partial x_j}}=\bar{X}_i^S-\frac{1}{2}\overline{\xi_j\xi_k}\frac{\partial^2\bar{X}_i}{\partial x_j\partial x_k}+O(\varepsilon^3), \tag{2.52}$$

$$\begin{aligned}
&\frac{\partial}{\partial x_j}\left[\overline{\xi_ju_k'}\frac{\partial\bar{u}_i}{\partial x_k}\right]=\overline{\xi_j\frac{\partial u_k'}{\partial x_j}}\frac{\partial\bar{u}_i}{\partial x_k}+\overline{\xi_ju_k'}\frac{\partial^2\bar{u}_i}{\partial x_j\partial x_k}\\
&=\bar{u}_k^S\frac{\partial\bar{u}_i}{\partial x_k}-\frac{1}{2}\overline{\xi_j\xi_l}\frac{\partial^2\bar{u}_k}{\partial x_j\partial x_l}\frac{\partial\bar{u}_i}{\partial x_k}+\overline{\xi_ju_k'}\frac{\partial^2\bar{u}_i}{\partial x_j\partial x_k}+O(\varepsilon^3).
\end{aligned} \tag{2.53}$$

Replacing equations from (2.49) to (2.53) into equation (2.48), we obtain:

$$\begin{aligned}
&\bar{D}^L\bar{u}_i^S+2\left(\Omega\times\bar{\mathbf{u}}^S\right)_i+\bar{X}_i^S+\frac{1}{\rho}\frac{\partial}{\partial x_j}\left(\overline{\xi_j\frac{\partial p'}{\partial x_i}}\right)+\frac{1}{2\rho}\overline{\xi_j\xi_k}\frac{\partial^3\bar{p}}{\partial x_i\partial x_j\partial x_k}\\
&=\frac{\partial\left(\overline{u_i'u_j'}\right)}{\partial x_j}-\bar{u}_k^S\frac{\partial\bar{u}_i}{\partial x_k}+O(\varepsilon^3).
\end{aligned} \tag{2.54}$$

Equation (2.54) expresses the relationship between the evolution of Stokes drift and the disturbance of fluid particles. This is the basis to develop Quasi-Eulerian mean equations of motion.

From (2.14) and (2.15) the first term on the right-hand side of equation (2.54) can be decomposed into the wave and turbulence components, such as:

$$-\frac{\partial\left(\overline{u_i' u_j'}\right)}{\partial x_j} = -\frac{\partial\left(\overline{\tilde{u}_i \tilde{u}_j}\right)}{\partial x_j} - \frac{\partial\left(\overline{u_i^t u_j^t}\right)}{\partial x_j}, \tag{2.55}$$

where, $\tilde{u}_i$ and $u_i^t$ are $i^{th}$- components of wave and turbulent velocities, respectively. It is stressed that an assumption of no correlation between wave and turbulent quantities is employed in this step.

Using the definition of Quasi-Eulerian mean quantity (2.11) the GLM equation (2.26) can be rewritten as:

$$\begin{aligned} &\bar{D}^L \bar{u}_i + 2\left(\Omega \times \bar{\mathbf{u}}\right)_i + \delta_{i3} g + \frac{1}{\rho}\frac{\partial \bar{p}}{\partial x_i} + \bar{X}_i = -\bar{D}^L \bar{u}_i^S - 2\left(\Omega \times \bar{\mathbf{u}}^S\right)_i - \bar{X}_i^S \\ &-\frac{1}{\rho}\overline{\frac{\partial}{\partial x_j}\left(\xi_j \frac{\partial p'}{\partial x_i}\right)} - \frac{1}{2\rho}\overline{\xi_j \xi_k}\frac{\partial^3 \bar{p}}{\partial x_i \partial x_j \partial x_k} + O(\varepsilon^3). \end{aligned} \tag{2.56}$$

Inserting equations (2.54) and (2.55) into equation (2.56) we obtain the momentum equation expressed in terms of Quasi-Eulerian mean velocity, i.e.:

$$\frac{D\bar{u}_i}{Dt} + 2\left(\Omega \times \bar{\mathbf{u}}\right)_i + \delta_{i3} g + X_i = -\frac{1}{\rho}\frac{\partial \bar{p}}{\partial x_i} - \frac{\partial\left(\overline{\tilde{u}_i \tilde{u}_j}\right)}{\partial x_j} + \frac{1}{\rho}\frac{\partial \bar{\tau}_{ij}}{\partial x_j} + O(\varepsilon^3), \tag{2.57}$$

where, $\bar{\tau}_{ij} = -\rho\overline{u_i^t u_j^t}$ is the turbulent stress tensor.

The momentum equation (2.57) includes four variables: three components of Quasi-Eulerian mean velocity $\bar{\mathbf{u}}$ and pressure $\bar{p}$. Effects of waves and turbulence can be modeled as source terms. The momentum equation can be solved in combination with the continuity equation. The turbulent effect is expressed in the form of Reynolds turbulent stress, which can be calculated by using existing turbulent submodels, and the wave effect following an appropriate wave model.

## 2.3 Derivation of the Quasi-Eulerian mean mass conservation equation

The mass conservation equation is necessary to close the set of equations of the mean motion. The mass conservation is simplified under the assumption of slow modulation of

the waves (assumption A2). For an incompressible fluid (assumption A1), the mass conservation equation is expressed by (AM):

$$\frac{\partial \overline{u}^L}{\partial x}+\frac{\partial \overline{v}^L}{\partial y}+\frac{\partial \overline{w}^L}{\partial z}=\frac{1}{2}\left(\frac{\partial^3 \overline{\xi_j \xi_k}}{\partial t \partial x_j \partial x_k}+\overline{u}_l^L \frac{\partial^3 \overline{\xi_j \xi_k}}{\partial x_l \partial x_j \partial x_k}\right). \tag{2.58}$$

In the following, the vertical GLM velocity is assumed a small quantity, i.e., $\overline{w}^L = O(\varepsilon)$. Using assumption A2 the right-hand side of equation (2.58) is simplified as:

$$\frac{1}{2}\left(\frac{\partial^3 \overline{\xi_j \xi_k}}{\partial t \partial x_j \partial x_k}+\overline{u}_l^L \frac{\partial^3 \overline{\xi_j \xi_k}}{\partial x_l \partial x_j \partial x_k}\right)=\frac{\partial}{\partial t}\left(\frac{1}{2}\frac{\partial^2 \overline{\xi_3^2}}{\partial z^2}\right)+O(\varepsilon^3). \tag{2.59}$$

Notice that Quasi-Eulerian mean quantities are averaged over the wave period. Therefore, on the scale of the mean current, the right-hand side of equation (2.59), generally, differs from zero. According to the definition of Stokes correction in AM, the term in brackets on the right-hand side of equation (2.59) is the Stokes correction of the mean position of fluid-particle $\overline{Z}^S$, i.e.:

$$\overline{Z}^S=\frac{1}{2}\frac{\partial^2 \overline{\xi_3^2}}{\partial z^2}+O(\varepsilon^3). \tag{2.60}$$

In stationary waves, the temporal derivative of $\overline{Z}^S$ is zero, so equation (2.58) becomes:

$$\frac{\partial \overline{u}}{\partial x}+\frac{\partial \overline{v}}{\partial y}+\frac{\partial \overline{w}}{\partial z}=-\left(\frac{\partial \overline{u}^S}{\partial x}+\frac{\partial \overline{v}^S}{\partial y}+\frac{\partial \overline{w}^S}{\partial z}\right). \tag{2.61}$$

However, in nonstationary waves, the right-hand side of equation (2.59) differs from zero and is also of second-order in the disturbance amplitude. In general, the continuity equation (2.58) is rewritten as:

$$\frac{\partial \overline{u}}{\partial x}+\frac{\partial \overline{v}}{\partial y}+\frac{\partial \overline{w}}{\partial z}=\frac{\partial \overline{Z}^S}{\partial t}-\left(\frac{\partial \overline{u}^S}{\partial x}+\frac{\partial \overline{v}^S}{\partial y}+\frac{\partial \overline{w}^S}{\partial z}\right). \tag{2.62}$$

Equation (2.62) indicates that the divergence of Quasi-Eulerian mean velocity is compensated by the divergence of Stokes drift and the time variation of Stokes correction of the mean position of the fluid particle. As pointed out by Tamura *et al.* (2012), the divergence of Stokes drift might cause vertical velocity which is comparable to Ekman velocity and has important effects to the upper ocean dynamics. Besides, the divergence of Stokes drift also contributes to the set-down/setup of mean water level.

Combined with the momentum equation (2.57) we had a set of four independent equations in four unknowns as long as the wave and turbulent motions are described by an appropriate wave theory and a relation to the mean flow, respectively. In principle, these equations can be solved numerically.

# 3

# THREE-DIMENSIONAL WAVE RADIATION STRESS AND VORTEX FORCE REPRESENTATIONS[2]

[2] This Chapter is based on the publication: Nguyen, D.T., Reniers, A.J.H.M., Roelvink, D., 2021b. Relationship between Three-Dimensional Radiation Stress and Vortex-Force Representations. Ibid., 791.

## 3.1 INTRODUCTION

There are two representations of wave-averaged effects on the currents called 'radiation stress' and 'vortex force'. Both representations have been applied widely in the ocean and coastal numerical models.

The radiation stress representation was introduced by Longuet-Higgins and Stewart (1960). It was successful in explaining the transfer of momentum flux from the waves to the mean current. However, it is a two-dimensional (2D) tensor, and as such it is only suitable for depth-averaged numerical models. The extension of the 'traditional' radiation stress concept to three-dimensional (3D) space has been the subject of many studies. In Xia *et al.* (2004), the 3D radiation stress was inferred from the classical 2D radiation stress concept of Longuet-Higgins and Stewart (1960). This method was also applied by Mellor (2015). However, as indicated by Ardhuin *et al.* (2017), this method is "incorrect because of a derivation error". Recently, Nguyen *et al.* (2021a) obtained a depth-dependent wave radiation stress tensor in the Generalized Lagrangian Mean (GLM) framework. It was applied in their Quasi-Eulerian mean equations of motion. With the use of the depth-dependent wave radiation stress formulation, their equations were successfully validated with various experimental data in conditions of waves combined with currents.

The vortex force representation is an alternative way to express the mean effect of waves on the current. It was first introduced by Craik and Leibovich (1976) to explain the evolution of Langmuir circulations. The vortex-force representation involves a gradient of the Bernoulli head and a vortex force. This concept has been widely applied by the ocean and coastal communities such as McWilliams *et al.* (2004), Newberger and Allen (2007), Ardhuin *et al.* (2008) Michaud *et al.* (2011); and Bennis *et al.* (2011).

In Lane *et al.* (2007), a comparison of 'radiation stress' and 'vortex force' representations was made. Their study showed that these two representations are equivalent in the condition of conservative waves. However, the relationship between these two representations for non-conservative waves was not addressed in their study.

In this Chapter, the concept of three-dimensional wave radiation stress tensor is introduced. Besides, the relationship between three-dimensional wave radiation stress and vortex-force representations in both conditions of conservative waves and non-conservative waves is presented in detail. In this study, the concept of conservative wave means the wave propagates without wave energy dissipation, and the concept of non-conservative wave means the wave propagates with the presence of wave energy dissipation (due to breaking wave, roller wave, or bottom friction).

## 3.2 THREE-DIMENSIONAL WAVE RADIATION STRESS REPRESENTATION

The components of three-dimensional wave radiation stress $S$ are defined by:

$$S_{11} = \rho\left(\overline{\tilde{u}^2} - \overline{\tilde{w}^2}\right) \qquad S_{12} = \rho\overline{\tilde{u}\tilde{v}} \qquad S_{13} = \rho\overline{\tilde{u}\tilde{w}}, \tag{3.1}$$

$$S_{21} = \rho\overline{\tilde{v}\tilde{u}} \qquad S_{22} = \rho\left(\overline{\tilde{v}^2} - \overline{\tilde{w}^2}\right) \qquad S_{23} = \rho\overline{\tilde{v}\tilde{w}}, \tag{3.2}$$

$$S_{31} = \rho\overline{\tilde{w}\tilde{u}} \qquad S_{32} = \rho\overline{\tilde{w}\tilde{v}} \qquad S_{33} = 0. \tag{3.3}$$

The modulation of wave amplitude is assumed slowly in the horizontal direction. Then, local linear wave theory is applied to calculate the following wave forcing terms: $\partial S_{11}/\partial x$, $\partial S_{12}/\partial y$, $\partial S_{21}/\partial x$, $\partial S_{22}/\partial y$, $\partial S_{31}/\partial x$, $\partial S_{32}/\partial y$.

Using local linear wave theory, components of wave velocity are:

$$\tilde{u} = \frac{k_1\sigma a}{k}\frac{\cosh k(z+h)}{\sinh kh}\cos\left(k_1x + k_2y - \sigma t\right), \tag{3.4}$$

$$\tilde{v} = \frac{k_2\sigma a}{k}\frac{\cosh k(z+h)}{\sinh kh}\cos\left(k_1x + k_2y - \sigma t\right), \tag{3.5}$$

where, $a$ is the wave amplitude, $k$ is the wave number, $k_\alpha$ ($\alpha = 1;2$ represents for horizontal direction) is the component of wave number in the $\alpha$ direction, $h$ is still water depth, and $\sigma = \sqrt{gk\tanh kh}$ is the angular frequency of the wave.

From equations (3.4) and (3.5), the vertical component of wave velocity is calculated from the continuity equation for the wave motion:

$$\begin{aligned}\tilde{w} = {} & \sigma a\frac{\sinh k(z+h)}{\sinh kh}\sin\left(k_1x + k_2y - \sigma t\right) \\ & -\frac{\sigma}{k^2}\frac{\sinh k(z+h)}{\sinh kh}\left(k_1\frac{\partial a}{\partial x} + k_2\frac{\partial a}{\partial y}\right)\cos\left(k_1x + k_2y - \sigma t\right).\end{aligned} \tag{3.6}$$

From equations (3.4), 3.5), and (3.6) we obtain:

$$S_{11} = \rho g k a^2\left(\frac{k_1^2}{k^2}\frac{\cosh^2 k(z+h)}{\sinh 2kh} - \frac{\sinh^2 k(z+h)}{\sinh 2kh}\right), \tag{3.7}$$

$$S_{12} = S_{21} = \rho g a^2\frac{k_1k_2}{k}\frac{\cosh^2 k(z+h)}{\sinh 2kh}, \tag{3.8}$$

$$S_{22} = \rho g k a^2\left(\frac{k_2^2}{k^2}\frac{\cosh^2 k(z+h)}{\sinh 2kh} - \frac{\sinh^2 k(z+h)}{\sinh 2kh}\right), \tag{3.9}$$

$$S_{31} = -\frac{\rho g k_1 a}{2k^2}\frac{\sinh 2k(z+h)}{\sinh 2kh}\left(k_1\frac{\partial a}{\partial x}+k_2\frac{\partial a}{\partial y}\right), \tag{3.10}$$

$$S_{32} = -\frac{\rho g k_2 a}{2k^2}\frac{\sinh 2k(z+h)}{\sinh 2kh}\left(k_1\frac{\partial a}{\partial x}+k_2\frac{\partial a}{\partial y}\right). \tag{3.11}$$

In the condition of conservative waves propagating in deep water, the wave forcing which is caused by normal components of wave radiation stress, $\partial S_{13}/\partial z$ and $\partial S_{23}/\partial z$, can be calculated by the local linear wave theory. We have:

$$S_{13} = -\frac{\rho g k_1 a}{2k^2}\frac{\sinh 2k(z+h)}{\sinh 2kh}\left(k_1\frac{\partial a}{\partial x}+k_2\frac{\partial a}{\partial y}\right), \tag{3.12}$$

$$S_{23} = -\frac{\rho g k_2 a}{2k^2}\frac{\sinh 2k(z+h)}{\sinh 2kh}\left(k_1\frac{\partial a}{\partial x}+k_2\frac{\partial a}{\partial y}\right). \tag{3.13}$$

However, in the presence of dissipative forcing, the local linear wave theory is no longer suitable to calculate $S_{13}$ and $S_{23}$. The vertical distribution of the normal components of wave radiation stress in dissipative waves was analyzed by Deigaard and Fredsøe (1989). Their study is restricted to the shallow water waves, where the horizontal wave velocity is assumed to be depth independent. This results in the linear variation of $S_{13}$ and $S_{23}$ with depth. Usually, the horizontal wave velocity is a depth-dependent quantity (e.g., wind waves in deep water) in which case more general formulas for $S_{13}$ and $S_{23}$ are required. In general, the normal components of wave radiation stress can be decomposed into conservative and decay parts, such as:

$$S_{13} = \rho\left(\overline{\tilde{u}\tilde{w}}_{CS} + \overline{\tilde{u}\tilde{w}}_{DC}\right), \tag{3.14}$$

$$S_{23} = \rho\left(\overline{\tilde{v}\tilde{w}}_{CS} + \overline{\tilde{v}\tilde{w}}_{DC}\right), \tag{3.15}$$

where, the subscripts *CS* and *DC* represent the conservative and decay parts of normal components of wave radiation stress, respectively.

### 3.2.1 Conservative part of the normal component of the wave radiation stress in weak ambient current

In this part, the ambient current is assumed small in comparison with the near-bed orbital velocity, i.e. $|\bar{\mathbf{u}}| \ll \mathbf{u}_{orb}$, and the surface waves are approximated irrotational. Then, the effect of mean currents on the wave radiation stress is neglected. The local linear wave theory can be used to calculate conservative parts of normal components of wave radiation stress. The above assumptions were also employed by McWilliams *et al.* (2004) to obtain an asymptotic theory for the interaction of waves and currents in coastal water.

Then, conservative parts of normal components of wave radiation stress are given by:

$$\overline{\tilde{u}\tilde{w}}_{CS} = -\frac{k_1 ga}{2k^2}\frac{\sinh 2k(z+h)}{\sinh 2kh}\left(k_1\frac{\partial a}{\partial x}+k_2\frac{\partial a}{\partial y}\right), \tag{3.16}$$

$$\overline{\tilde{v}\tilde{w}}_{CS} = -\frac{k_2 ga}{2k^2}\frac{\sinh 2k(z+h)}{\sinh 2kh}\left(k_1\frac{\partial a}{\partial x}+k_2\frac{\partial a}{\partial y}\right). \tag{3.17}$$

The above formulas agree with the results obtained by You (1997) and Groeneweg (1999) when the incident angle of the wave is zero ( $\theta = 0^0$ ).

### 3.2.2 Conservative part of the normal component of the wave radiation stress in a strong ambient current

As pointed out by Supharatid *et al.* (1992) and Nielsen and You (1997), the ambient current has a significant impact on the vertical distribution of wave radiation stress. Therefore, in the presence of a strong ambient current, equations (3.16) and (3.17) are no longer suitable. The normal component of the wave radiation stress is enhanced by a factor $C_{WR} = \left(C_{WR,1}, C_{WR,2}\right)$ representing the effect of the ambient current. Equations (3.16) and (3.17) become:

$$\overline{\tilde{u}\tilde{w}}_{CS} = -\frac{C_{WR,1}k_1 ga}{2k^2}\frac{\sinh 2k(z+h)}{\sinh 2kh}\left(k_1\frac{\partial a}{\partial x}+k_2\frac{\partial a}{\partial y}\right), \tag{3.18}$$

$$\overline{\tilde{v}\tilde{w}}_{CS} = -\frac{C_{WR,2}k_2 ga}{2k^2}\frac{\sinh 2k(z+h)}{\sinh 2kh}\left(k_1\frac{\partial a}{\partial x}+k_2\frac{\partial a}{\partial y}\right). \tag{3.19}$$

For regular wave, the empirical factors $C_{WR,1}$ and $C_{WR,2}$ are calculated by (Nielsen and You, 1997):

$$C_{WR,1} = 1+100\frac{\overline{u_*}}{\sigma a}\frac{(z+h)}{D}, \tag{3.20}$$

$$C_{WR,2} = 1+100\frac{\overline{v_*}}{\sigma a}\frac{(z+h)}{D}, \tag{3.21}$$

where, $\left(\overline{u_*}, \overline{v_*}\right)$ is the friction velocity, and $D = h+\overline{\zeta}$ with $\overline{\zeta}$ is the Quasi-Eulerian mean water level.

As indicated by Ockenden and Soulsby (1994), for a substantial part of the time, the bottom shear stresses caused by random waves exceed those caused by the corresponding regular waves. In this study, formulas (3.18) and (3.19) are modified to apply to random waves as follows:

$$C_{WR,1} = 1 + 100\sqrt{2}\,\frac{\overline{u_*}}{\sigma a}\,\frac{(z+h)}{D}, \tag{3.22}$$

$$C_{WR,2} = 1 + 100\sqrt{2}\,\frac{\overline{v_*}}{\sigma a}\,\frac{(z+h)}{D}, \tag{3.23}$$

where, $a = 0.5H_{rms}$ with $H_{rms}$ is the root mean square wave height. The empirical coefficient is approximated to unity when the ambient current is small in comparison with the near-bed orbital velocity. The friction velocity components caused by waves and currents are calculated by:

$$\overline{u_*} = \sqrt{\overline{\tau}_{b,1}/\rho} \qquad \overline{v_*} = \sqrt{\overline{\tau}_{b,2}/\rho}, \tag{3.24}$$

where, $\overline{\tau}_b = \left(\overline{\tau}_{b,1}, \overline{\tau}_{b,2}\right)$ is the mean of total bed-shear stress caused by waves and currents.

### 3.2.3 Decay-related part of normal components of the wave radiation stress

Outside the bottom boundary layer, the decayed-related part of wave radiation stress gradient is caused by the dissipative forcing, i.e.:

$$\frac{\partial \overline{\tilde{u}\tilde{w}}_{DC}}{\partial z} = -\frac{F_{br,1}(z)}{\rho} - \frac{F_{mx,1}(z)}{\rho}, \tag{3.25}$$

$$\frac{\partial \overline{\tilde{v}\tilde{w}}_{DC}}{\partial z} = -\frac{F_{br,2}(z)}{\rho} - \frac{F_{mx,2}(z)}{\rho}, \tag{3.26}$$

where, $F_{br} = \left(F_{br,1}, F_{br,2}\right)$ represents the effect of breaking waves and rollers, and $F_{mx} = \left(F_{mx,1}, F_{mx,2}\right)$ represents the wave-induced mixing. The vertical distribution of the wave-induced forcing terms $F_{br}$ and $F_{mx}$ can be estimated by empirical formulas proposed by Uchiyama *et al.* (2010).

Therefore, with a correction for the effect of Coriolis forcing on Stokes drift, the wave radiation stress can be expressed by:

$$\frac{1}{\rho}\left(\frac{\partial S_{11}}{\partial x} + \frac{\partial S_{12}}{\partial y} + \frac{\partial S_{13}}{\partial z}\right) = \frac{\partial\left(\overline{\tilde{u}^2} - \overline{\tilde{w}^2}\right)}{\partial x} + \frac{\partial \overline{\tilde{u}\tilde{v}}}{\partial y} + \frac{\partial \overline{\tilde{u}\tilde{w}}_{CS}}{\partial z} - f\overline{v}^S - \frac{F_{br,1}}{\rho} - \frac{F_{mx,1}}{\rho}, \tag{3.27}$$

$$\frac{1}{\rho}\left(\frac{\partial S_{21}}{\partial x} + \frac{\partial S_{22}}{\partial y} + \frac{\partial S_{23}}{\partial z}\right) = \frac{\partial \overline{\tilde{v}\tilde{u}}}{\partial x} + \frac{\partial\left(\overline{\tilde{v}^2} - \overline{\tilde{w}^2}\right)}{\partial y} + \frac{\partial \overline{\tilde{v}\tilde{w}}_{CS}}{\partial z} + f\overline{u}^S - \frac{F_{br,2}}{\rho} - \frac{F_{mx,2}}{\rho}, \tag{3.28}$$

$$\frac{1}{\rho}\left(\frac{\partial S_{31}}{\partial x}+\frac{\partial S_{32}}{\partial y}+\frac{\partial S_{33}}{\partial z}\right)=\frac{\partial \overline{\tilde{w}\tilde{u}}}{\partial x}+\frac{\partial \overline{\tilde{w}\tilde{v}}}{\partial y}, \tag{3.29}$$

where, $f=2\Omega\sin\phi$ as Coriolis frequency, and $\phi$ the latitude at the given position.

## 3.3 VORTEX FORCE REPRESENTATION

Another way to express the effect of waves on currents is using vortex-force representation. This method was proposed by McWilliams *et al.* (2004). In their work, the surface waves are assumed slow varying, weakly nonlinear, and irrotational up to second-order of the wave amplitude. Further, the mean currents are assumed to vary slowly and are small in comparison with the near-bed orbital velocity, i.e., $|\bar{\mathbf{u}}| \ll \mathbf{u}_{orb}$.

In vortex force representation, the wave-induced forcing is given by:

$$VF_1=\frac{\partial J}{\partial x}-\bar{v}^S\left[f+\left(\frac{\partial \bar{v}}{\partial x}-\frac{\partial \bar{u}}{\partial y}\right)\right]+\bar{w}^S\frac{\partial \bar{u}}{\partial z}, \tag{3.30}$$

$$VF_2=\frac{\partial J}{\partial y}+\bar{u}^S\left[f+\left(\frac{\partial \bar{v}}{\partial x}-\frac{\partial \bar{u}}{\partial y}\right)\right]+\bar{w}^S\frac{\partial \bar{v}}{\partial z}, \tag{3.31}$$

$$VF_3=-\left(\bar{u}^S\frac{\partial \bar{u}}{\partial z}+\bar{v}^S\frac{\partial \bar{v}}{\partial z}\right), \tag{3.32}$$

where, $VF_i$ is wave-induced forcing in terms of vortex force representation, and $J$ is wave-induced kinematic pressure defined by:

$$J=\frac{gka^2}{2\sinh 2kh}. \tag{3.33}$$

## 3.4 RELATIONSHIP BETWEEN WAVE RADIATION STRESS AND VORTEX FORCE REPRESENTATIONS

In this section, the effects of turbulence and non-wave dissipative forcing $X$ are neglected. Multiplying equation (2.17) with $\partial\xi_j/\partial x_i$ and averaging over wave period to obtain the following equation for the evolution of Lagrangian disturbance velocity $u^l$:

$$\overline{\frac{\partial \xi_j}{\partial x_i}\bar{D}^L u_j^l}+\overline{\frac{\partial \xi_j}{\partial x_i}\left(2(\Omega\times\mathbf{u})_j\right)^l}+\overline{\frac{\partial \xi_j}{\partial x_i}\left(\frac{\partial \Phi}{\partial x_j}\right)^l}+\overline{\frac{\partial \xi_j}{\partial x_i}\left(\frac{1}{\rho}\frac{\partial p}{\partial x_j}\right)^l}=0. \tag{3.34}$$

The pseudo-momentum $\mathbf{p}_i^0$ defined by (Andrews and McIntyre, 1978):

$$\mathbf{p}_i^0 = -\overline{\frac{\partial \xi_j}{\partial x_i} u_j^l}. \tag{3.35}$$

Using the relation (2.8) and definition (3.35), the first term on the left-hand side of equation (3.34) can be expressed as:

$$\begin{aligned}
&\overline{\frac{\partial \xi_j}{\partial x_i} \bar{D}^L u_j^l} = \bar{D}^L \left( \overline{\frac{\partial \xi_j}{\partial x_i} u_j^l} \right) - \overline{u_j^l \bar{D}^L \left( \frac{\partial \xi_j}{\partial x_i} \right)} = \bar{D}^L \left( \overline{\frac{\partial \xi_j}{\partial x_i} u_j^l} \right) \\
&- \left[ \overline{u_j^l \frac{\partial}{\partial x_i} \left( \bar{D}^L \xi_j \right)} - \overline{\frac{\partial \xi_j}{\partial x_k} u_j^l} \frac{\partial \bar{u}_k^L}{\partial x_i} \right] = - \left[ \bar{D}^L \mathbf{p}_i^0 + \frac{1}{2} \frac{\partial \overline{\left( u_j^l u_j^l \right)}}{\partial x_i} + \mathbf{p}_k^0 \frac{\partial \bar{u}_k^L}{\partial x_i} \right].
\end{aligned} \tag{3.36}$$

The second term on the left-hand side of equation (3.34) is approximated by:

$$\overline{\frac{\partial \xi_j}{\partial x_i} \left( 2(\Omega \times \mathbf{u})_j \right)^l} \approx \overline{\frac{\partial \xi_j}{\partial x_i} \left( 2(\Omega \times \mathbf{u}')_j \right)} \approx -2(\Omega \times \bar{\mathbf{u}}^S)_i. \tag{3.37}$$

From equation (2.18) the third term on the left-hand side of equation (3.34) can be neglected, i.e.:

$$\overline{\frac{\partial \xi_j}{\partial x_i} \left( \frac{\partial \Phi}{\partial x_j} \right)^l} = \overline{\frac{\partial \xi_j}{\partial x_i} \left( \delta_{j3} g \right)^l} = 0. \tag{3.38}$$

The relationship between Lagrangian disturbance and Quasi-Eulerian disturbance is given by relationship (2.27). Then, the fourth term on the left-hand side of equation (3.34) can be expressed as:

$$\overline{\frac{\partial \xi_j}{\partial x_i} \left( \frac{\partial p}{\partial x_j} \right)^l} = \frac{\partial \bar{p}^S}{\partial x_i} - \overline{\xi_j \frac{\partial^2 p'}{\partial x_i \partial x_j}} - \frac{1}{2} \overline{\xi_j \xi_k} \frac{\partial^3 \bar{p}}{\partial \xi_i \partial x_k \partial x_j} + O(\varepsilon^3), \tag{3.39}$$

where, $\bar{p}^S$ is Stokes correction of mean pressure.

Then, equation (3.34) becomes:

$$\begin{aligned}
&-\bar{D}^L \mathbf{p}_i^0 - \frac{1}{2} \frac{\partial \overline{\left( u_j^l u_j^l \right)}}{\partial x_i} - \mathbf{p}_k^0 \frac{\partial \bar{u}_k^L}{\partial x_i} - 2(\Omega \times \bar{\mathbf{u}}^S)_i + \frac{1}{\rho} \frac{\partial \bar{p}^S}{\partial x_i} \\
&= \frac{1}{\rho} \overline{\xi_j \frac{\partial^2 p'}{\partial x_i \partial x_j}} + \frac{1}{2\rho} \overline{\xi_j \xi_k} \frac{\partial^3 \bar{p}}{\partial \xi_i \partial x_k \partial x_j}.
\end{aligned} \tag{3.40}$$

From equation (2.54) we have:

$$\frac{\partial\left(\overline{u_i' u_j'}\right)}{\partial x_j}-\frac{\partial\overline{\tilde{w}'^2}}{\partial x_i}=\bar{D}^L\bar{u}_i^S+2\left(\Omega\times\bar{\mathbf{u}}^S\right)_i+\bar{u}_k^S\frac{\partial\bar{u}_i}{\partial x_k}-\frac{\partial\overline{\tilde{w}'^2}}{\partial x_i}$$
$$+\frac{1}{\rho}\frac{\partial}{\partial x_j}\left(\overline{\xi_j\frac{\partial p'}{\partial x_i}}\right)+\frac{1}{2\rho}\overline{\xi_j\xi_k}\frac{\partial^3\bar{p}}{\partial x_i\partial x_j\partial x_k}+O(\varepsilon^3). \tag{3.41}$$

If the effect of turbulence is neglected then the Quasi-Eulerian disturbance $\varphi'$ is replaced by wave quantity $\tilde{\varphi}$. From equations (3.40) and (3.41) we obtain:

$$\frac{\partial\left(\overline{\tilde{u}_i\tilde{u}_j}\right)}{\partial x_j}-\frac{\partial\overline{\tilde{w}^2}}{\partial x_i}=\frac{\partial}{\partial x_i}\left[\frac{\bar{p}^S}{\rho}-\frac{1}{2}\overline{\left(u_j^l u_j^l\right)}-\overline{\tilde{w}^2}\right]-\bar{u}_j^S\left(\frac{\partial\bar{u}_j}{\partial x_i}-\frac{\partial\bar{u}_i}{\partial x_j}\right)$$
$$-\bar{D}^L\left(\mathbf{p}_i^0-\bar{u}_i^S\right)-\left(\mathbf{p}_j^0-\bar{u}_j^S\right)\frac{\partial\bar{u}_j^L}{\partial x_i}+O(\varepsilon^3). \tag{3.42}$$

Equation (3.42) expresses the general relationship between wave radiation stress and the vortex-force representations. In this, the first term on the right-hand side represents the changes in the wave-related Bernouilli head, and the second term on the right-hand side of equation (3.42) expresses the vortex force of the mean current. The remaining terms on the right-hand side are a function of the mismatch between the pseudo momentum and the Stokes drift. According to Andrews and McIntyre (1978), the Stokes drift is defined by:

$$\bar{u}_i^S=\overline{\xi_j\frac{\partial\tilde{u}_i}{\partial x_j}}+\frac{1}{2}\overline{\xi_j\xi_k}\frac{\partial^2\bar{u}_i}{\partial x_j\partial x_k}+O\left(\varepsilon^3\right). \tag{3.43}$$

From definitions (3.35) and (3.43) we obtain:

$$\mathbf{p}_i^0-\bar{u}_i^S\approx\overline{\xi_j\left(\frac{\partial\tilde{u}_j}{\partial x_i}-\frac{\partial\tilde{u}_i}{\partial x_j}\right)}-\frac{1}{2}\overline{\xi_3^2}\frac{\partial^2\bar{u}_i}{\partial z^2}+O(\varepsilon^3). \tag{3.44}$$

The first term on the right-hand side of equation (3.44) expresses the effect of rotation of the wave, and the second term relates to the shear effect of the mean current. The calculation of the first term on the right-hand side of equation (3.44) requires a rotational wave theory. However, the use of rotational wave theory is still a challenge for coastal and ocean applications. In the next sections, the right-hand side of equation (3.42) will be expressed explicitly under specific conditions of the waves combined with the mean currents.

### 3.4.1 Conservative waves

In this part, the following conditions are applied:

i) The waves are conservative and irrotational up to the second-order of wave amplitude.

ii) The mean currents are slow variation and small in comparison with near-bed orbital velocity, i.e. $\left|\overline{\mathbf{u}}\right| \ll \mathbf{u}_{orb}$.

The above conditions were also used by McWilliams *et al.* (2004) to obtain the vortex force representation. With conditions (i) and (ii), the formula (3.44) becomes:

$$\mathbf{p}_i^0 - \overline{u}_i^S = O(\varepsilon^3). \tag{3.45}$$

Thus, the pseudo-momentum $\mathbf{p}_i^0$ can be approximated by the Stokes drift $\overline{u}_i^S$. Therefore, the last two terms on the right-hand side of equation (3.42) can be neglected giving:

$$\frac{\partial\left(\overline{\tilde{u}_i\tilde{u}_j}\right)}{\partial x_j} - \frac{\partial\overline{\tilde{w}^2}}{\partial x_i} = \frac{\partial}{\partial x_i}\left[\frac{\overline{p}^S}{\rho} - \frac{1}{2}\overline{\left(u_j^l u_j^l\right)} - \overline{\tilde{w}^2}\right] - \overline{u}_j^S\left(\frac{\partial\overline{u}_j}{\partial x_i} - \frac{\partial\overline{u}_i}{\partial x_j}\right) + O(\varepsilon^3). \tag{3.46}$$

The term $u_j^l u_j^l / 2$ is the Bernoulli head defined in the GLM framework. From the relationship (2.27) we obtain:

$$\frac{1}{2}\overline{\left(u_j^l u_j^l\right)} = \frac{1}{2}\overline{\left(\tilde{u}_j\tilde{u}_j\right)} + K, \tag{3.47}$$

where, the term $K$ is a correction to the Bernoulli head defined by:

$$K = \overline{\tilde{u}_j\xi_k}\frac{\partial\overline{u}_j}{\partial x_k} + \frac{\overline{\xi_k^2}}{2}\left(\frac{\partial\overline{u}_j}{\partial x_k}\right)^2. \tag{3.48}$$

Using linear wave theory we obtain:

$$\frac{\overline{p}^S}{\rho} - \frac{1}{2}\overline{\left(\tilde{u}_j\tilde{u}_j\right)} - \overline{\tilde{w}^2} = \frac{gka^2}{2\sinh 2kh}. \tag{3.49}$$

Combining (3.47) and (3.49) gives:

$$\frac{\partial}{\partial x_i}\left[\frac{\overline{p}^S}{\rho} - \frac{1}{2}\overline{\left(u_j^l u_j^l\right)} - \overline{\tilde{w}^2}\right] = \frac{\partial\left(J+K\right)}{\partial x_i}, \tag{3.50}$$

where, the term $J$ is defined by (3.33).

In the ocean and coastal environment, it is usually that $\partial\overline{w}/\partial x_\alpha \ll \overline{u}_\alpha/\partial z$. Therefore, the term $\overline{u}_i^S\partial\overline{w}/\partial x_\alpha$ can be neglected in the vortex force representation. From equation (3.50) and including the Coriolis effect in the radiation stress forcing equation (3.46) can be expressed explicitly as:

$$\frac{1}{\rho}\left(\frac{\partial S_{11}}{\partial x} + \frac{\partial S_{12}}{\partial y} + \frac{\partial S_{13}}{\partial z}\right) = \frac{\partial\left(J+K\right)}{\partial x} - \overline{v}^S\left[f + \left(\frac{\partial\overline{v}}{\partial x} - \frac{\partial\overline{u}}{\partial y}\right)\right] + \overline{w}^S\frac{\partial\overline{u}}{\partial z} + O(\varepsilon^3), \tag{3.51}$$

$$\frac{1}{\rho}\left(\frac{\partial S_{21}}{\partial x}+\frac{\partial S_{22}}{\partial y}+\frac{\partial S_{23}}{\partial z}\right)=\frac{\partial\left(J+K\right)}{\partial y}+\overline{u}^{S}\left[f+\left(\frac{\partial \overline{v}}{\partial x}-\frac{\partial \overline{u}}{\partial y}\right)\right]+\overline{w}^{S}\frac{\partial \overline{v}}{\partial z}+O(\varepsilon^{3}), \quad (3.52)$$

$$\frac{1}{\rho}\left(\frac{\partial S_{31}}{\partial x}+\frac{\partial S_{32}}{\partial y}+\frac{\partial S_{33}}{\partial z}\right)=\frac{\partial K}{\partial z}-\left(\overline{u}^{S}\frac{\partial \overline{u}}{\partial z}+\overline{v}^{S}\frac{\partial \overline{v}}{\partial z}\right)+O(\varepsilon^{3}). \quad (3.53)$$

Equations (3.51)-(3.53) show the relationship between radiation stress and vortex force representations in conservative waves. The right-hand side of these equations is vortex force representation obtained by McWilliams *et al.* (2004) with a correction of the Bernoulli head $K$. Therefore, in conditions of weakly nonlinear waves and weak ambient current, the radiation stress and vortex force representations are equivalent.

## 3.4.2 Non-conservative waves

In this section, the relationship between radiation stress and vortex force representations will be studied in the following conditions:

i) The evolution of the waves is dominated by dissipative processes, such as breaking waves, rollers, white-capping, and bottom friction.

ii) The mean currents are slowly varying and small in comparison with near-bed orbital velocity, i.e. $\left|\overline{\mathbf{u}}\right| \ll \mathbf{u}_{\mathrm{orb}}$.

In the presence of non-conservative processes, the last two terms on the right-hand side of equation (3.42) express the evolution of the rotation of the waves. In the presence of wave dissipation, we do not have any relationship between $\overline{u}_i^S$ and $\mathbf{p}_i^0$. If the current is small in comparison with the wave velocity then its effect on the wave-induced forcing can be neglected. The evolution of the rotation of the waves is approximated by dissipative wave forcing, i.e.:

$$\overline{D}^{L}\left(\mathbf{p}_i^0-\overline{u}_i^S\right)+\left(\mathbf{p}_j^0-\overline{u}_j^S\right)\frac{\partial \overline{u}_j^L}{\partial x_i}=\frac{F_{br,i}}{\rho}+\frac{F_{mx,i}}{\rho}. \quad (3.54)$$

From equations (3.50) and (3.54) equation (3.42) is now expressed as:

$$\begin{aligned}\frac{1}{\rho}\left(\frac{\partial S_{11}}{\partial x}+\frac{\partial S_{12}}{\partial y}+\frac{\partial S_{13}}{\partial z}\right)&=\frac{\partial\left(J+K\right)}{\partial x}-\overline{v}^{S}\left[f+\left(\frac{\partial \overline{v}}{\partial x}-\frac{\partial \overline{u}}{\partial y}\right)\right]\\&+\overline{w}^{S}\frac{\partial \overline{u}}{\partial z}-\frac{F_{br,1}}{\rho}-\frac{F_{mx,1}}{\rho}+O(\varepsilon^{3}),\end{aligned} \quad (3.55)$$

$$\frac{1}{\rho}\left(\frac{\partial S_{21}}{\partial x}+\frac{\partial S_{22}}{\partial y}+\frac{\partial S_{23}}{\partial z}\right)=\frac{\partial\left(J+K\right)}{\partial y}+\overline{u}^{S}\left[f+\left(\frac{\partial \overline{v}}{\partial x}-\frac{\partial \overline{u}}{\partial y}\right)\right]$$
$$+\overline{w}^{S}\frac{\partial \overline{v}}{\partial z}-\frac{F_{br,2}}{\rho}-\frac{F_{mx,2}}{\rho}+O(\varepsilon^{3}), \tag{3.56}$$

$$\frac{1}{\rho}\left(\frac{\partial S_{31}}{\partial x}+\frac{\partial S_{32}}{\partial y}+\frac{\partial S_{33}}{\partial z}\right)=\frac{\partial K}{\partial z}-\left(\overline{u}^{S}\frac{\partial \overline{u}}{\partial z}+\overline{v}^{S}\frac{\partial \overline{v}}{\partial z}\right)+O(\varepsilon^{3}). \tag{3.57}$$

Equations (3.55)-(3.57) expresses the relationship between radiation stress and vortex force representations in the condition of non-conservative waves propagating on a weak current. It shows that the wave radiation stress gradient is the total of vortex-force and nonconservative wave forcing.

## 3.5 CONCLUSIONS

In this Chapter, a three-dimensional wave radiation stress formalism was introduced. In this formalism, the effects of non-conservative waves and ambient current on three-dimensional wave radiation stress are taken into account. An empirical coefficient $C_{WR}$ was proposed to account for the effect of strong ambient current on the vertical distribution of wave radiation stress components.

Besides, the relationship between 3D wave radiation stress and vortex force representations was proven mathematically. It showed that:

i) In conservative waves and weak ambient current, the wave radiation stress and vortex force representations are equivalent.

ii) In non-conservative waves and weak ambient current, the wave radiation stress representation is equivalent to the total of vortex force and wave-induced dissipative forcing terms.

# 4

# EQUATIONS OF MOTION IN THE HYDROSTATIC ASSUMPTION

## 4.1 QUASI-EULERIAN MEAN EQUATIONS OF MOTION

### 4.1.1 Momentum equation of motion

In this Chapter, equations of mean motion are obtained in the hydrostatic assumption for the mean flow. This means that acceleration of mean velocity and dissipative forcing are neglected in the vertical momentum equation. This assumption is suitable for most hydrodynamic problems in the deep ocean and coastal zones.

From equation (2.57) the Quasi-Eulerian mean vertical momentum equation is expressed explicitly as:

$$\frac{D\overline{w}}{Dt}+g+X_3=-\frac{1}{\rho}\frac{\partial\overline{p}}{\partial z}-\frac{\partial\overline{\tilde{u}\tilde{w}}}{\partial x}-\frac{\partial\overline{\tilde{v}\tilde{w}}}{\partial y}-\frac{\partial\overline{\tilde{w}^2}}{\partial z}+\frac{1}{\rho}\frac{\partial\overline{\tau}_{31}}{\partial x}+\frac{1}{\rho}\frac{\partial\overline{\tau}_{32}}{\partial y}+\frac{1}{\rho}\frac{\partial\overline{\tau}_{33}}{\partial z}+O(\varepsilon^3). \quad (4.1)$$

With the use of hydrostatic assumption for the mean flow equation (4.1) becomes:

$$\frac{1}{\rho}\frac{\partial\overline{p}}{\partial z}+g+\frac{\partial\overline{\tilde{u}\tilde{w}}}{\partial x}+\frac{\partial\overline{\tilde{v}\tilde{w}}}{\partial y}+\frac{\partial\overline{\tilde{w}^2}}{\partial z}=O(\varepsilon^3). \quad (4.2)$$

According to Longuet-Higgins and Stewart (1964), hydrostatic pressure $\overline{p}^H$ is defined by:

$$\overline{p}^H=\overline{p}+\rho\overline{\tilde{w}^2}. \quad (4.3)$$

The vertical momentum equation (4.2) becomes:

$$\frac{1}{\rho}\frac{\partial\overline{p}^H}{\partial z}+g+\frac{\partial\overline{\tilde{u}\tilde{w}}}{\partial x}+\frac{\partial\overline{\tilde{v}\tilde{w}}}{\partial y}=O(\varepsilon^3). \quad (4.4)$$

Substituting equation (4.3) into the momentum equation (2.57) and using the formulations (3.27) and (3.28) to obtain the following Quasi-Eulerian mean horizontal momentum equations:

$$\frac{\partial\overline{u}}{\partial t}+\overline{u}\frac{\partial\overline{u}}{\partial x}+\overline{v}\frac{\partial\overline{u}}{\partial y}+\overline{w}\frac{\partial\overline{u}}{\partial z}-f\overline{v}=-\frac{1}{\rho}\frac{\partial\overline{p}^H}{\partial x}-\left[\frac{\partial\left(\overline{\tilde{u}^2}-\overline{\tilde{w}^2}\right)}{\partial x}+\frac{\partial\overline{\tilde{u}\tilde{v}}}{\partial y}+\frac{\partial\overline{\tilde{u}\tilde{w}}_{CS}}{\partial z}\right]-f\overline{v}^S \quad (4.5)$$
$$+\frac{F_{br,1}}{\rho}+\frac{F_{mx,1}}{\rho}+\frac{1}{\rho}\left(\frac{\partial\overline{\tau}_{11}}{\partial x}+\frac{\partial\overline{\tau}_{12}}{\partial y}+\frac{\partial\overline{\tau}_{13}}{\partial z}\right)+\upsilon\Delta\overline{u}+O(\varepsilon^3),$$

$$\frac{\partial\overline{v}}{\partial t}+\overline{u}\frac{\partial\overline{v}}{\partial x}+\overline{v}\frac{\partial\overline{v}}{\partial y}+\overline{w}\frac{\partial\overline{v}}{\partial z}+f\overline{u}=-\frac{1}{\rho}\frac{\partial\overline{p}^H}{\partial y}-\left[\frac{\partial\overline{\tilde{u}\tilde{v}}}{\partial x}+\frac{\partial\left(\overline{\tilde{v}^2}-\overline{\tilde{w}^2}\right)}{\partial y}+\frac{\partial\overline{\tilde{v}\tilde{w}}_{CS}}{\partial z}\right]+f\overline{u}^S \quad (4.6)$$
$$+\frac{F_{br,2}}{\rho}+\frac{F_{mx,2}}{\rho}+\frac{1}{\rho}\left(\frac{\partial\overline{\tau}_{21}}{\partial x}+\frac{\partial\overline{\tau}_{22}}{\partial y}+\frac{\partial\overline{\tau}_{23}}{\partial z}\right)+\upsilon\Delta\overline{v}+O(\varepsilon^3).$$

Equations (4.5) and (4.6) are Quasi-Eulerian mean horizontal momentum equations in hydrostatic assumption. The mean velocity will be solved when coupling these equations with the mass conservation equation presented below.

### 4.1.2 Depth-integrated continuity equation

The mass conservation equation is given by (2.62). At the second-order of the wave amplitude, the Stokes correction of the mean position of a fluid particle $\overline{Z}^S$ can be estimated by:

$$\overline{Z}^S = k^2 a^2 \frac{\cosh 2k(z+h)}{\sinh^2 kh} + O(\varepsilon^3). \tag{4.7}$$

The Quasi-Eulerian mean water level is calculated by solving the depth-integrated mass conservation equation. Vertical integration of the continuity equation (2.62) to obtain:

$$\int_{-h}^{\overline{\zeta}^L} \frac{\partial \overline{u}^L}{\partial x} dz + \int_{-h}^{\overline{\zeta}^L} \frac{\partial \overline{v}^L}{\partial y} dz + \overline{w}^L(\overline{\zeta}^L) - \overline{w}^L(-h) = \int_{-h}^{\overline{\zeta}^L} \frac{\partial \overline{Z}^S}{\partial t} dz, \tag{4.8}$$

where, $\overline{\zeta}^L = \overline{\zeta} + \overline{\zeta}^S$ is the GLM water surface, and $\overline{\zeta}^S$ is Stokes correction of mean water level and approximated by:

$$\overline{\zeta}^S = \frac{ka^2}{2\tanh kh} + O(\varepsilon^3). \tag{4.9}$$

From equations (4.7) and (4.9) we have:

$$\overline{\zeta}^S = \int_{-h}^{\overline{\zeta}^L} \overline{Z}^S dz + O(\varepsilon^3). \tag{4.10}$$

Equation (4.10) suggests that the Stokes correction of the mean water level is the cumulative effect of the Stokes correction of the mean position of the fluid particles.

Applying Leibniz integral rule for the first and the second terms on the left-hand side of equation (4.8) we obtain:

$$\int_{-h}^{\overline{\zeta}^L} \frac{\partial \overline{u}^L}{\partial x} dz = \frac{\partial}{\partial x} \int_{-h}^{\overline{\zeta}^L} \overline{u}^L dz - \overline{u}^L(\overline{\zeta}^L) \frac{\partial \overline{\zeta}^L}{\partial x} - \overline{u}^L(-h) \frac{\partial h}{\partial x}, \tag{4.11}$$

$$\int_{-h}^{\overline{\zeta}^L} \frac{\partial \overline{v}^L}{\partial y} dz = \frac{\partial}{\partial y} \int_{-h}^{\overline{\zeta}^L} \overline{v}^L dz - \overline{v}^L(\overline{\zeta}^L) \frac{\partial \overline{\zeta}^L}{\partial y} - \overline{v}^L(-h) \frac{\partial h}{\partial y}. \tag{4.12}$$

The boundary conditions at the water surface and water bottom are given by:

$$\overline{w}^L(\overline{\zeta}^L) = \frac{\partial \overline{\zeta}^L}{\partial t} + \overline{u}^L(\overline{\zeta}^L) \frac{\partial \overline{\zeta}^L}{\partial x} + \overline{v}^L(\overline{\zeta}^L) \frac{\partial \overline{\zeta}^L}{\partial y}, \tag{4.13}$$

$$\overline{w}^L(-h) = -\left[\frac{\partial h}{\partial t} + \overline{u}^L(-h)\frac{\partial h}{\partial x} + \overline{v}^L(-h)\frac{\partial h}{\partial y}\right]. \tag{4.14}$$

Replacing of (4.11)-(4.14) into equation (4.8) we obtain:

$$\frac{\partial\left(\overline{\zeta}+h\right)}{\partial t} + \frac{\partial}{\partial x}\int_{-h}^{\overline{\zeta}^L}\overline{u}dz + \frac{\partial}{\partial y}\int_{-h}^{\overline{\zeta}^L}\overline{v}dz = -\frac{\partial}{\partial x}\left(\int_{-h}^{\overline{\zeta}^L}\overline{u}^S dx\right) - \frac{\partial}{\partial y}\left(\int_{-h}^{\overline{\zeta}^L}\overline{v}^S dy\right). \tag{4.15}$$

Equation (4.15) is the depth-integrated continuity equation. The solution of this equation gives the evolution of the mean water level.

When local linear wave theory is employed the Stokes drift is expressed explicitly by:

$$\overline{u}^S(z) = \frac{\sigma k_1 a^2}{2}\frac{\cosh 2k(z+h)}{\sinh^2 kh} + O(\varepsilon^3), \tag{4.16}$$

$$\overline{v}^S(z) = \frac{\sigma k_2 a^2}{2}\frac{\cosh 2k(z+h)}{\sinh^2 kh} + O(\varepsilon^3). \tag{4.17}$$

## 4.2 GENERALIZED LAGRANGIAN MEAN EQUATIONS OF MOTION

### 4.2.1 Momentum equation of motion

In this section, the Quasi-Eulerian mean equations of motion are expressed in terms of GLM quantities assuming hydrostatic conditions.

According to Ardhuin *et al.* (2008), hydrostatic pressure $\overline{p}^H$ is calculated by:

$$\overline{p}^H = \overline{p}_a + \rho g\left(\overline{\zeta} - z\right), \tag{4.18}$$

Besides, using local linear wave theory to calculate Stokes correction of mean pressure we obtain:

$$\overline{p}^S = \rho g\left(\overline{\tilde{w}^2} + \overline{\zeta}^S\right). \tag{4.19}$$

Then, hydrostatic pressure $\overline{p}^H$ can be calculated by:

$$\overline{p}^H = \overline{p}_a + \rho g\left(\overline{\zeta}^L - z\right) - \left(\overline{p}^S - \rho g\overline{\tilde{w}^2}\right). \tag{4.20}$$

From relationship (2.11) and equation (4.20) equations (4.5) and (4.6) can be expressed in terms of GLM quantities as:

$$\begin{aligned}
&\frac{\partial \overline{u}^L}{\partial t}+\overline{u}^L\frac{\partial \overline{u}^L}{\partial x}+\overline{v}^L\frac{\partial \overline{u}^L}{\partial y}+\overline{w}^L\frac{\partial \overline{u}^L}{\partial z}-f\overline{v}^L=-\frac{1}{\rho}\frac{\partial \overline{p}_a}{\partial x}-g\frac{\partial \overline{\zeta}^L}{\partial x}\\
&-\left(\frac{\partial \overline{\tilde{u}^2}}{\partial x}+\frac{\partial \overline{\tilde{u}\tilde{v}}}{\partial y}+\frac{\partial \overline{\tilde{u}\tilde{w}}_{CS}}{\partial z}\right)+\frac{F_{br,1}}{\rho}+\frac{F_{mx,1}}{\rho}+\frac{1}{\rho}\frac{\partial \overline{p}^S}{\partial x}\\
&+\frac{1}{\rho}\left(\frac{\partial \overline{\tau}_{11}^L}{\partial x}+\frac{\partial \overline{\tau}_{12}^L}{\partial y}+\frac{\partial \overline{\tau}_{13}^L}{\partial z}\right)+T_1+\upsilon\Delta\overline{u}^L+O(\varepsilon^3),
\end{aligned} \tag{4.21}$$

$$\begin{aligned}
&\frac{\partial \overline{v}^L}{\partial t}+\overline{u}^L\frac{\partial \overline{v}^L}{\partial x}+\overline{v}^L\frac{\partial \overline{v}^L}{\partial y}+\overline{w}^L\frac{\partial \overline{v}^L}{\partial z}+f\overline{u}^L=-\frac{1}{\rho}\frac{\partial \overline{p}_a}{\partial y}-g\frac{\partial \overline{\zeta}^L}{\partial y}\\
&-\left(\frac{\partial \overline{\tilde{u}\tilde{v}}}{\partial x}+\frac{\partial \overline{\tilde{v}^2}}{\partial y}+\frac{\partial \overline{\tilde{v}\tilde{w}}_{CS}}{\partial z}\right)+\frac{F_{br,2}}{\rho}+\frac{F_{mx,2}}{\rho}+\frac{1}{\rho}\frac{\partial \overline{p}^S}{\partial y}\\
&+\frac{1}{\rho}\left(\frac{\partial \overline{\tau}_{21}^L}{\partial x}+\frac{\partial \overline{\tau}_{22}^L}{\partial y}+\frac{\partial \overline{\tau}_{23}^L}{\partial z}\right)+T_2+\upsilon\Delta\overline{v}^L+O(\varepsilon^3),
\end{aligned} \tag{4.22}$$

where, the terms $T_1$ and $T_2$ are defined by:

$$T_1=\overline{D}^L\overline{u}^S+\overline{u}^S\frac{\partial \overline{u}^L}{\partial x}+\overline{v}^S\frac{\partial \overline{u}^L}{\partial y}+\overline{w}^S\frac{\partial \overline{u}^L}{\partial z}-\upsilon\Delta\overline{u}^S, \tag{4.23}$$

$$T_2=\overline{D}^L\overline{v}^S+\overline{u}^S\frac{\partial \overline{v}^L}{\partial x}+\overline{v}^S\frac{\partial \overline{v}^L}{\partial y}+\overline{w}^S\frac{\partial \overline{v}^L}{\partial z}-\upsilon\Delta\overline{v}^S. \tag{4.24}$$

The term $T_\alpha$ is of second-order of the wave amplitude and should not be neglected, especially in dissipative waves.

### 4.2.2 Mass conservation equation of motion

The mass conservation equation in the GLM framework is given by:

$$\frac{\partial \overline{u}^L}{\partial x}+\frac{\partial \overline{v}^L}{\partial y}+\frac{\partial \overline{w}^L}{\partial z}=\frac{\partial \overline{Z}^S}{\partial t}. \tag{4.25}$$

The depth-integrated mass conservation equation written is:

$$\frac{\partial\left(\overline{\zeta}^L+h\right)}{\partial t}+\frac{\partial}{\partial x}\int_{-h}^{\overline{\zeta}^L}\overline{u}^L dz+\frac{\partial}{\partial y}\int_{-h}^{\overline{\zeta}^L}\overline{v}^L dz=\frac{\partial \overline{\zeta}^S}{\partial t}. \tag{4.26}$$

The right-hand side of equation (4.26) is a term of second-order of wave amplitude. It can be neglected in case of stationary waves.

## 4.3 EQUATIONS OF MEAN MOTION IN VORTEX FORCE REPRESENTATION

In this section, the new Quasi-Eulerian mean equations are expressed in terms of vortex force representation. It is noticed that the vortex force representation is only valid in the condition of weak ambient current, i.e. $\left|\overline{\mathbf{u}}\right| \ll \mathbf{u}_{\mathrm{orb}}$.

From the relationship between radiation stress and vortex force representation (3.55)-(3.56), the Quasi-Eulerian mean horizontal momentum equations (4.5) and (4.6) are rewritten as:

$$\frac{\partial \overline{u}}{\partial t}+\overline{u}\frac{\partial \overline{u}}{\partial x}+\overline{v}\frac{\partial \overline{u}}{\partial y}+\overline{w}\frac{\partial \overline{u}}{\partial z}-f\overline{v}=-\frac{1}{\rho}\frac{\partial \overline{p}^{H}}{\partial x}-\frac{\partial\left(J+K\right)}{\partial x}+\overline{v}^{S}\left[f+\left(\frac{\partial \overline{v}}{\partial x}-\frac{\partial \overline{u}}{\partial y}\right)\right] \tag{4.27}$$
$$-\overline{w}^{S}\frac{\partial \overline{u}}{\partial z}+\frac{F_{br,1}}{\rho}+\frac{F_{mx,1}}{\rho}+\frac{1}{\rho}\left(\frac{\partial \overline{\tau}_{11}}{\partial x}+\frac{\partial \overline{\tau}_{12}}{\partial y}+\frac{\partial \overline{\tau}_{13}}{\partial z}\right)+\upsilon_{mol}\Delta\overline{u}+O(\varepsilon^{3}),$$

$$\frac{\partial \overline{v}}{\partial t}+\overline{u}\frac{\partial \overline{v}}{\partial x}+\overline{v}\frac{\partial \overline{v}}{\partial y}+\overline{w}\frac{\partial \overline{v}}{\partial z}+f\overline{u}=-\frac{1}{\rho}\frac{\partial \overline{p}^{H}}{\partial y}-\frac{\partial\left(J+K\right)}{\partial y}-\overline{u}^{S}\left[f+\left(\frac{\partial \overline{v}}{\partial x}-\frac{\partial \overline{u}}{\partial y}\right)\right] \tag{4.28}$$
$$-\overline{w}^{S}\frac{\partial \overline{v}}{\partial z}+\frac{F_{br,2}}{\rho}+\frac{F_{mx,2}}{\rho}+\frac{1}{\rho}\left(\frac{\partial \overline{\tau}_{21}}{\partial x}+\frac{\partial \overline{\tau}_{22}}{\partial y}+\frac{\partial \overline{\tau}_{23}}{\partial z}\right)+\upsilon_{mol}\Delta\overline{v}+O(\varepsilon^{3}).$$

The vertical momentum equation is given by (4.4), the mass conservation equation is given by equation (2.62), and the depth-integrated mass conservation equation is given by equation (4.15).

# 5

# APPLICATIONS[3]

[3] This Chapter is based on the publication: Nguyen, D.T., Jacobsen, N.G., Roelvink, D., 2021a. Development and Validation of Quasi-Eulerian Mean Three-Dimensional Equations of Motion Using the Generalized Lagrangian Mean Method. Ibid., 76.

## 5.1 MODEL IMPLEMENTATION

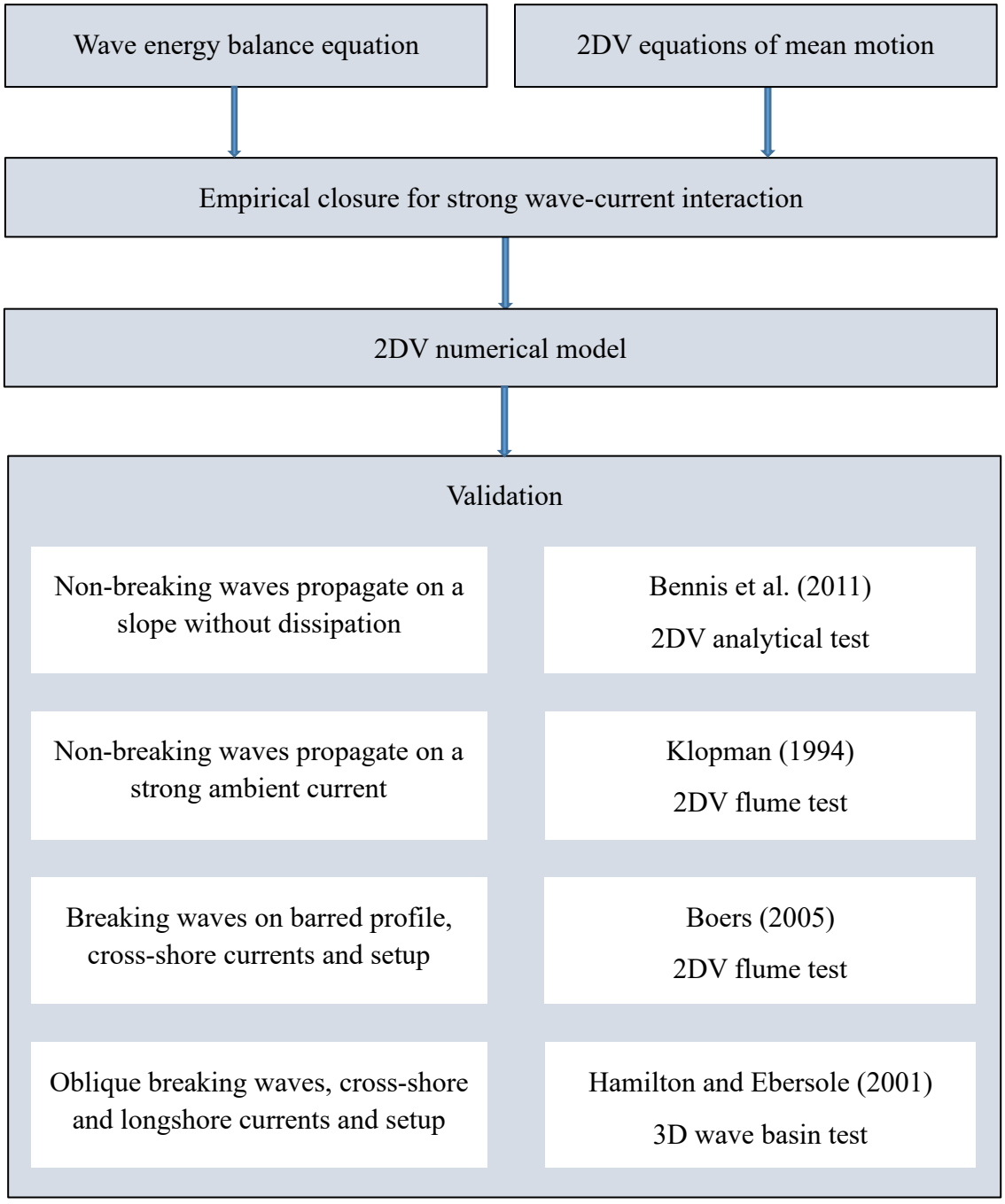


*Figure 5.1 A flowchart of the validation scheme*

A 2DV numerical model was developed based on Quasi-Eulerian mean equations of motion. Various tests of wave combined with current were employed to validate the new equations of motion. In these tests, the wave period, wave frequency, and wave number are assumed slowly variations in time and space. Therefore, the wave energy balance

equation is applied instead of the wave action balance equation. A flowchart of the validation scheme is described in Figure 5.1.

### 5.1.1 Wave energy balance equation

In this Chapter, we assume that the relative wave frequency, wave period, and wavenumber are slowly variations in the experimental flumes. Then, the wave energy balance equation can be applied instead of the wave action balance equation.

If the wave field is assumed uniform in the *y*-direction then the wave balance equation is given by (Roelvink and Reniers, 2011):

$$\frac{\partial E}{\partial t}+\frac{\partial}{\partial x}\left(Ec_g\cos\theta\right)+D_w+D_f=0. \tag{5.1}$$

where, $E=\rho g H_{rms}^2/8$ is the wave energy density with $H_{rms}$ is the root mean square wave height, $c_g$ is the wave group velocity, $\theta$ is the incident angle of the wave, $D_w$ is the wave energy dissipation rate due to breaking wave, $D_f$ is the wave energy dissipation rate due to bottom friction.

The wave energy dissipation rate due to breaking wave is calculated by (Battjes and Janssen, 1978):

$$D_w=\frac{1}{4}\rho g\alpha_b f_p Q_b\frac{H_{br}^3}{h}, \tag{5.2}$$

where, $f_p=2\pi/T_p$ is the peak frequency and $T_p$ is the peak period of the wave, $\alpha_b$ is a constant of order one, $H_{br}$ is the breaking wave height, and $Q_b$ is the fraction of breaking wave given by the following relationship:

$$Q_b=\exp\left(-\left(\frac{H_{br}^2}{H_{rms}^2}\left(1-Q_b\right)\right)\right). \tag{5.3}$$

The breaking wave height is calculated by Miche criterion, i.e.:

$$H_{br}=\frac{0.88}{k}\tanh\left(\frac{\gamma kh}{0.88}\right), \tag{5.4}$$

where, $\gamma$ is the breaking index ($\approx 0.6-0.8$). This index can be calculated by the following equation (Battjes and Stive, 1985):

$$\gamma=0.5+0.4\tanh\left(33\frac{H_{rms}}{L_{rms}}\right), \tag{5.5}$$

with $L_{rms}$ is the root mean square wavelength at deep water.

To calculate the mean current in the surfzone, an additional component called roller is included (Svendsen, 1984). The idea is that some fractions of breaking waves $\alpha_r$ (from 0 to 1) are transferred to the roller before dissipating. The evolution equation for the roller energy density is given by (Roelvink and Reniers, 2011):

$$\frac{\partial E_r}{\partial t} + \frac{\partial \left( E_r c \cos\theta \right)}{\partial x} = \alpha_r D_w - D_r, \tag{5.6}$$

where, $E_r$ is the roller energy density, $c$ is the wave celerity, and $D_r$ is the roller wave dissipation rate calculated by (Nairn *et al.*, 1991):

$$D_r = 2\beta \frac{gE_r}{c}, \tag{5.7}$$

where, $\beta$ is the mean slope under the roller.

The bottom friction dissipation rate is calculated by (Putnam and Johson, 1949):

$$D_f = \left| \overline{\tau_b \tilde{\mathbf{u}}_b} \right|, \tag{5.8}$$

where, $\tilde{\mathbf{u}}_b$ is the horizontal wave velocity vector above the bottom boundary layer, and $\tau_b$ is the instantaneous total bed shear stress. Simply, the instantaneous total bed shear stress can be decomposed as:

$$\tau_b = \tau_w + \left| \overline{\tau}_{cw} \right|, \tag{5.9}$$

where, $\tau_w$ is the wave-induced bed shear stress, and $\overline{\tau}_{cw}$ is the bed-shear stress due to the mean current. Then, equation (5.8) can be rewritten as:

$$D_f = D_{f,w} + D_{f,cw}, \tag{5.10}$$

where, $D_{f,w}$ is the wave energy dissipation caused by wave-induced bed shear stress, and $D_{f,cw}$ is the wave energy dissipation caused by mean current-induced bed shear stress defined by:

$$D_{f,w} = \left| \overline{\tau_w \tilde{\mathbf{u}}_b} \right|, \tag{5.11}$$

$$D_{f,cw} = \overline{\left| \overline{\tau}_{cw} \right| \left| \tilde{\mathbf{u}}_b \right|}. \tag{5.12}$$

The wave-induced bed shear stress $\tau_w$ is calculated by (Soulsby, 1997):

$$\tau_w = \frac{1}{2} \rho f_w \left| \tilde{\mathbf{u}}_b \right| \tilde{\mathbf{u}}_b, \tag{5.13}$$

where, $f_w$ is the friction factor for wave motion calculated by:

$$f_w = 1.39\left(\frac{A_{orb}}{z_0}\right)^{-0.52}, \tag{5.14}$$

with $A_{orb} = |\mathbf{u}_{orb}| T_p / 2\pi$ is the semi-orbital excursion, and $z_0$ is the bottom roughness height. The near-bed orbital velocity amplitude is calculated by:

$$|\mathbf{u}_{orb}| = \frac{\sigma H_{rms}}{2\sinh kh}. \tag{5.15}$$

For random waves, we use the assumption of the Gaussian distribution of the wave velocity. According to Guza and Thornton (1985), we have:

$$\overline{|\tilde{\mathbf{u}}_b|^2} = s^2, \tag{5.16}$$

$$\overline{|\tilde{\mathbf{u}}_b|^3} = 1.60\left(\overline{|\tilde{\mathbf{u}}_b|^2}\right)^{3/2}, \tag{5.17}$$

where, $s$ is the near-bed standard deviation of the velocity. The Gaussian moments can express by 'equivalent monochromatic wave' moments by the following relationship:

$$\overline{|\tilde{\mathbf{u}}_b|^2} = 0.5|\mathbf{u}_{orb}|^2. \tag{5.18}$$

Therefore, the relationship (5.17) can be expressed as:

$$\overline{|\tilde{\mathbf{u}}_b|^3} = 0.57|\mathbf{u}_{orb}|^3. \tag{5.19}$$

It furthermore follows that the mean of the absolute velocity reads:

$$\overline{|\tilde{\mathbf{u}}_b|} = \frac{\sqrt{2}s}{\sqrt{\pi}} = \frac{|\mathbf{u}_{orb}|}{\sqrt{\pi}}. \tag{5.20}$$

Therefore, the wave energy dissipations caused by wave-induced friction and current-induced friction are calculated, respectively, by:

$$D_{f,w} = 0.28\rho f_w |\mathbf{u}_{orb}|^3, \tag{5.21}$$

$$D_{f,cw} = \frac{1}{\sqrt{\pi}}|\overline{\tau}_{cw}||\mathbf{u}_{orb}|. \tag{5.22}$$

According to Van Rijn (2011), the magnitude of the near-bed current can be calculated by:

$$\overline{|\mathbf{u}_b|} = \sqrt{\overline{\mathbf{u}}_b^2 + \frac{1}{2}|\mathbf{u}_{orb}|^2}, \tag{5.23}$$

where, $\overline{\mathbf{u}}_b = \left(\overline{u}_b, \overline{v}_b\right)$ is horizontal mean velocity near the bed. Then, the mean bed shear stress for combined waves and currents $\overline{\tau}_{cw}$ is calculated by:

$$\overline{\tau}_{cw} = -\frac{1}{2}\rho f_{cw}\overline{\mathbf{u}}_b\sqrt{\overline{\mathbf{u}}_b^2 + \frac{1}{2}\left|\mathbf{u}_{orb}\right|^2}, \tag{5.24}$$

where, $f_{cw}$ is the friction factor of the mean current. The formula (5.24) was derived for monochromatic waves. For random waves, we modify the formula (5.24) based on the approximate practical formula of Feddersen *et al.* (2000) to obtain:

$$\overline{\tau}_{cw} = -\frac{1}{2}\rho f_{cw}\overline{\mathbf{u}}_b\sqrt{(1.16s)^2 + \overline{\mathbf{u}}_b{}^2}. \tag{5.25}$$

The friction factor of the mean current is given by:

$$f_{cw} = 0.242\left[\log\left(12h/k_a\right)\right]^{-2}, \tag{5.26}$$

where, $k_a$ is the apparent roughness calculated from the near-bed layer thickness calculated by:

$$k_a = 30\delta/e, \tag{5.27}$$

with $e$ is the base of the natural logarithm, and $\delta$ is the bottom boundary layer thickness.

In current-only condition, the boundary layer thickness is given by (Van Rijn, 2011):

$$\delta = ez_0. \tag{5.28}$$

In wave-only condition, the bottom boundary layer thickness is calculated by (Jonsson and Carlsen, 1976), i.e.:

$$\delta = 0.072A_{orb}\left(A_{orb}/k_n\right)^{-0.25}. \tag{5.29}$$

In the condition of waves combined with current, Van Rijn (2011) proposed the following formula:

$$\delta = 0.2A_{orb}\left(A_{orb}/k_n\right)^{-0.25}, \tag{5.30}$$

where, $k_n = 30z_0$ is the Nikuradse roughness. However, equation (5.30) does not account for the effect of near-bed mean current on the bottom boundary layer thickness. Therefore, it is only suitable if the near-bed mean current is small in comparison with the near-bed orbital velocity. When the near-bed current is significant and is comparable to the orbital velocity the following formula is proposed:

$$\delta = 0.2A_{orb}\left(A_{orb}/k_n\right)^{-0.25}\left(1+\left|\overline{\mathbf{u}}_b\right|/\left|\mathbf{u}_{orb}\right|\right). \tag{5.31}$$

It is clear that when $|\bar{\mathbf{u}}_b| \ll |\mathbf{u}_{orb}|$ the formula (5.31) reduces to formula (5.30).

## 5.1.2 The 2DV governing equations

In this part, a two-dimensional numerical model is developed based on the Quasi-Eulerian mean equations of motion, which were developed in the previous part. The model is written for the variation of hydrodynamic properties in the *x*- and *z*-directions (2DV model). All hydrodynamic properties are assumed to be uniform in the *y*-direction. The accelerations of mean vertical velocity and dissipative forcing are neglected in the vertical momentum equation of mean motion. Besides, the horizontal variation of the mean atmospheric pressure at the water surface and Coriolis' effect are assumed small and neglected.

Using equation (4.18) momentum equations in the 2DV model are given by:

$$\frac{\partial \bar{u}}{\partial t}+\bar{u}\frac{\partial \bar{u}}{\partial x}+\bar{w}\frac{\partial \bar{u}}{\partial z}-\upsilon\Delta\bar{u}=-g\frac{\partial \bar{\zeta}}{\partial x}-\frac{\partial\left(\overline{\tilde{u}^2}-\overline{\tilde{w}^2}\right)}{\partial x}-\frac{\partial \overline{\tilde{u}\tilde{w}}}{\partial z}+\frac{1}{\rho}\left(\frac{\partial \bar{\tau}_{11}}{\partial x}+\frac{\partial \bar{\tau}_{13}}{\partial z}\right)+O(\varepsilon^3), \quad (5.32)$$

$$\frac{\partial \bar{v}}{\partial t}+\bar{u}\frac{\partial \bar{v}}{\partial x}+\bar{w}\frac{\partial \bar{v}}{\partial z}-\upsilon\Delta\bar{v}=-\frac{\partial \overline{\tilde{u}\tilde{v}}}{\partial x}-\frac{\partial \overline{\tilde{v}\tilde{w}}}{\partial z}+\frac{1}{\rho}\left(\frac{\partial \bar{\tau}_{21}}{\partial x}+\frac{\partial \bar{\tau}_{23}}{\partial z}\right)+O(\varepsilon^3), \quad (5.33)$$

where, only molecular viscosity is considered as non-wave dissipative forcing and $\upsilon$ is molecular viscosity.

The components of turbulence stress tensor are parameterized by:

$$\bar{\tau}_{11}=\rho\upsilon_h^T\frac{\partial \bar{u}}{\partial x}, \qquad \bar{\tau}_{13}=\rho\upsilon_v^T\frac{\partial \bar{u}}{\partial z}, \quad (5.34)$$

$$\bar{\tau}_{21}=\rho\upsilon_h^T\frac{\partial \bar{v}}{\partial x}, \qquad \bar{\tau}_{23}=\rho\upsilon_v^T\frac{\partial \bar{v}}{\partial z}, \quad (5.35)$$

where, $\upsilon_h^T$ and $\upsilon_v^T$ are horizontal and vertical turbulent viscosities, respectively. In this study, horizontal turbulent viscosity is assumed a constant $\upsilon_h^T=1.0\times10^{-3}$ m$^2$/s, and vertical turbulent viscosity is assumed a constant-parabolic distribution, i.e.:

$$\upsilon_v^T(z)=\begin{cases}\kappa\delta\left(1-\dfrac{\delta}{h}\right)\bar{\mathbf{u}}_{*,c} & if\ (z+h)\le\delta\\ -\kappa z\left(1+\dfrac{z}{h}\right)\bar{\mathbf{u}}_{*,c} & otherwise\end{cases}, \quad (5.36)$$

where, $\kappa=0.41$ is the Von Karman constant, $\bar{\mathbf{u}}_{*,c}=\sqrt{|\bar{\tau}_c|/\rho}$ is friction velocity caused by mean current, and $\bar{\tau}_c$ is the bed shear stress caused by mean current calculated by:

$$\overline{\tau}_c = -\frac{1}{2}\rho f_{cw}\left|\overline{\mathbf{u}}_b\right|\overline{\mathbf{u}}_b. \tag{5.37}$$

In the condition of stationary waves, Quasi-Eulerian mean continuity equation in the 2DV model is:

$$\frac{\partial \overline{u}}{\partial x}+\frac{\partial \overline{w}}{\partial z}=-\frac{\partial \overline{u}^S}{\partial x}-\frac{\partial \overline{w}^S}{\partial z}. \tag{5.38}$$

If the bed level is fixed then depth-integrated continuity equation is simplified as:

$$\frac{\partial \overline{\zeta}}{\partial t}+\frac{\partial}{\partial x}\int_{-h}^{\overline{\zeta}^L}\overline{u}dz=-\frac{\partial}{\partial x}\left(\int_{-h}^{\overline{\zeta}^L}\overline{u}^S dx\right). \tag{5.39}$$

### 5.1.3 Vertical distribution of wave-induced forcing

In the 2DV model, the vertical distribution of the wave-induced forcing $F_{br}$ and $F_{mx}$ is estimated using the empirical formula proposed by Uchiyama *et al.* (2010). The breaking and roller forcing is calculated by:

$$F_{br}=\frac{\left(1-\alpha_r\right)D_w+D_r}{\sigma}\mathbf{k}f^b(z), \tag{5.40}$$

where, $f^b(z)$ represents the penetration of momentum associated with breaking waves and rollers. Here, the Type I and Type III of function $f^b(z)$ proposed by Uchiyama *et al.* (2010) is employed, i.e.:

$$\text{Type I:}\quad f^b(z)=\frac{1-\tanh\left[k_b(\overline{\zeta}-z)\right]^4}{\int_{-h}^{\overline{\zeta}}\left(1-\tanh\left[k_b(\overline{\zeta}-z')\right]^4 dz'\right)}, \tag{5.41}$$

$$\text{Type III:}\quad f^b(z)=\frac{\cosh\left[k_b(\overline{\zeta}-z)\right]}{\int_{-h}^{\overline{\zeta}}\cosh\left[k_b(\overline{\zeta}-z')\right]dz'}, \tag{5.42}$$

where, $k_b=\left(a_b H_{rms}\right)^{-1}$ is the vertical length scale controlling the penetration depth of the breaking wave, and $a_b$ is a $O(1)$ constant. Type I is applied for the deep water and type III for the shallow water (characterized by the ratio $h/L$).

The wave-induced momentum mixing is parameterized similar to turbulent stress (Uchiyama *et al.*, 2010), i.e.:

$$F_{mx}=-\frac{\partial}{\partial z}\left[\rho\left(K_b+K_{fr}\right)\frac{\partial \overline{\mathbf{u}}}{\partial z}\right], \tag{5.43}$$

where, $K_{fr}$ is the wave-induced mixing coefficient due to the wave decay at the bottom, and $K_b$ is the wave-induced mixing coefficient due to breaking waves.

The vertical distribution of the wave-induced mixing coefficients $K_{fr}$ and $K_b$ are necessary to calculate the wave-induced forcing $F_{mx}$. In this study, the wave-induced mixing coefficient $K_{fr}$ is parameterized similar to the turbulent viscosity, i.e.:

$$K_{fr} = \begin{cases} \kappa\delta\left(1-\dfrac{\delta}{h}\right)\overline{\mathbf{u}}_{*,cw} & if\ (z+h) \le \delta \\ -\kappa z\left(1+\dfrac{z}{h}\right)\overline{\mathbf{u}}_{*,cw} & otherwise \end{cases}, \tag{5.44}$$

where, $\overline{\mathbf{u}}_{*,cw} = \overline{\mathbf{u}}_{*} - \overline{\mathbf{u}}_{*,c}$ is a component of friction velocity which arises in the presence of the waves.

The wave-induced mixing coefficient $K_b$ is calculated following the empirical formula given by Uchiyama *et al.* (2010), i.e.:

$$K_b(z) = c_b\left(\frac{(1-\alpha_r)D_w + D_r}{\rho}\right)^{1/3} H_{rms} D f^{Kv}(z), \tag{5.45}$$

where, $c_b$ is a $O(0.1)$ parameter, and $f^{Kv}(z)$ is a decay function. Here, we use two types of decay function $f^{Kv}(z)$, i.e. Type I and Type III, proposed by Uchiyama *et al.* (2010). Type I for the deep water application, and Type III for the shallow water application.

$$\text{Type I:}\quad f^{Kv}(z) = \frac{1-\tanh\left[k_{Kv}(\overline{\zeta}-z)\right]^4}{\int_{-h}^{\overline{\zeta}}\left(1-\tanh\left[k_{Kv}(\overline{\zeta}-z')\right]^4 dz'\right)}, \tag{5.46}$$

$$\text{Type III:}\quad f^{Kv}(z) = \frac{\cosh\left[k_{Kv}(\overline{\zeta}-z)\right]}{\int_{-h}^{\overline{\zeta}}\cosh\left[k_{Kv}(\overline{\zeta}-z')\right]dz'}, \tag{5.47}$$

with $k_{Kv} = \left(a_{Kv}H_{rms}\right)^{-1}$ is the decay length controlling the penetration depth of the wave-induced mixing, and $a_{Kv}$ is $O(1)$ constant.

In the following, we define $F_{tot}$ as the total of wave-induced mixing and current-induced turbulent forcing, i.e.:

$$\frac{F_{tot,1}}{\rho} = \frac{1}{\rho}\left(F_{mx,1} + \frac{\partial\overline{\tau}_{11}}{\partial x} + \frac{\partial\overline{\tau}_{13}}{\partial z}\right) = \left(\upsilon_v + K_{fr} + K_b\right)\frac{\partial\overline{u}}{\partial z} + \frac{\partial}{\partial x}\left(\upsilon_h^T\frac{\partial\overline{u}}{\partial x}\right), \tag{5.48}$$

$$\frac{F_{tot,2}}{\rho}=\frac{1}{\rho}\left(F_{mx,2}+\frac{\partial\overline{\tau}_{21}}{\partial x}+\frac{\partial\overline{\tau}_{23}}{\partial z}\right)=\left(\upsilon_v+K_{fr}+K_b\right)\frac{\partial\overline{v}}{\partial z}+\frac{\partial}{\partial x}\left(\upsilon_h^T\frac{\partial\overline{v}}{\partial x}\right). \tag{5.49}$$

Defining $F_w$ as the total of wave-induced forcing caused by the conservative part of the wave radiation stress and breaking wave and roller-induced forcing, i.e.:

$$\frac{F_{w,1}}{\rho}=-\left[\frac{\partial\left(\overline{\tilde{u}^2}-\overline{\tilde{w}^2}\right)}{\partial x}+\frac{\partial\overline{\tilde{u}\tilde{w}}_{CS}}{\partial z}\right]+\frac{F_{br,1}}{\rho}, \tag{5.50}$$

$$\frac{F_{w,2}}{\rho}=-\left[\frac{\partial\overline{\tilde{u}\tilde{v}}}{\partial x}+\frac{\partial\overline{\tilde{v}\tilde{w}}_{CS}}{\partial z}\right]+\frac{F_{br,2}}{\rho}. \tag{5.51}$$

The total forcing $\left(F_w+F_{tot}\right)$ then represents the total effects of waves and turbulence on the mean current.

## 5.2 NUMERICAL APPROXIMATION

The 2DV equations of mean motion are discretized based on the finite difference method on a fully staggered grid (C-grid). An implicit numerical scheme has been used to discretize these equations. Finally, the tri-diagonal matrix algorithm (Thomas algorithm) has been used to solve these equations. In the model, the water level is approximated at the grid point $(i,k)$, the horizontal component of velocity at $(i+1/2,k)$, and the vertical component of velocity at $(i,k+1/2)$. The advection terms are approximated following the principles described in Stelling and Busnelli (2001). This method ensures the conservation of properties near large local gradient areas. The 2DV model developed in this study is a time-domain model starting from rest and simulating to equilibrium in all cases.

## 5.3 ADIABATIC TEST

The adiabatic test, described in Bennis *et al.* (2011), is a seemingly simple but challenging test of the derived equations since any imbalance leads to strong spurious circulations. This test was applied first by Ardhuin *et al.* (2008). In this, a steady monochromatic small-amplitude wave propagates over a slope without dissipation. This test has an exact solution by solving Laplace's equation for the instantaneous velocity potential with given bottom, surface, and lateral boundary conditions (Ardhuin *et al.*, 2008). In the work of Ardhuin *et al.* (2008), the adiabatic test was solved by using the NTUA-nl2 model (National Technical University of Athens numerical model) developed by Belibassakis and Athanassoulis (2002). The Quasi-Eulerian mean current is depth uniform.

### 5.3.1 Bathymetry

The bathymetry is symmetrical and varies slowly from 4 m to 6 m in the x-direction and is uniform in the y-direction (Figure 5.2). The maximum bottom slope is 2.6x10-2, and the reflection coefficient is $R = 1.4 \times 10^{-9}$, so we can neglect the reflected wave in the momentum balance (Ardhuin *et al.*, 2008).

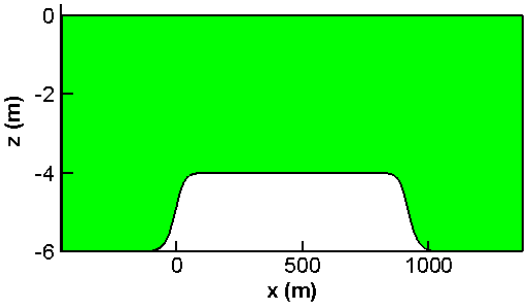


*Figure 5.2 Bathymetry of the computational area*

### 5.3.2 Boundary conditions

At the boundary, a regular wave with 1.02 m height and a period of 5.26 s is imposed. This is also the wave that was used by Ardhuin *et al.* (2008), and Bennis *et al.* (2011) to test their model in adiabatic condition. The mean water level at the boundary is given by:

$$\overline{\zeta} = -\frac{ka^2}{2\sinh 2kh}. \tag{5.52}$$

At the inflow boundary, the Quasi-Eulerian mean velocity is vertical uniform and given by:

$$\overline{u}(z) = -\frac{1}{h+\overline{\zeta}^L}\int_{-h}^{\overline{\zeta}^L} \overline{u}^S(z)dz. \tag{5.53}$$

At the outflow boundary, the Neumann boundary condition is applied, i.e.:

$$\frac{\partial \overline{u}}{\partial x} = -\frac{\partial \overline{u}^S}{\partial x}. \tag{5.54}$$

### 5.3.3 Numerical results

Figure 5.3 shows the spatial distribution of Stokes drift in the *x*-direction. It shows that the Stokes drift is constant over the horizontal bed and the magnitude of the Stokes drift increases with a decrease in water depth and vice versa.

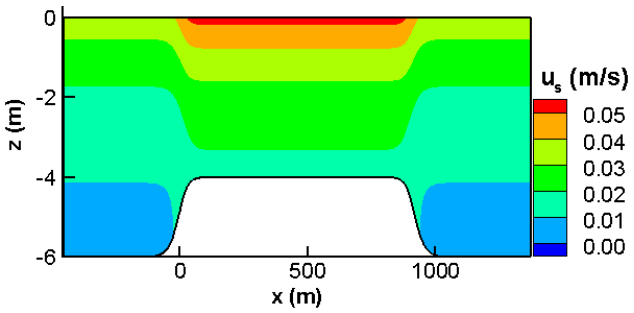


*Figure 5.3 Spatial distribution of Stokes drift*

The comparison of mean water level calculated by the numerical model and mean water level calculated by the formula of Longuet-Higgins and Stewart (1964) is given in Figure 5.4. It shows a perfect agreement between the two calculation methods.

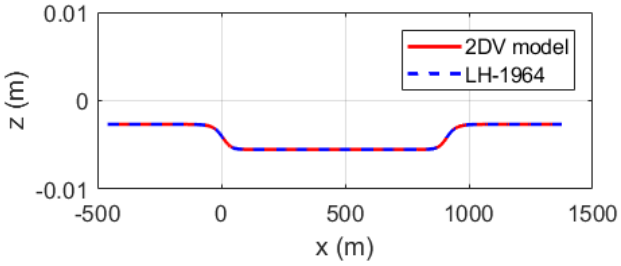


*Figure 5.4 Distribution of mean water level*

In the adiabatic condition, the total forcing $F_{tot,1}$ was zero. The vertical distribution of the wave forcing term $F_{w,1}/\rho$ is presented in Figure 5.5. It shows that wave-induced forcing $F_{w,1}/\rho$ was zero when the waves propagated over a flat bed. On a sloping bed, this forcing was not nil and was distributed uniformly over depth. Then, the total forcing $\left(F_{w,1}+F_{tot,1}\right)$ was depth-uniform in the adiabatic condition.

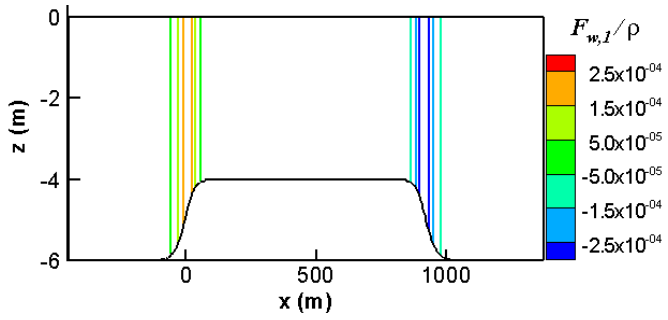


*Figure 5.5 Distribution of $F_{w,1}/\rho$ $(m/s^2)$*

When the wave propagates over a slope, the change of the wave height leads to the change of Stokes drift. Due to the conservation of mass and momentum the Quasi-Eulerian mean

velocity also changes. However, the vertical integration of total flow is still unchanged, and in this case, it equals zero, i.e.:

$$\int_{-h}^{\bar{\zeta}^L} \bar{u}^L dz = 0. \tag{5.55}$$

Since all dissipative forcing was absent, the Quasi-Eulerian mean horizontal velocity was uniformly distributed over the vertical. However, the GLM velocity inherited the non-uniformity from the Stokes drift (Figure 5.6a). Figure 5.6b presents the Quasi-Eulerian mean velocity calculated with the 2DV model. It proves that Quasi-Eulerian mean equations of motion passed the adiabatic test.

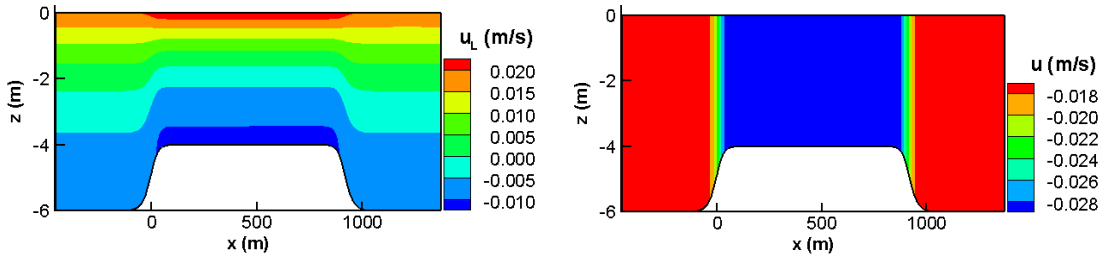


(a) GLM velocity (b) Quasi-Eulerian mean velocity

*Figure 5.6 Vertical distribution of horizontal mean velocity*

## 5.4 MEAN CURRENTS IN THE PRESENCE OF NON-BREAKING WAVES

In the experiment of Klopman (1994), the vertical distribution of the mean current was measured in three different types of waves: monochromatic waves, bi-chromatic waves, and random waves. The experiments were performed for four conditions of ambient currents: currents only (CO), waves only (WO), waves following currents (WFC), and waves opposing currents (WOC). The wave height was chosen so that no wave breaking took place. Therefore, the bottom friction plays an important role in the vertical distribution of the mean current. In the following, the experimental data for random waves were employed to validate the 2DV numerical model.

### 5.4.1 Input parameters

The experiment was performed in a wave flume that has a horizontal flat bottom. The flume has a size of 45 m long, 1 m wide, and 0.5 m deep. The total discharge was kept constant: $Q = 0.$ m$^3$/s for the case wave-only, and $Q = 0.08$ m$^3$/s for the remaining cases. The properties of the random waves at the wave paddle are given in Table 5-1.

*Table 5-1 Wave properties at the paddle*

| **Wave type** | $T_p$ (s) | $H_{rms}$ (m) | $h$ (m) |
|---|---|---|---|
| Random | 1.7 | 0.1 | 0.5 |

The flow velocities were measured at the center of the channel, i.e., 22.5 m from the wave paddle. Two Laser-Doppler Velocimetry flow meters (LDV's) were used to measure flow velocity components. The vertical distributions of Eulerian-mean velocities measured at the center of the flume are present in Figure 5.7.

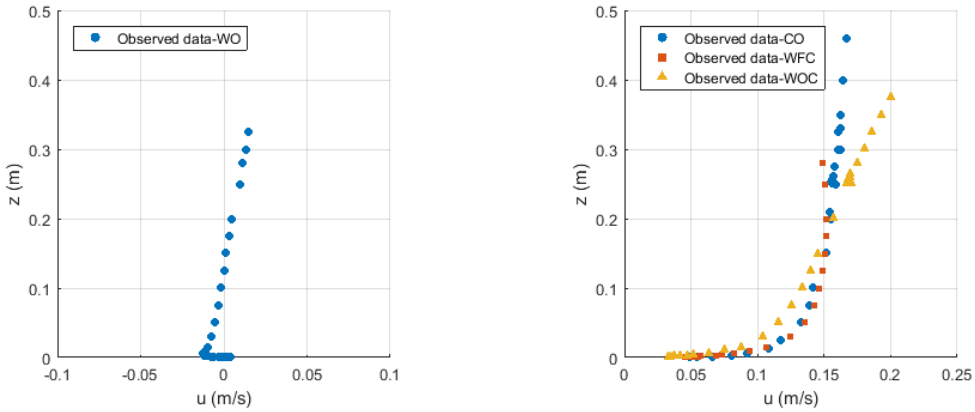


(a) Wave only (b) Wave combined with current

*Figure 5.7 Vertical distribution of the Eulerian-mean velocity*

On the left-hand side of Figure 5.7 (WO condition), the wave propagates from the right-hand side to the left-hand side. The wave-induced streaming near the bed is in the same direction as the propagation of the surface waves. The horizontal mean velocity changes sign at the height $z \approx 0.13$ m (Klopman, 1994). Outside the bottom streaming layer, the mean velocity varies almost linearly. On the right-hand side of Figure 5.7, we present the vertical distribution of horizontal mean velocity in three conditions: CO, WFC, and WOC. It shows that vertical profiles of mean current change significantly in the presence of surface waves. In the WFC condition, the velocity shear $\partial\overline{u} / \partial z$ is negative in the upper part of the water column (z/h > 0.4). In the WOC condition, the mean velocity decreases near the bed (z/h < 0.4) and increases near the surface (z/h > 0.4) in comparison with the current-only condition.

By linear extrapolation of the velocities in a semi-logarithmic scale, Klopman (1994) obtained the friction velocity $u_* \approx 7.3$ mm/s. The vertical distribution of the Reynolds shear stress $-\overline{u^t w^t}$ is present in Figure 5.8. The bottom shear stress was estimated by Klopman (1994) at about $\overline{\tau}_b / \rho = 4.6 \times 10^{-5}$ m$^2$/s$^2$, corresponding to the friction velocity of

$u_* = \sqrt{\overline{\tau}_b / \rho} \approx 6.7$ mm/s. Then, the friction velocity calculated from the bed shear stress is slightly smaller than obtained from the velocity profile.

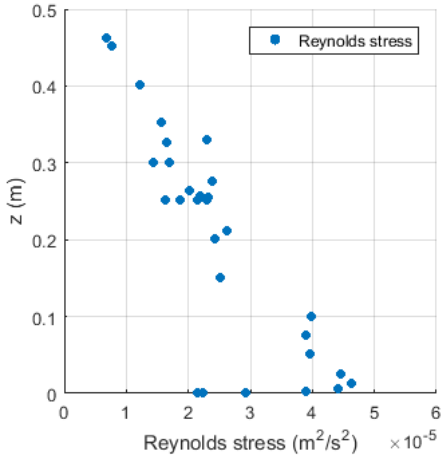


*Figure 5.8 Vertical distribution of observed Reynolds shear stress $\overline{-u^t w^t}$ in the CO condition*

## 5.4.2 Boundary conditions

a) Surface and bottom boundary conditions

In the model, the total shear stress is assumed to vanish at the mean water surface, since non-breaking waves are considered, i.e.:

$$\left[\left(\upsilon_v + K_{fr}\right)\frac{\partial \overline{u}}{\partial z}\right]_{z=\overline{\zeta}} = 0, \tag{5.56}$$

where, $\upsilon_v = \upsilon_v^T + \upsilon_{mol}$.

At the bottom, the bottom boundary condition is given by:

$$\left[\left(\upsilon_v + K_{fr}\right)\frac{\partial \overline{u}}{\partial z}\right]_{z=-h} = -\frac{kD_f}{\rho\sigma} - \frac{\overline{\tau}_{cw}}{\rho}. \tag{5.57}$$

b) Lateral boundary conditions

At the outflow boundary, the boundary condition for the mean water level and the mean current is given by:

$$\overline{\zeta} = -\frac{ka^2}{2\sinh 2kh}, \tag{5.58}$$

$$\frac{\partial \overline{u}}{\partial x} = -\frac{\partial \overline{u}^S}{\partial x}. \tag{5.59}$$

At the inflow boundary, the Quasi-Eulerian mean velocity is given by:

$$\overline{u}(z) = \frac{1}{h + \overline{\zeta}^L} \overline{Q}^L - \overline{u}^S(z), \tag{5.60}$$

where, $\overline{Q}^L$ is the mean of total discharge through the pipe.

### 5.4.3 The numerical results

The experiment of Klopman (1994) is simulated by the 2DV model with spatial steps of $\Delta x = 0.15\,\text{m}$, $\Delta z = 0.0025\,\text{m}$, and a time step of $\Delta t = 0.5\,\text{s}$. In the experiment, due to small technical issues, there was uncertainty in the measured discharge (see Klopman (1994) for more detail). However, these errors were not corrected in his document. Generally, the measured discharge is expressed as a total of the real discharge and error discharge, i.e.:

$$Q_{measured} = Q_{real} + Q_{err}, \tag{5.61}$$

where, $Q_{real}$ is the real discharge through the wave flume, $Q_{measured}$ is the measured discharge, and $Q_{err}$ is the error of flow discharge. In the CO condition, it was found that when $Q_{err}$ approximates to 0.003 $\text{m}^3\text{s}^{-1}$ (3.75% of the real discharge) a good agreement between numerical results and experimental data was obtained. In waves combined with current conditions, the error of flow discharge is assumed similar to the current only condition. In the WO condition, flow discharge $Q_{err}$ is zero by definition. In all tests, the bed roughness is kept constant $z_0 = 4.0\times10^{-5}\,\text{m}$, corresponding to a Nikuradse roughness of $k_n = 1.2\times10^{-3}\,\text{m}$. In Table 2, the bottom boundary thickness is presented. In the condition of waves combined with current, bottom boundary thickness $\delta$ was calculated by two methods: the formula of Van Rijn (2011) and its modified formula 62. The results are presented in Table 5-2.

*Table 5-2 Bottom boundary thickness $\delta$ in different waves and current condition*

| **Conditions** | Formula (5.31) ($\times10^{-3}$ m) | Van Rijn (2011) ($\times10^{-3}$ m) |
|---|---|---|
| CO | 0.1 | 0.1 |
| WO | 1.3 | 1.3 |
| WFC | 5.3 | 3.6 |
| WOC | 4.9 | 3.6 |

The wave energy dissipation in different conditions of waves combined with the current is present in Table 5-3. It shows that with the same wave height and ambient current velocity, the wave energy dissipation due to the following current is bigger than due to opposing current. The wave energy dissipation due to current-induced bottom friction $D_{f,cw}$ approximates 42% and 31% of the total energy dissipation $D_f$ due to bottom friction in the WFC, and WOC conditions, respectively. Moreover, the energy dissipation due to bottom friction in the WFC condition is bigger than that in the WOC condition.

*Table 5-3 Wave energy dissipation*

| **Conditions** | $D_{f,w}(\mathrm{W/m^2})$ | $D_{f,cw}(\mathrm{W/m^2})$ |
|---|---|---|
| WO | 0.046 | 0 |
| WFC | 0.044 | 0.032 |
| WOC | 0.045 | 0.020 |

Table 5-4 presents the characteristics of the mean flow near the bed calculated by the 2DV model. It shows that bottom stress in conditions of waves combined with the current was much higher than that in conditions of WO and CO. This is because momentum mixing under wave-current interaction conditions was much higher than in conditions of both WO and CO (see for instance the discussion in Chapter 3 of Deigaard (1992)).

*Table 5-4 Characteristics of the near-bed mean flow*

| **Conditions** | $\lvert\overline{u}_b\rvert$ ($\times 10^{-2}$ m/s) | $\lvert\overline{\tau}_b\rvert$ ($\times 10^{-2}$ kgm$^2$/s$^2$) | $u_*$ ($\times 10^{-2}$ m/s) |
|---|---|---|---|
| CO | 8.16 | 5.4 | 0.74 |
| WO | 0.9 | 0.21 | 0.13 |
| WFC | 8.10 | 37.67 | 1.94 |
| WOC | 5.86 | 24.6 | 1.56 |

The vertical distribution of Reynolds turbulent viscosity is present in Figure 5.9. It shows that the viscosity in WFC condition is bigger than in WOC condition, and viscosity in waves combined with current conditions is bigger than in CO condition. Moreover, the viscosity in the WO condition is much smaller than in other conditions.

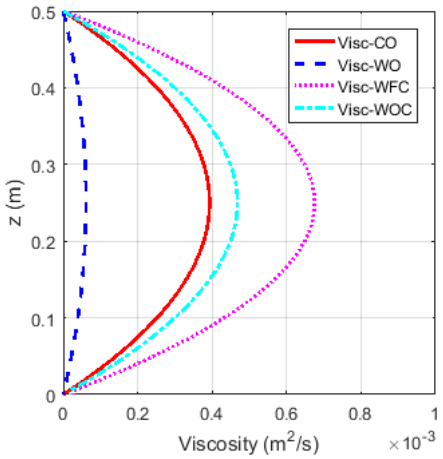


*Figure 5.9 Reynolds turbulent viscosity ($\upsilon_v^T$)*

In Figure 5.10, the conservative part of $\overline{\tilde{u}\tilde{w}}$ in different conditions of waves combined with the current was plotted. It clearly shows that the ambient current had a significant impact on the normal component of the wave radiation stress. Moreover, the conservative part of the normal component of wave radiation stress $\overline{\tilde{u}\tilde{w}}$ in the condition of the following waves was slightly bigger than that in the condition of the opposing waves.

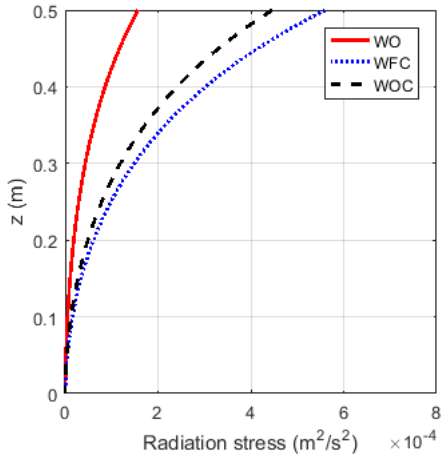


*Figure 5.10 Vertical distribution of the wave radiation stress component $\overline{\tilde{u}\tilde{w}}_{CS}$*

In non-breaking waves, the wave-induced forcing term $F_{w,1}/\rho$ only represents the effect of the conservative part of the wave radiation stress. Figure 5.11 shows the vertical distributions of forcing term $F_{w,1}/\rho$ and mixing term $F_{tot,1}/\rho$ at the center of the wave flume. In all three tests, i.e., WO, WFC, and WOC, the forcing $F_{w,1}$ is completely

compensated by total mixing $F_{tot,1}$ at any water depth level. The total of these two forcing terms, i.e., $\left(F_{w,1}+F_{tot,1}\right)$, is depth-uniform in the non-breaking wave condition.

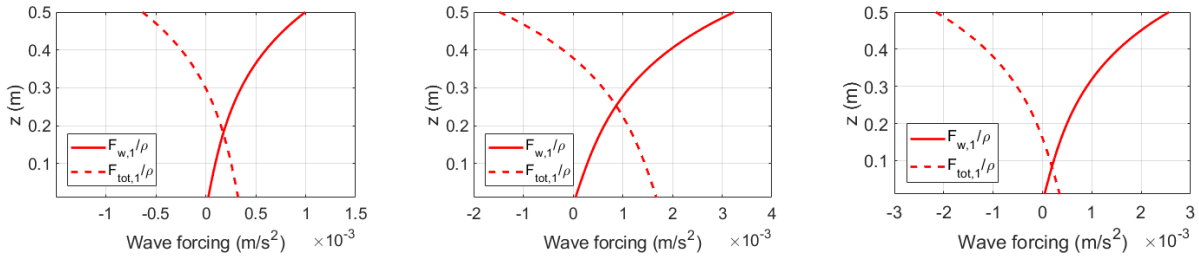


(a) WO (b) WFC (c) WOC

*Figure 5.11 Vertical distribution of wave-induced forcing terms*

Figure 5.12 shows the vertical distribution of Reynolds turbulent stress at the center of the wave flume. Near the bed, the turbulent stress calculated by the 2DV numerical model is about $\overline{\tau}_b/\rho \approx 54.4\times10^{-6}\,\mathrm{m}^2/\mathrm{s}^2$, and the corresponding friction velocity is 7.4 mm/s (Table 5-4), which is in good agreement with the friction velocity obtained from the mean velocity profile by Klopman (1994), i.e. 7.3 mm/s.

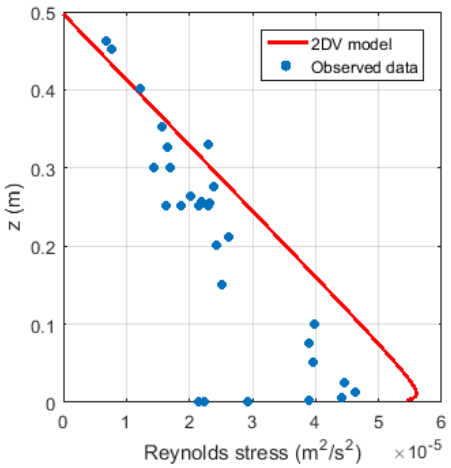


*Figure 5.12 Spatial distribution of Quasi-Eulerian mean velocity in the CO condition*

The spatial distribution of the Quasi-Eulerian mean velocity calculated with the 2DV model in the condition of CO is given in Figure 5.13. The (vertically uniform) inflow boundary was specified at position $x=0$ m.

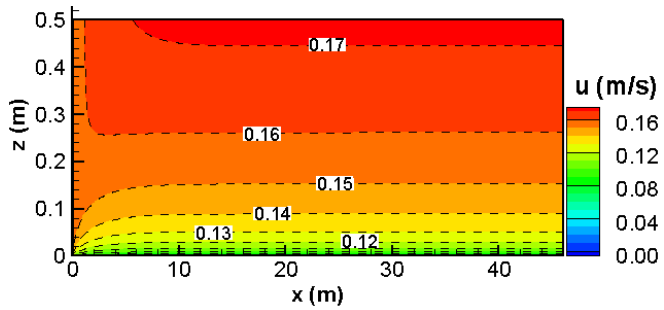


*Figure 5.13 Spatial distribution of Quasi-Eulerian mean velocity in CO condition*

The comparison between numerical results and experimental data in the middle of the flume is given in Figure 5.14. The comparison is given in both the linear scale and semilogarithmic scale. It shows that the mean current profile calculated with the 2DV model closely followed the experimental data. The agreement was good not only in the upper part of the water column but also close to the bed.

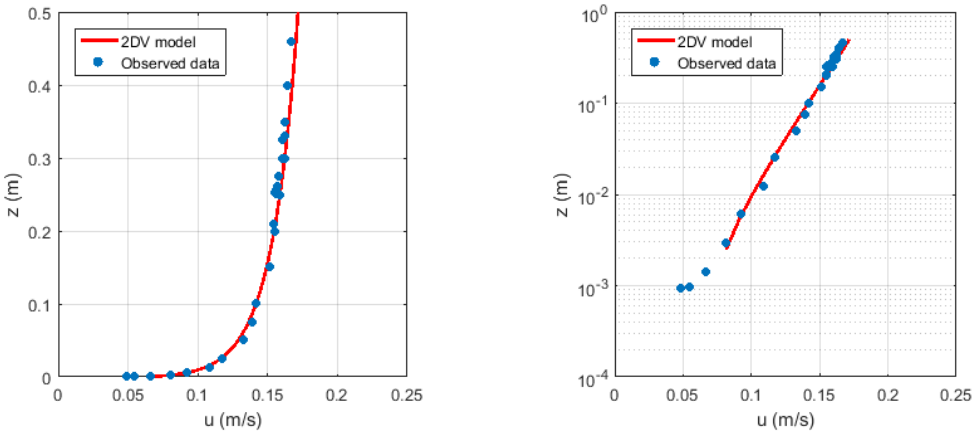


(a) Linear scale (b) Semilogarithmic scale

*Figure 5.14 Vertical distribution of Quasi-Eulerian mean velocity in CO condition*

In Figure 5.15, the spatial distributions of Stokes drift and Quasi-Eulerian mean velocity in the WO condition are presented. In this, surface waves are imposed at $x = 45$ m and propagated towards the left. The Stokes drift was in the direction of the waves, whereas the Quasi-Eulerian mean velocity was in the opposite direction. The magnitude of Stokes drift and Quasi-Eulerian mean velocity decreased in the wave propagation direction due to the effect of bottom friction. However, the momentum transport of total flow through any vertical section was zero.

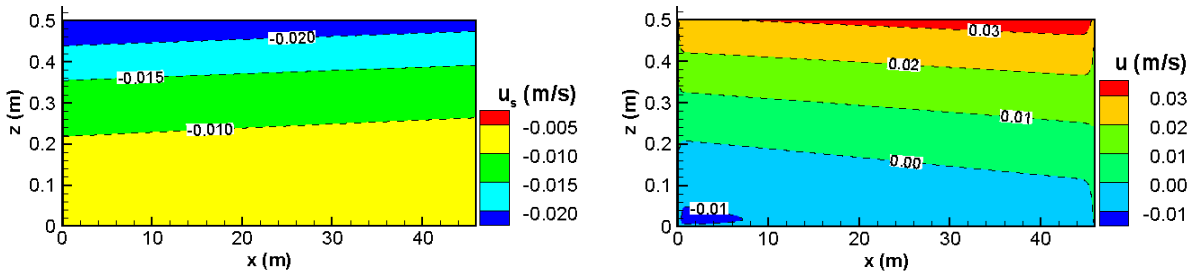


(a) Stokes drift (b) Quasi-Eulerian mean velocity

*Figure 5.15 Spatial distribution of mean velocity fields in the WO condition*

The comparison between the Quasi-Eulerian mean velocity calculated with the 2DV model and experimental data in the WO condition is given in Figure 5.16. It shows a very good agreement between model results and experimental data in the whole vertical section even on both linear scale and semilogarithmic scale. The near-bed wave-induced streaming is in the wave propagation direction. The mean horizontal velocity varied near-linearly from above the bottom streaming layer up to the mean surface level.

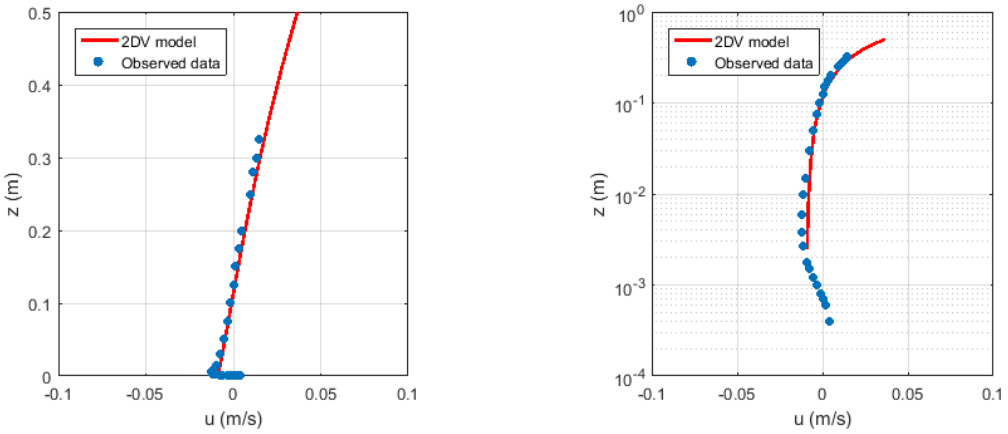


(a) Linear scale (b) Semilogarithmic scale

*Figure 5.16 Vertical distribution of Quasi-Eulerian mean velocity in the WO condition*

The spatial distribution of Quasi-Eulerian mean velocity in conditions of WFC and WOC is presented in Figure 5.17. In the case of WFC, the magnitude of the mean velocity was not the biggest at the water surface but located inside the water column. In the case of WOC, the magnitude of velocity increased from the bottom to the water surface.

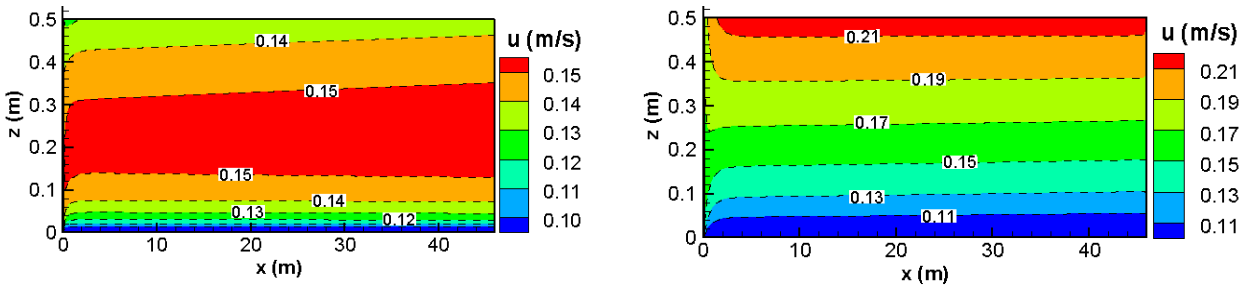


(a) WFC (b) WOC

*Figure 5.17 Spatial distribution of Quasi-Eulerian mean velocity*

Figure 5.18 shows the comparisons between experimental data and numerical model results under the condition of waves combined with the current on a linear scale. It shows that the vertical profile of the mean velocity calculated by the 2DV model fits well with experimental data in the whole water column. The agreement holds for both WFC and WOC conditions.

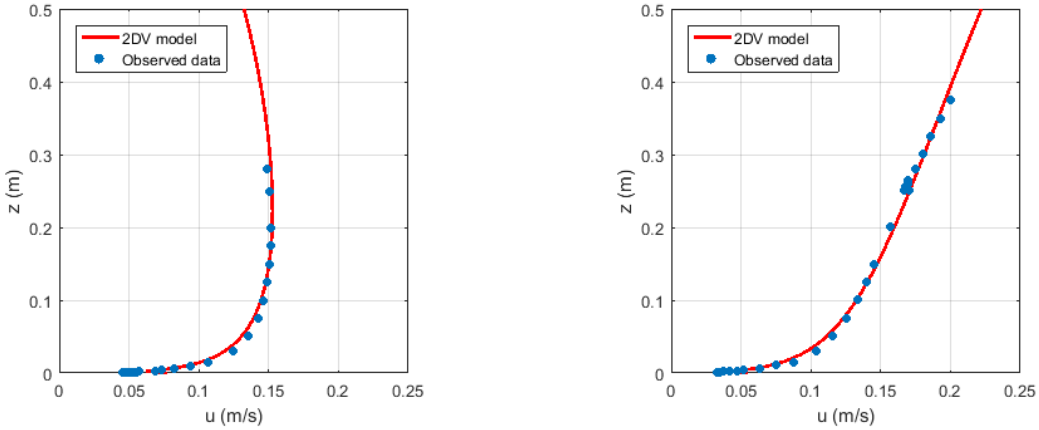


(a) WFC (b) WOC

*Figure 5.18 Distribution of Quasi-Eulerian mean velocity in the linear scale*

In Figure 5.19, the semilogarithmic scale is employed to see the agreement between the 2DV model results and experimental results.

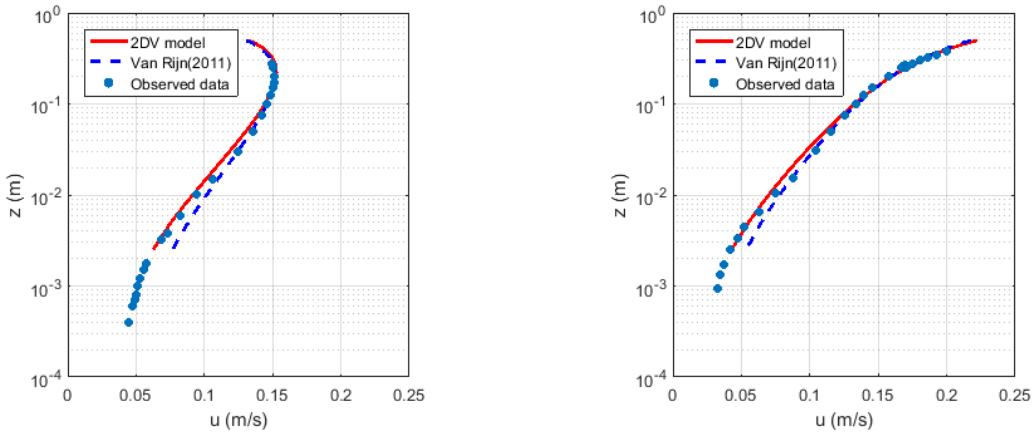


(a) WFC (b) WOC

*Figure 5.19 Distribution of Quasi-Eulerian mean velocity in the semilogarithmic scale*

It shows that the agreement between the 2DV model results and experimental data was very good even in the area very close to the bed. Besides, the mean current velocity profiles using the boundary layer thickness formulation proposed by Van Rijn (2011) (Formula (5.30)) were also plotted (dashed line). The result calculated by the modified formulation (5.31) was better than the result calculated by the formulation of Van Rijn (2011), especially in the region close to the bed. It is noticed that the formula to calculate boundary layer thickness $\delta$, i.e., Formula (5.31), is an extension of the formula proposed by Van Rijn (2011) (Formula (5.30)). In Formula (5.31), the effect of near-bed current is accounted for when calculating $\delta$. Table 2 presents boundary layer thickness $\delta$ in different conditions of waves combined with the current. In the wave-only condition, formulas (5.31) and (5.30) are identical. However, the difference between them is significant in cases of a strong ambient current.

## 5.5 BREAKING WAVES PROPAGATING IN A WAVE FLUME

### 5.5.1 Bathymetry and the wave properties at the boundary

The experiment of Boers (2005) was carried out in a wave flume with dimensions of 40 m long, 1.05 m high, and 0.8 m wide. The bottom of the flume is filled with sand and mortar on the top layer. Two breaker bars are designed at the bottom. The still water level is fixed at the level z = 0 m. Bottom profile of calculation area is depicted in Figure 5.20.

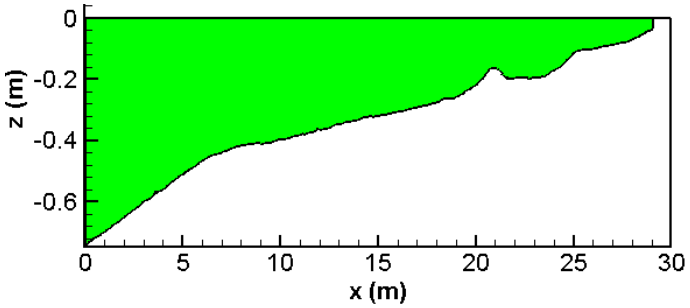


*Figure 5.20 The bottom profile*

Two wave conditions with the highest and lowest wave height at the boundary in the experiment of Boers (2005) are employed in this work (tests 1B and 1C). The properties of the waves at the offshore boundary are given in Table 5-5, where $H_s$ is the significant wave height of the waves.

*Table 5-5 Wave properties at the offshore boundary.*

| **Experiment** | $H_s$ **(m)** | $T_p$ **(s)** |
|---|---|---|
| Test 1B | 0.206 | 2.03 |
| Test 1C | 0.103 | 3.33 |

## 5.5.2 Boundary conditions

a) Surface and bottom boundary conditions

At the GLM water surface, the total shear stress is assumed to vanish, i.e.:

$$\left[\left(\upsilon_v + K_{fr} + K_b\right)\frac{\partial \overline{u}}{\partial z}\right]_{z=\overline{\xi}^L} = 0, \tag{5.62}$$

where, $\upsilon_v = \upsilon_{mol} + \upsilon_v^T$.

At the bed, the momentum dissipated by bottom friction is assumed to be transferred to the vertical mixing, i.e.:

$$\left[\left(\upsilon_v + K_{fr} + K_b\right)\frac{\partial \overline{u}}{\partial z}\right]_{z=-h} = -\frac{k_1 D_f}{\rho\sigma} - \frac{\overline{\tau}_{cw,x}}{\rho}. \tag{5.63}$$

b) Lateral boundary conditions

At the offshore boundary, the following conditions are applied:

$$\overline{\zeta} = -\frac{ka^2}{2\sinh 2kD}, \tag{5.64}$$

$$\overline{u} = -\frac{1}{h+\overline{\zeta}^L}\int_{-h}^{\overline{\zeta}^L} \overline{u}^S dz. \tag{5.65}$$

At the land boundary, the GLM velocity is zero. Then, we have:

$$\overline{u}(z) = -\overline{u}^S(z). \tag{5.66}$$

### 5.5.3 Model validation

In the experiment, the cross-shore distribution of significant wave height was calculated from the zeroth-order spectral moment of surface elevation (Boers, 2005), that is:

$$H_s = 4\sqrt{\int_0^{f_N} S(f)df}, \tag{5.67}$$

where, $S(f)$ is the spectral energy density, and $f_N$ is the Nyquist frequency of the measurements ($\approx 10$ Hz).

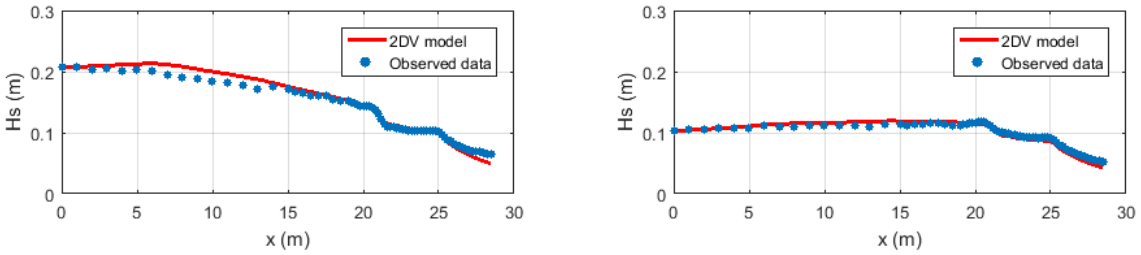


(a) Test 1B (b) Test 1C

*Figure 5.21 Distribution of significant wave height*

The significant wave height in the 2DV numerical model is calculated from the wave energy balance equation (5.1). In Figure 5.21, the spatial distributions of significant wave height in tests 1B and 1C are presented. In this, the dots present the experimental data, and the solid line presents the numerical model results. It shows that the numerical model results fit well with measured data. In test 1B, the experimental data was slightly lower than the model results in the region from x = 5 m to x = 14 m. In test 1C, the recirculation was rather small then a better agreement between two kinds of data was obtained.

Figure 5.22 shows the vertical distribution of the forcing term $F_{w,1}/\rho$ and total mixing term $F_{tot,1}/\rho$ at $x = 22.9$ m. It shows that the wave-induced forcing $F_{w,1}/\rho$ is completely balanced by total mixing $F_{tot,1}/\rho$. Total forcing $\left(F_{w,1}+F_{tot,1}\right)$ is depth-uniform in breaking wave conditions.

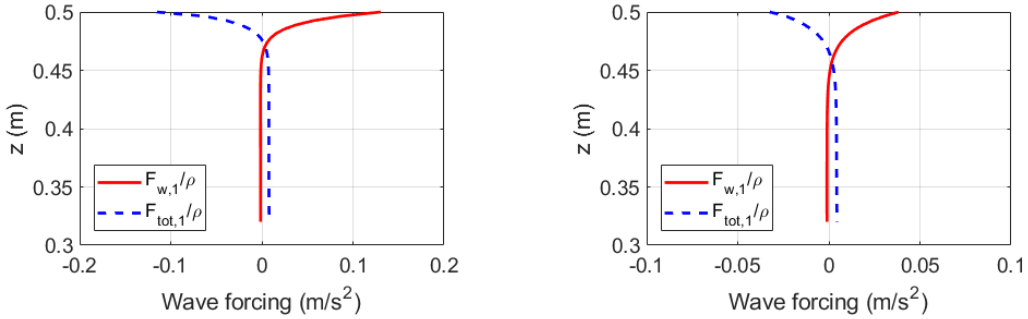


(a) Test 1B (b) Test 1C

*Figure 5.22 Distribution of wave-induced forcing terms at* $x = 22.9\,m$

The comparison of the mean water level calculated by the 2DV numerical model with measured data is given in Figure 5.23. In both tests, the calculated mean water level fits well with measured data even in the breaking wave area.

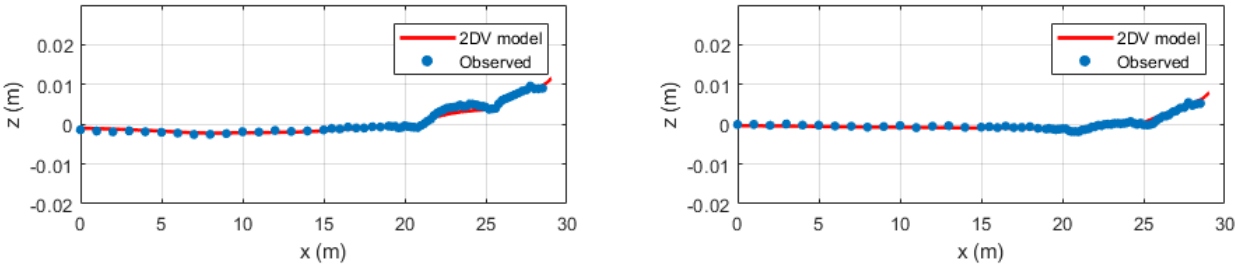


(a) Test 1B (b) Test 1C

*Figure 5.23 Distribution of mean water level* $\overline{\zeta}$

The horizontal distribution of Stokes drifts and Quasi-Eulerian mean velocities calculated by the 2DV model is presented in Figure 5.24.

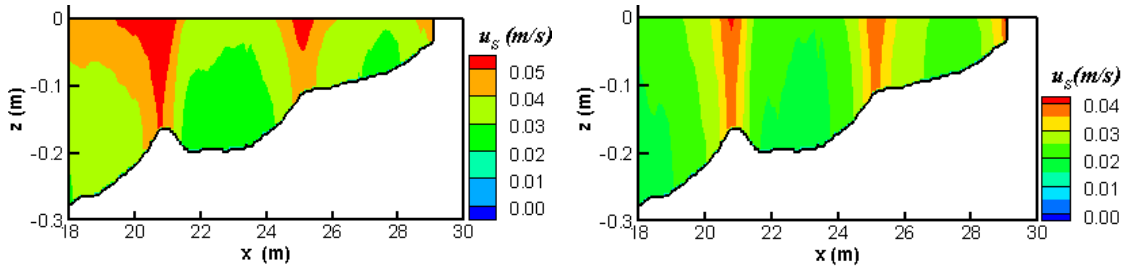


(a) Test 1B (b) Test 1C

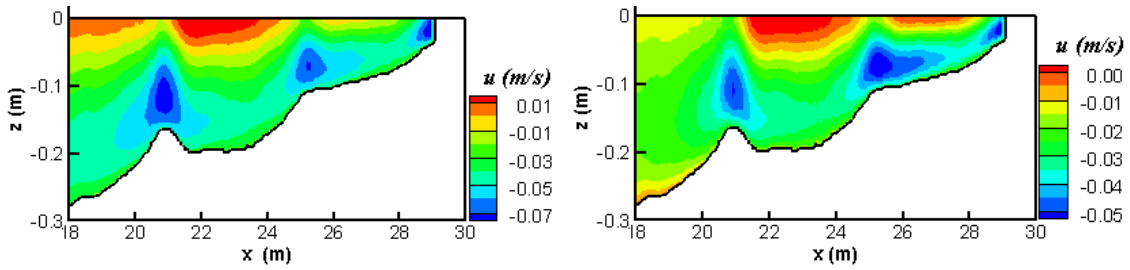


(c) Test 1B (d) Test 1C

*Figure 5.24 Distribution of Stokes drift (a,b) and Quasi-Eulerian mean velocity (c,d)*

Figure 5.24(a) and Figure 5.24(b) show the spatial distribution of Stokes drift in Test 1B and Test 1C. The Stokes drift reaches local maximum above the peak of sandbars. Figure 5.24(c) and Figure 5.24(d) present the spatial distribution of Quasi-Eulerian mean velocity in Test 1B and Test 1C, respectively. We can see a spatial lag between the location of the maximum wave-induced current at the surface level and the location of the breaking wave. This spatial lag is caused by roller effects. Besides, Figure 5.24(c) and Figure 5.24(d) show that the direction of the mean current at the upper part of the water column is shoreward. Whereas, the mean current at the lower part of the water column is offshore direction.

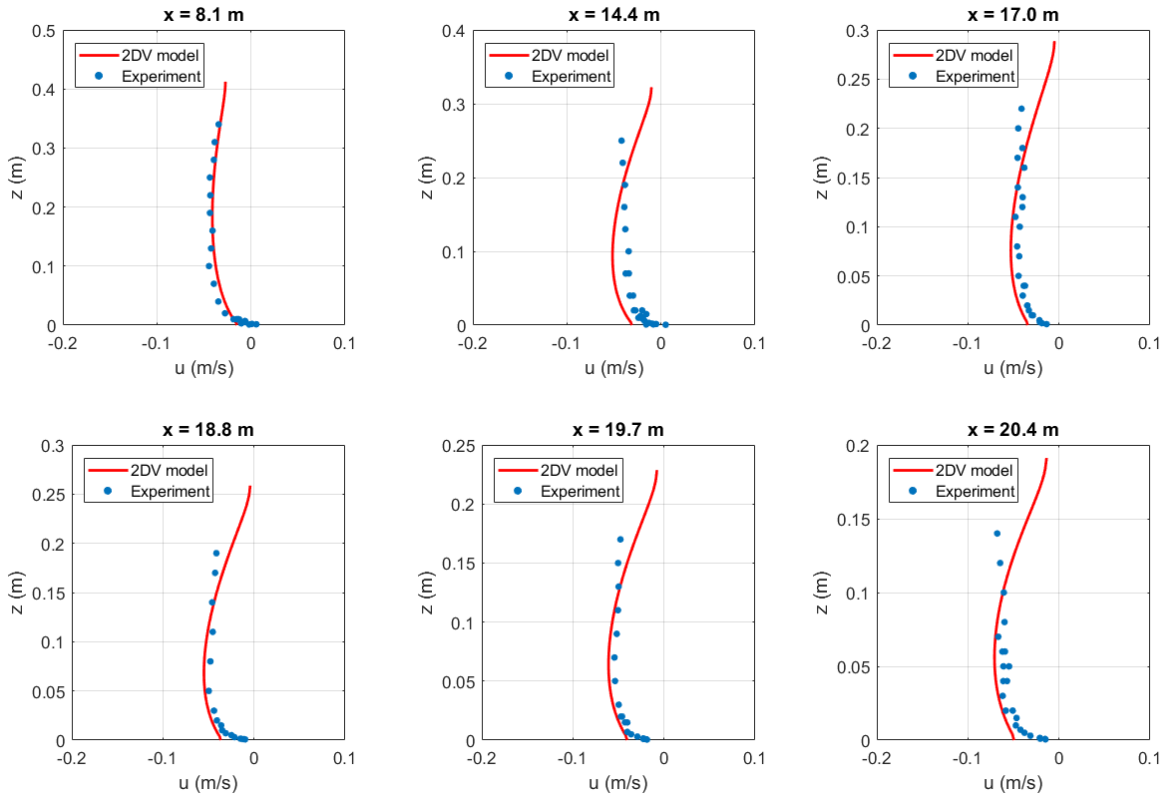

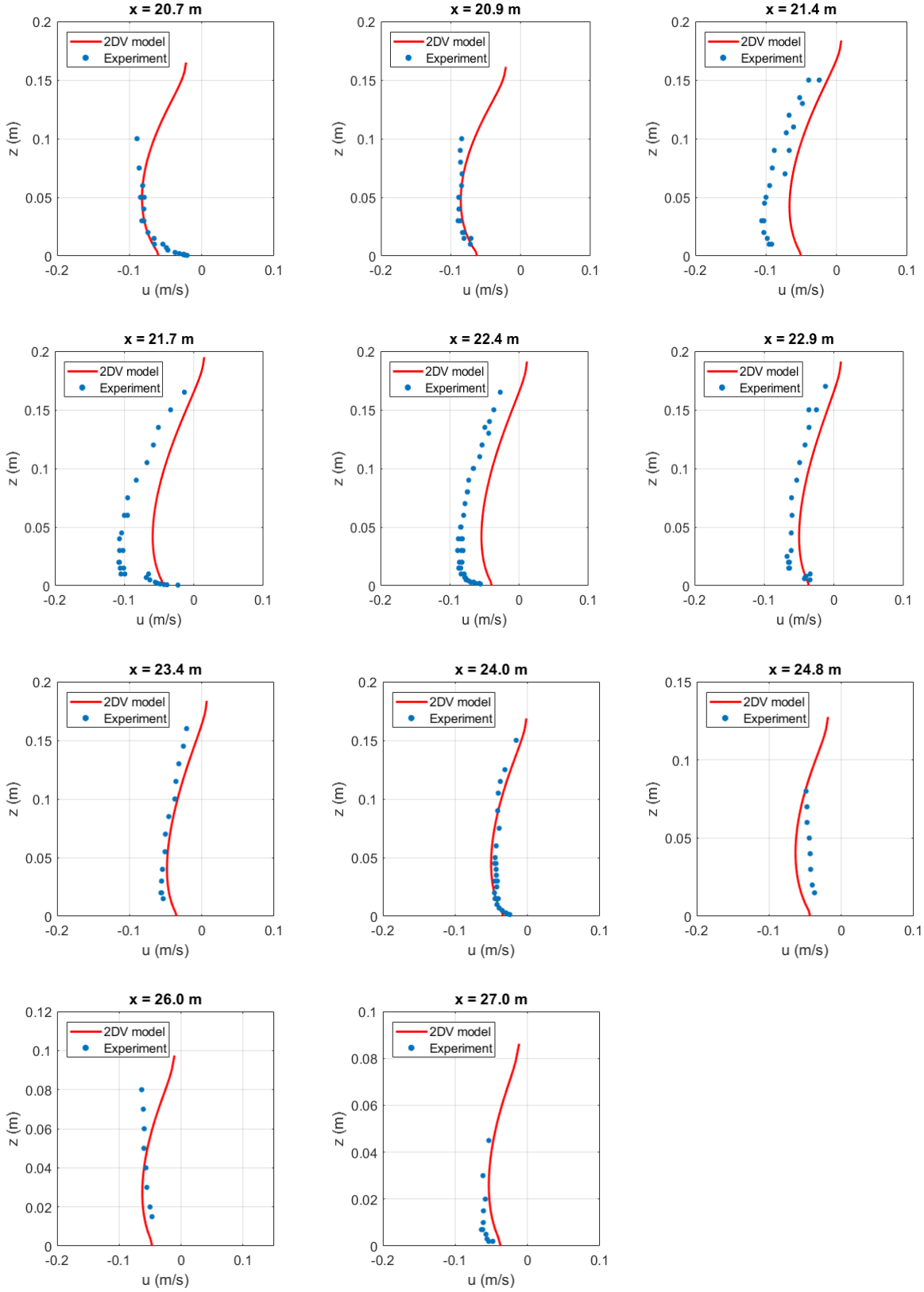


*Figure 5.25 Vertical distribution of horizontal mean velocity in test 1B*

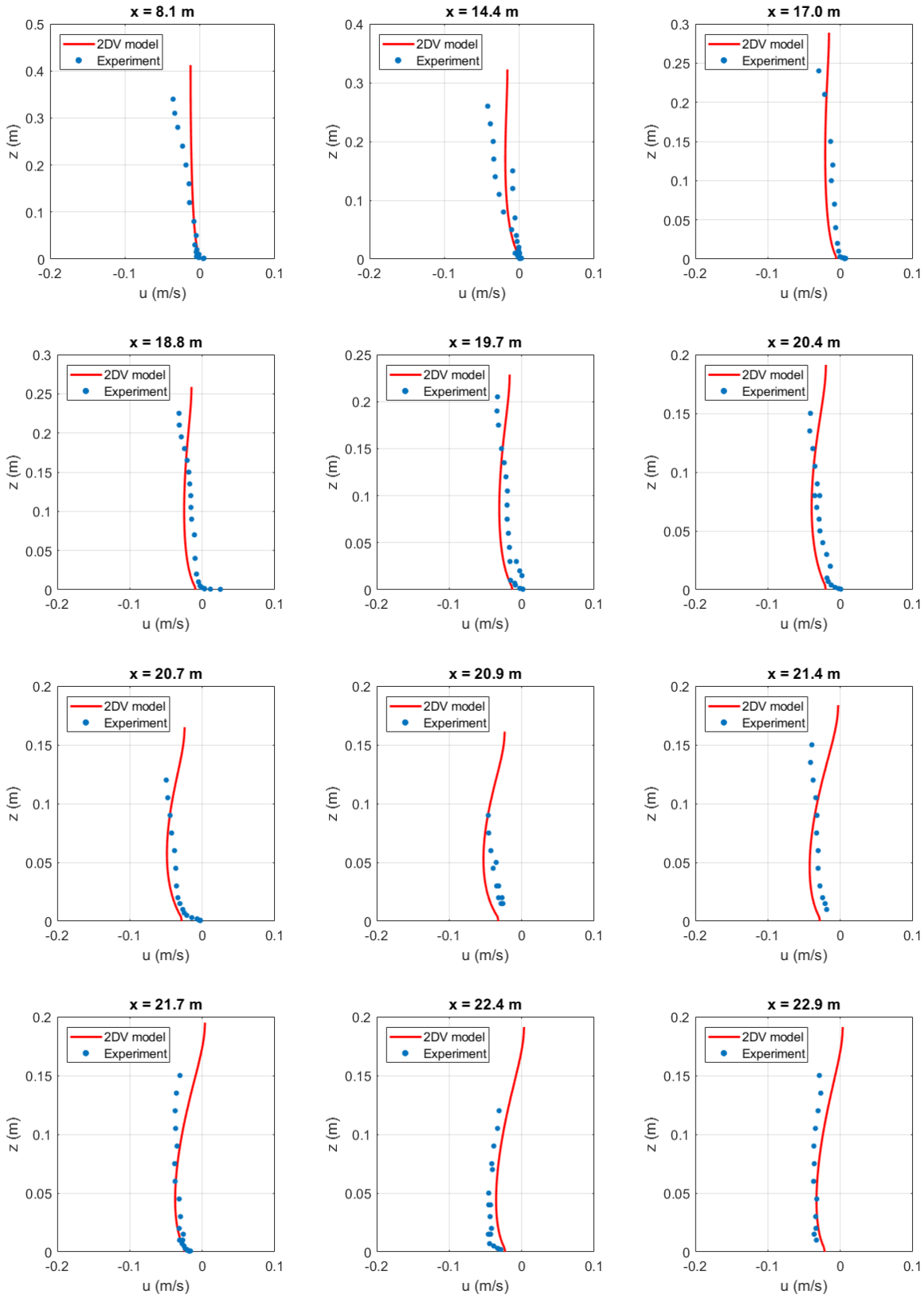
x = 8.1 m
x = 14.4 m
x = 17.0 m
x = 18.8 m
x = 19.7 m
x = 20.4 m
x = 20.7 m
x = 20.9 m
x = 21.4 m
x = 21.7 m
x = 22.4 m
x = 22.9 m
2DV model
Experiment
z (m)
u (m/s)

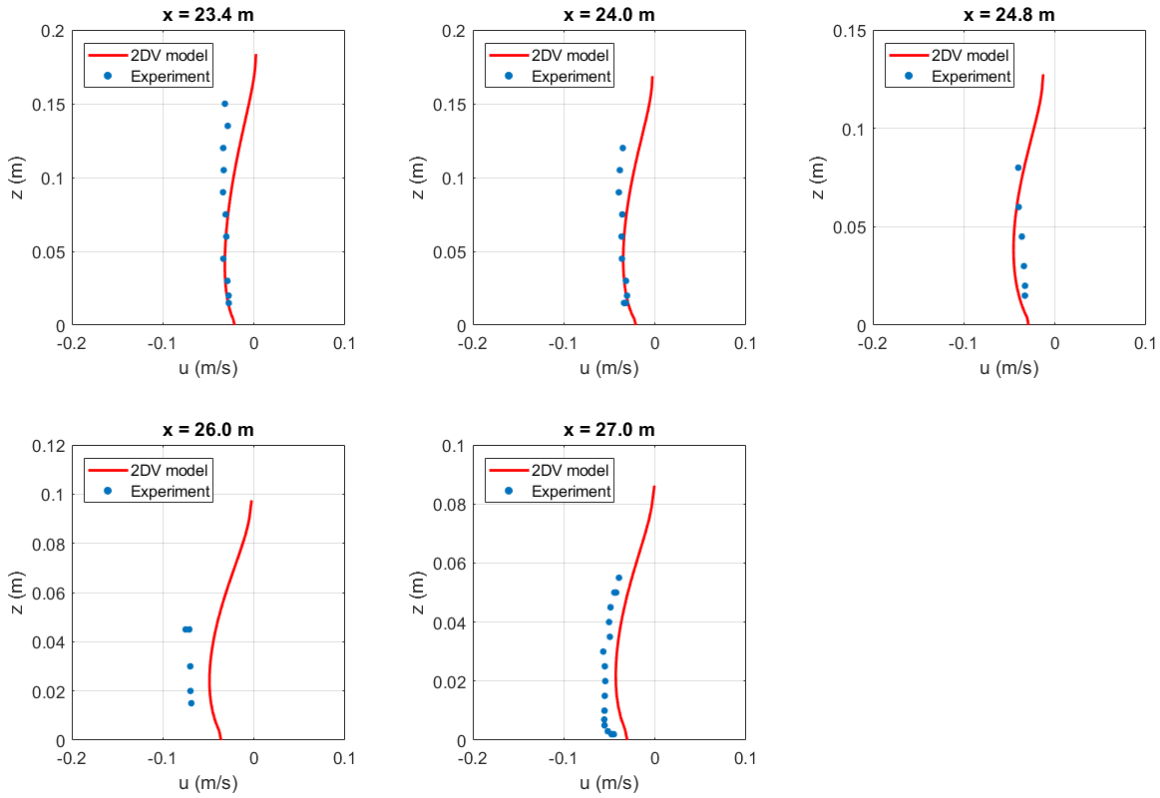


*Figure 5.26 Vertical distribution of horizontal mean velocity in test 1C*

The comparison between Quasi-Eulerian mean velocities calculated by the 2DV numerical model and measured data along the wave flume is given in Figure 5.25 and Figure 5.26.

Overall, the 2DV model simulated quite well the vertical distribution of the mean velocity. In comparison with test 1B, the model results for test 1C show a better agreement with experimental data, especially near the sandbars. It suggests that empirical formulas of Uchiyama *et al.* (2010) can be applied well for small-amplitude waves. For the waves of high amplitude, these empirical formulas just give qualitative results in the breaking zone. Besides, in the 2DV model, the roller-induced mass flux is not taken into account. The inclusion of that flux might improve the results. Further research on the wave forcing in breaking wave areas is needed.

## 5.6 BREAKING WAVES PROPAGATING IN A LARGE-SCALE FACILITY

### 5.6.1 Laboratory setup

In this section, the 2DV model was employed to simulate the cross-shore and the longshore currents with the input data obtained from the large-scale sediment transport

facility (LSTF). The design of the LSTF is presented in detail in the paper of Hamilton and Ebersole (2001). The facility has dimensions of approximately 30 m cross-shore by 50 m longshore by 1.4 m deep. The concrete beach has a longshore dimension of 31 m and a cross-shore dimension of 21 m, with a slope of 1:30. Unidirectional long-crested waves were generated with four piston-type wave generators. An active pumping and recirculation system comprised of 20 independent pumps and pipelines was used to control the cross-shore distribution of mean longshore current. Pumping rates were adjusted iteratively to converge toward the proper setting, based on the measurements along the beach.

The wave conditions at the offshore boundary are given in Table 5-6. The TMA spectrum (self-similar spectral shape) with the width parameter of 3.3 was employed. It is an extension of deep water spectrum JONSWAP for applications in shallow water.

*Table 5-6 Incident wave properties at the boundary*

| **Wave type** | $T_p$ (s) | $H_s$ (m) | $\theta\left(^0\right)$ | $h$ (m) |
|---|---|---|---|---|
| Irregular | 2.5 | 0.225 | 10 | 0.667 |

## 5.6.2 Boundary conditions

a) Surface and bottom boundary conditions

At the GLM water surface, the total shear stress is assumed to vanish. Therefore, the surface boundary conditions are:

$$\left[\left(\upsilon_v + K_{fr} + K_b\right)\frac{\partial \overline{u}}{\partial z}\right]_{z=\overline{\zeta}^L} = 0, \tag{5.68}$$

$$\left[\left(\upsilon_v + K_{fr} + K_b\right)\frac{\partial \overline{v}}{\partial z}\right]_{z=\overline{\zeta}^L} = 0, \tag{5.69}$$

where, $\upsilon_v = \upsilon_{mol} + \upsilon_v^T$.

The bottom boundary condition in the cross-shore direction is given by:

$$\left[\left(\upsilon_v + K_{fr} + K_b\right)\frac{\partial \overline{u}}{\partial z}\right]_{z=-h} = -\frac{k_1 D_f}{\rho\sigma} - \frac{\overline{\tau}_{cw,1}}{\rho}. \tag{5.70}$$

According to Longuet-Higgins (1970), the bed shear stress in the longshore direction can be calculated based on the local rate of energy dissipation. In the following, their formula is corrected with the bed shear stress caused by the mean current $\overline{\tau}_c$. Therefore, we have:

$$\overline{\tau}_{cw,2} = -\frac{k_2\left[\left(1-\alpha_r\right)D_w + D_r + D_f\right]}{\sigma} + \overline{\tau}_{c,2}. \tag{5.71}$$

From equations (5.25) and (5.71) the longshore current near the bed is calculated by:

$$\overline{v}_b = -\frac{2}{\rho f_{cw}\sqrt{(1.16s)^2 + \left(\overline{u}_b^2 + \overline{v}_b^2\right)}}\left\{\overline{\tau}_{c,2} - \frac{2k_2\left[\left(1-\alpha_r\right)D_w + D_r + D_f\right]}{\rho\sigma f_{cw}\sqrt{(1.16s)^2 + \left|\overline{\mathbf{u}}_b\right|^2}}\right\}. \tag{5.72}$$

b) Lateral boundary conditions

At the offshore, boundary conditions for Quasi-Eulerian mean water level and Quasi-Eulerian mean velocity components are:

$$\overline{\zeta} = -\frac{ka^2}{2\sinh 2kh}, \tag{5.73}$$

$$\overline{u} = -\frac{1}{h+\overline{\zeta}^L}\int_{-h}^{\overline{\zeta}^L}\overline{u}^S dz, \tag{5.74}$$

$$\overline{v} = \overline{u}\tan\theta. \tag{5.75}$$

At the land boundary, the GLM velocity in the $x$-direction is zero. Besides, the no-slip boundary condition is assumed for Quasi-Eulerian velocity in the $y$-direction. Then:

$$\overline{u}(z) = -\overline{u}^S(z), \tag{5.76}$$

$$\overline{v}(z) = 0. \tag{5.77}$$

## 5.6.3 Numerical results and discussion

Figure 5.27 shows the comparison of significant wave height between experimental data and numerical results calculated by the 2DV model. The comparison shows a very good agreement between experimental data and model results.

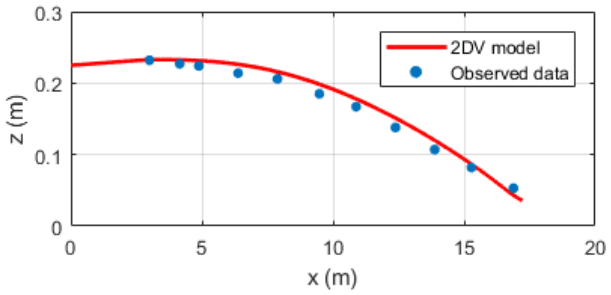


*Figure 5.27 Distribution of significant wave height*

In Figure 5.28, a comparison of the mean water level between experimental data and the 2DV model result is given. There was a small difference of about a few millimeters

outside the breaking zone. The difference between these two kinds of data was bigger in the area closer to the coastline. It might be due to the recirculation system of the facility or because the experimental data was for a closed basin, so the volume of water in the setup was taken from offshore.

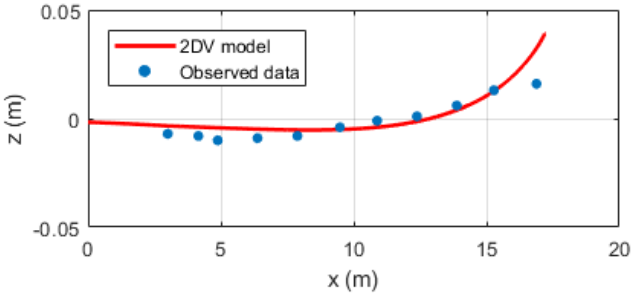


*Figure 5.28 Distribution of mean water level*

a) Cross-shore direction

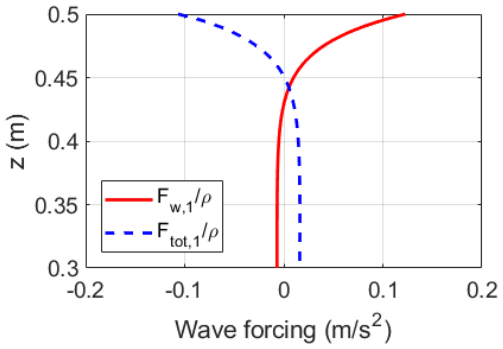


*Figure 5.29 Vertical distribution of wave-induced forcing terms*

Figure 5.29 presents the vertical distribution of wave forcing term $F_{w,1}/\rho$ and total mixing $F_{tot,1}/\rho$ at the location $x = 10.9$ m. It shows that momentum caused by wave forcing was completely compensated by total mixing. The total of these two forcing terms was depth uniform.

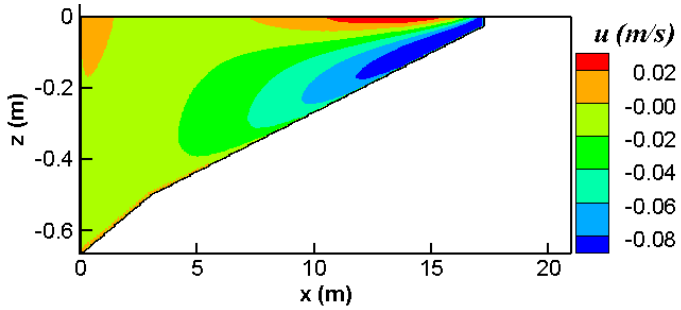


*Figure 5.30 Distribution of cross-shore velocity*

Figure 5.30 shows an overview of the spatial distribution of cross-shore velocity calculated by the 2DV model. It shows that outside the wave breaking zone, the vertical distribution of the Quasi-Eulerian mean velocity was almost uniform. However, inside the wave breaking zone, the mean velocity shows a strong vertical shear.

The LSTF data was also employed by Teles *et al.* (2013) to validate the TELEMAC 3D model. In Figure 5.31, comparisons of cross-shore mean velocities between experimental data, results of the TELEMAC 3D model, and results of the 2DV model were carried out at six cross-shore locations.

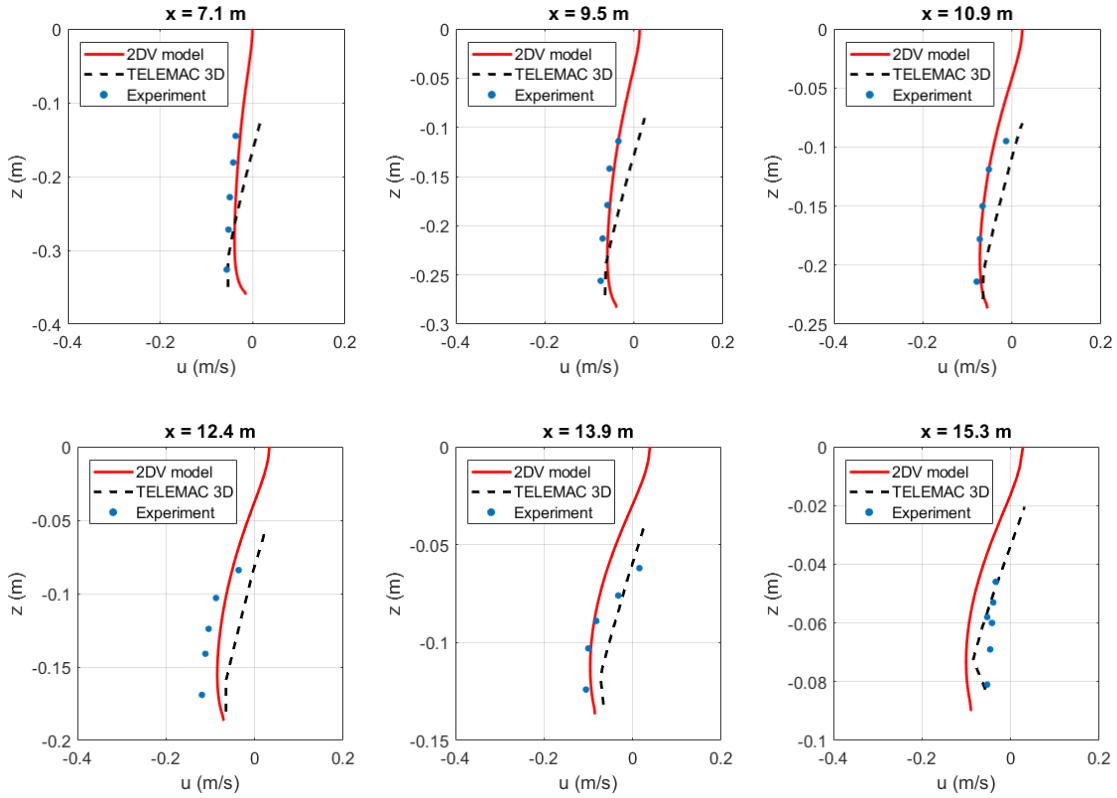


*Figure 5.31 Vertical profiles of cross-shore velocity*

The results obtained from the 2DV model fit quite well with the experimental data, and are much better than the results obtained by the TELEMAC 3D model in most of the cross-sections. Closer to the surface and the land boundary the difference between experimental data and 2DV model results became bigger. The difference might be due to the use of empirical formulas for the wave-induced forcing, and the return flow in the facility. Improvement of these formulas by making use of the large body of literature on the return flow profiles is recommendable but outside the scope of this study.

b) Longshore direction

Figure 5.32 shows the vertical distribution of the wave-induced forcing $F_{w,2}/\rho$ and total mixing $F_{tot,2}/\rho$ in the longshore direction at $x = 10.9$ m. It shows that the total mixing $F_{tot,2}$ is balanced by wave-induced forcing $F_{tot,2}$. The total forcing $\left(F_{w,2} + F_{tot,2}\right)$ is depth uniform.

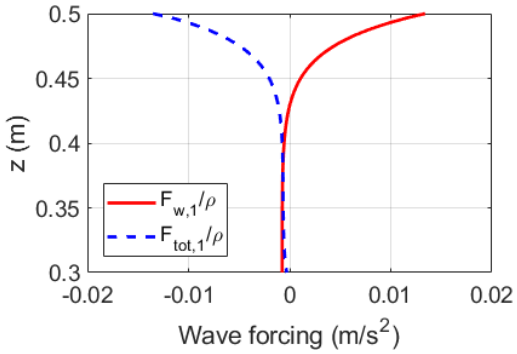


*Figure 5.32 Vertical distribution of wave-induced forcing terms*

The cross-shore distribution of the longshore velocity calculated by the 2DV numerical model is presented in Figure 5.33. According to the results, the longshore velocity increases shoreward. The maximum magnitude of the longshore velocity reached approximately 0.35 m/s at the position $x \approx 14$ m. After this point, the longshore velocity decreased toward the shoreline.

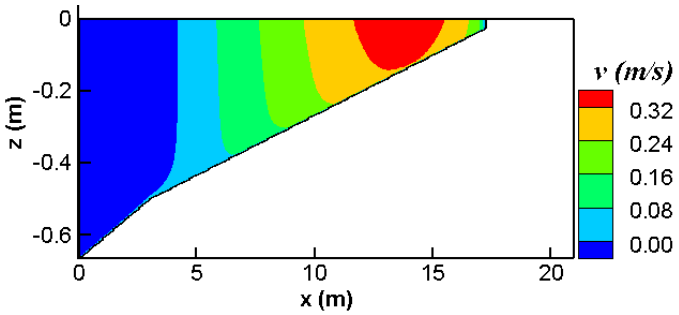


*Figure 5.33 Distribution of the longshore velocity*

In Figure 5.34, a comparison between experimental data and numerical results at one-third of the water depth above the bottom is given. It shows that the results obtained by the 2DV model agreed well with the experimental data and matched the observed cross-shore distribution better than the results obtained by the TELEMAC 3D model.

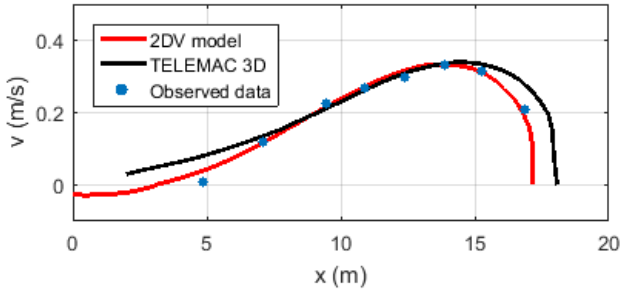


*Figure 5.34 Longshore velocity at* $z = -2h/3$

The comparison of the longshore velocities at different vertical cross-sections is given in Figure 5.35. The results of the TELEMAC 3D model show quite good agreement at four locations from x = 9.5 m to x = 13.9 m. However, at the location near the offshore x = 7.1 m and the location near the coastline x = 15.3 m the differences between experimental data and results from the TELEMAC 3D model were significant. In contrast, the results of the 2DV model show good agreement with experimental data at all six cross-sections.

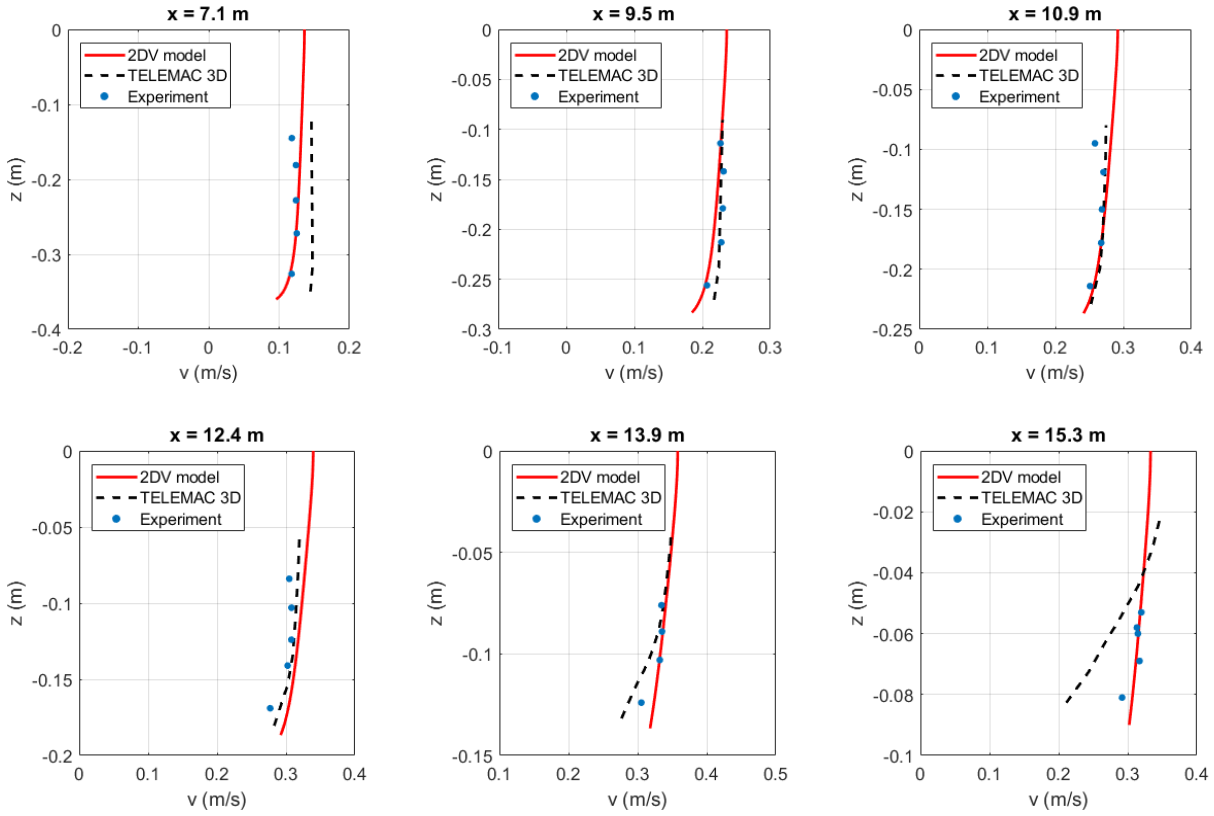


*Figure 5.35 Vertical profiles of the longshore velocity at different locations*

## 5.7 DISCUSSION

Following Van Rijn (2011), the bottom boundary layer thickness $\delta$ was calculated by the formula (5.30). In this, the effect of mean current on bottom boundary layer thickness was neglected. However, interactions of the current with the wave boundary layer and waves with current boundary layer led to the enhancement of current-induced friction, wave energy dissipation, and bed shear stress. Then, both waves and current should be considered in calculating bottom boundary thickness. In this study, the formula given by Van Rijn (2011) was modified to take into account the effect of ambient currents. The use of the modified formula provided a better agreement with experimental data than the use of the original formula of Van Rijn (2011).

In the work of Nielsen and You (1997), an empirical coefficient $C_{WR}$ was proposed to account for the effect of strong ambient currents on the vertical distribution of wave radiation stress components. However, that coefficient is only applied to regular waves. In this study, a modified formula was proposed to apply to random waves. With that modification, the mean current profiles calculated by the 2DV model agreed well with experimental data obtained by Klopman (1994).

In breaking wave conditions, dissipative wave forcing terms were estimated by using empirical formulas introduced by Uchiyama *et al.* (2010). The cross-shore velocity profiles obtained by the 2DV model showed good agreement with experimental data presented in the works of Boers (2005) and Hamilton and Ebersole (2001). However, there are differences between model results and observed data near the breaking points. It requires further research on the vertical distribution of wave breaking induced forcing. In the longshore direction, the effect of breaking wave-induced forcing was small. Then, the longshore current data calculated by the 2DV model fitted very well with experimental data.

The LSTF test was also employed by Teles *et al.* (2013) to validate the TELEMAC 3D model. That model was developed based on the work of Ardhuin *et al.* (2008), and Bennis *et al.* (2011). As indicated by Ardhuin *et al.* (2008), their equations are only expected to give qualitative results for surfzone applications. The comparison presented in the previous part also showed that the 2DV model obtained a better agreement with observed data than TELEMAC 3D model.

# 6

# COMPARISONS WITH OTHER SETS OF EQUATIONS OF MEAN MOTION[4]

[4] This Chapter is presented in the publication: Nguyen, D.T., Reniers, A.J.H.M., Roelvink, D., 2021b. Relationship between Three-Dimensional Radiation Stress and Vortex-Force Representations. Ibid., 791.

## 6.1 COMPARISON WITH EQUATIONS OF MOTION OF WALSTRA *ET AL.* (2001)

A set of equations of mean motion of Walstra *et al.* (2001) has been implemented in the Delft3D-FLOW model. Details of the implementation are given in Deltares (2014). It is the simplification of a set of equations developed by Groeneweg (1999). In the following, horizontal momentum equations of Walstra *et al.* (2001) are expressed with the addition of the Coriolis effect and gradient of atmospheric pressure, i.e.:

$$\begin{aligned}&\frac{\partial \overline{u}^L}{\partial t}+\overline{u}^L\frac{\partial \overline{u}^L}{\partial x}+\overline{v}^L\frac{\partial \overline{u}^L}{\partial y}+\overline{w}^L\frac{\partial \overline{u}^L}{\partial z}-f\overline{v}^L=-\frac{1}{\rho}\frac{\partial \overline{p}_a}{\partial x}-g\frac{\partial \overline{\zeta}^L}{\partial x}\\&+\frac{1}{\rho}\left(\frac{\overline{\tau}_{11}^L}{\partial x}+\frac{\overline{\tau}_{12}^L}{\partial y}+\frac{\overline{\tau}_{13}^L}{\partial z}\right)+\overline{S}_1^L,\end{aligned} \tag{5.78}$$

$$\begin{aligned}&\frac{\partial \overline{v}^L}{\partial t}+\overline{u}^L\frac{\partial \overline{v}^L}{\partial x}+\overline{v}^L\frac{\partial \overline{v}^L}{\partial y}+\overline{w}^L\frac{\partial \overline{v}^L}{\partial z}+f\overline{u}^L=-\frac{1}{\rho}\frac{\partial \overline{p}_a}{\partial y}-g\frac{\partial \overline{\zeta}^L}{\partial y}\\&+\frac{1}{\rho}\left(\frac{\overline{\tau}_{21}^L}{\partial x}+\frac{\overline{\tau}_{22}^L}{\partial y}+\frac{\overline{\tau}_{23}^L}{\partial z}\right)+\overline{S}_2^L,\end{aligned} \tag{5.79}$$

where, $\overline{\tau}^L$ is GLM turbulent stress, $\overline{S}_1^L$ and $\overline{S}_2^L$ are wave-induced driving forces given by:

$$\overline{S}_1^L=-\frac{1}{\rho}\left(\frac{\overline{\tau}_{11}^s}{\partial x}+\frac{\overline{\tau}_{12}^s}{\partial y}+\frac{\overline{\tau}_{13}^s}{\partial z}\right)-\left(\frac{\partial \overline{\tilde{u}^2}}{\partial x}+\frac{\partial \overline{\tilde{u}\tilde{v}}}{\partial y}+\frac{\partial \overline{\tilde{u}\tilde{w}}}{\partial z}\right)+\mathrm{O}(\varepsilon^3), \tag{5.80}$$

$$\overline{S}_2^L=-\frac{1}{\rho}\left(\frac{\overline{\tau}_{21}^s}{\partial x}+\frac{\overline{\tau}_{22}^s}{\partial y}+\frac{\overline{\tau}_{23}^s}{\partial z}\right)-\left(\frac{\partial \overline{\tilde{v}\tilde{u}}}{\partial x}+\frac{\partial \overline{\tilde{v}^2}}{\partial y}+\frac{\partial \overline{\tilde{v}\tilde{w}}}{\partial z}\right)+\mathrm{O}(\varepsilon^3), \tag{5.81}$$

where, $\overline{\tau}^S$ is Stokes correction of turbulent stress.

The depth-integrated continuity equation is:

$$\frac{\partial \overline{\zeta}^L}{\partial t}+\frac{\partial}{\partial x}\left(\int_{-h}^{\overline{\zeta}^L}\overline{u}^L dz\right)+\frac{\partial}{\partial y}\left(\int_{-h}^{\overline{\zeta}^L}\overline{v}^L dz\right)=0. \tag{5.82}$$

In Table 6-1, a comparison between equations of Walstra *et al.* (2001) and new equations expressed in the GLM framework is presented for the *x*-direction. It shows that the difference between Walstra *et al.* (2001) and equations of Nguyen *et al.* (2021a) mainly comes from the wave-induced forcing terms. It shows that the terms $T_1$ and $\rho^{-1}\partial\overline{p}^S/\partial x$ are absent in the conservative wave forcing term of Walstra *et al.* (2001). Those terms are considered in Groeneweg (1999), where $T_1$ corresponds to the evolution of $\overline{\xi_j u_i^l}$. The missing second-order of wave amplitude terms leads to an imbalance of the model and generates spurious oscillations, discussed below.

*Table 6-1 Comparison between equations of Walstra et al. (2001) and the new set of equations in the GLM framework*

| **Terms** | Walstra *et al.* (2001) | New equations |
|---|---|---|
| Pressure gradient | $-\frac{1}{\rho}\frac{\partial \overline{p}_a}{\partial x} - g\frac{\partial \overline{\zeta}^L}{\partial x}$ | $-\frac{1}{\rho}\frac{\partial \overline{p}_a}{\partial x} - g\frac{\partial \overline{\zeta}^L}{\partial x}$ |
| Conservative wave forcing | $-\left(\frac{\partial \overline{\tilde{u}^2}}{\partial x} + \frac{\partial \overline{\tilde{u}\tilde{v}}}{\partial y} + \frac{\partial \overline{\tilde{u}\tilde{w}}}{\partial z}\right)$ | $-\left(\frac{\partial \overline{\tilde{u}^2}}{\partial x} + \frac{\partial \overline{\tilde{u}\tilde{v}}}{\partial y} + \frac{\partial \overline{\tilde{u}\tilde{w}}_{CS}}{\partial z}\right)$ $+\frac{1}{\rho}\frac{\partial \overline{p}^S}{\partial x} + T_1$ |
| Non-conservative wave forcing | $-\frac{1}{\rho}\left(\frac{\overline{\tau}_{11}^s}{\partial x} + \frac{\overline{\tau}_{12}^s}{\partial y} + \frac{\overline{\tau}_{13}^s}{\partial z}\right)$ $\frac{F_{br,1}}{\rho}$ : applied as a surface stress $\frac{F_{fr,1}}{\rho}$ : applied as a bottom stress | $\frac{F_{br,1}}{\rho}$ : applied as a body force $\frac{F_{mx,1}}{\rho}$ : applied as a body force $\frac{F_{fr,1}}{\rho}$ : applied as a bottom stress |
| Turbulence | $\frac{1}{\rho}\left(\frac{\overline{\tau}_{11}^L}{\partial x} + \frac{\overline{\tau}_{12}^L}{\partial y} + \frac{\overline{\tau}_{13}^L}{\partial z}\right)$ | $\frac{1}{\rho}\left(\frac{\overline{\tau}_{11}^L}{\partial x} + \frac{\overline{\tau}_{12}^L}{\partial y} + \frac{\overline{\tau}_{13}^L}{\partial z}\right)$ |
| Mass conservation | $\frac{\partial \overline{\zeta}^L}{\partial t} + \frac{\partial}{\partial x}\left(\int_{-h}^{\overline{\zeta}^L} \overline{u}^L dz\right)$ $+\frac{\partial}{\partial y}\left(\int_{-h}^{\overline{\zeta}^L} \overline{v}^L dz\right) = 0$ | $\frac{\partial\left(\overline{\zeta}^L + h\right)}{\partial t} + \frac{\partial}{\partial x}\int_{-h}^{\overline{\zeta}^L} \overline{u}^L dz$ $+\frac{\partial}{\partial y}\int_{-h}^{\overline{\zeta}^L} \overline{v}^L dz = \frac{\partial \overline{\zeta}^S}{\partial t}$ |

Moreover, according to Nielsen and You (1997), the effect of a strong current on the normal component of wave radiation stress gradient $\partial\overline{\tilde{u}\tilde{w}}/\partial z$ is significant. This effect was not considered by Walstra *et al.* (2001). In new equations, the normal component of wave radiation stress is enhanced by a factor $C_{WR}$ that represents the effect of current on the wave radiation stress. The factor $C_{WR}$ is approximated to 1 in the condition of a weak current; however, it is significant in the presence of a strong current.

In Walstra *et al.* (2001), the breaking and roller wave-induced forcing term is provided as surface stress. The breaking induced turbulence is incorporated into the turbulence model as a surface boundary condition. However, this method is only suitable under the condition of strong vertical mixing due to breaking waves (Rascle *et al.*, 2006). In addition, the Stokes correction of turbulent stress is a term of third-order of the wave amplitude, i.e., $\rho^{-1}\partial\overline{\tau}_{ij}^{S}/\partial x_j = O(\varepsilon^3)$. Therefore, it can be neglected if equations of motion are expressed to the second-order of wave amplitude.

In new equations, the breaking wave and roller wave-induced forcing terms are applied as a body force. This method is suitable for both strong and weak vertical mixing conditions, where the empirical formulas proposed by Uchiyama *et al.* (2010) are applied to calculate the vertical distribution of wave breaking induced forcing term.

The mass conservation equation of Walstra *et al.* (2001) is equivalent to the new mass conservation equation if the surface waves change slowly in time.

In the following, an adiabatic test proposed by Bennis *et al.* (2011) is employed to test the equations of Walstra *et al.* (2001). In this, a monochromatic wave propagates on a slope without dissipation. This is a simple but very challenging test since any imbalanced forces might lead to a spurious oscillation of the mean current. The horizontal mean current should be uniform in a vertical direction even if the wave propagates on a sloping bed. The new equations were successful in testing with the adiabatic condition.

In adiabatic condition, momentum equations (5.78) and (5.79) becomes:

$$\frac{\partial\overline{u}^{L}}{\partial t}+\overline{u}^{L}\frac{\partial\overline{u}^{L}}{\partial x}+\overline{v}^{L}\frac{\partial\overline{u}^{L}}{\partial y}+\overline{w}^{L}\frac{\partial\overline{u}^{L}}{\partial z}=-g\frac{\partial\overline{\zeta}^{L}}{\partial x}-\left(\frac{\partial\overline{\tilde{u}^{2}}}{\partial x}+\frac{\partial\overline{\tilde{u}\tilde{v}}}{\partial y}+\frac{\partial\overline{\tilde{u}\tilde{w}}}{\partial z}\right), \tag{5.83}$$

$$\frac{\partial\overline{v}^{L}}{\partial t}+\overline{u}^{L}\frac{\partial\overline{v}^{L}}{\partial x}+\overline{v}^{L}\frac{\partial\overline{v}^{L}}{\partial y}+\overline{w}^{L}\frac{\partial\overline{v}^{L}}{\partial z}=-g\frac{\partial\overline{\zeta}^{L}}{\partial y}-\left(\frac{\partial\overline{\tilde{v}\tilde{u}}}{\partial x}+\frac{\partial\overline{\tilde{v}^{2}}}{\partial y}+\frac{\partial\overline{\tilde{v}\tilde{w}}}{\partial z}\right), \tag{5.84}$$

Depth-integrated continuity equation is:

$$\frac{\partial\overline{\zeta}^{L}}{\partial t}+\frac{\partial}{\partial x}\left(\int_{-h}^{\overline{\zeta}^{L}}\overline{u}^{L}dz\right)+\frac{\partial}{\partial y}\left(\int_{-h}^{\overline{\zeta}^{L}}\overline{v}^{L}dz\right)=0. \tag{5.85}$$

The spatial distribution of Quasi-Eulerian mean horizontal velocity calculated by equations of Walstra *et al.* (2001) is presented in Figure 2a. That result was obtained after 30 min of simulation time. On the slope, the horizontal velocity is non-uniform in the vertical direction. Moreover, the model is unstable and the mean velocity increases to infinity in time. Thus, equations of Walstra *et al.* (2001) do not pass the adiabatic test. The imbalance is caused by the omission of the second-order terms $\rho^{-1}\partial\overline{p}^{S}/\partial x_{\alpha}$ and $T_{\alpha}$.

Figure 6.1b presents the distribution of Quasi-Eulerian mean flow simulated with new equations of motion that include these terms showing the correct depth-uniform horizontal mean velocity on the slope.

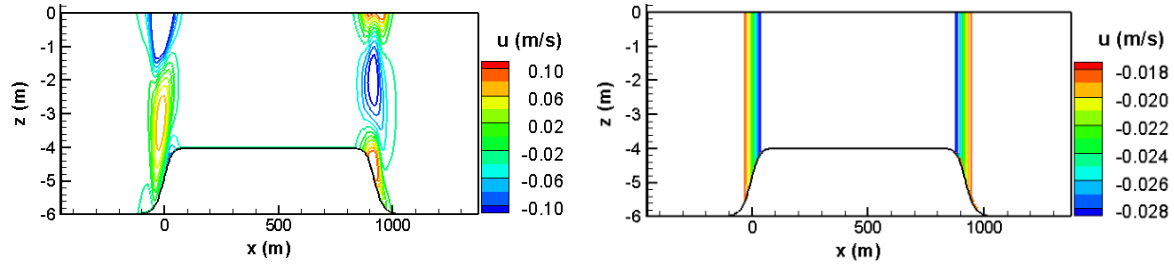


(a) Calculated by equations of Walstra *et al.* (2001)

(b) Calculated by 2DV model

*Figure 6.1 Distribution of Quasi-Eulerian mean horizontal velocity*

## 6.2 COMPARISON WITH EQUATIONS OF MOTION OF BENNIS *ET AL.* (2011)

In Bennis *et al.* (2011), the Quasi-Eulerian mean equations of Ardhuin *et al.* (2008) were employed. In this, dissipative wave forcing terms are expressed explicitly using empirical formulas. Their horizontal momentum equations are expressed by:

$$\frac{\partial \overline{u}}{\partial t}+\overline{u}\frac{\partial \overline{u}}{\partial x}+\overline{v}\frac{\partial \overline{u}}{\partial y}+\overline{w}\frac{\partial \overline{u}}{\partial z}-f\overline{v}+\frac{1}{\rho}\frac{\partial \overline{p}^{H}}{\partial x}=-\frac{\partial J}{\partial x}+\overline{v}^{S}\left[f+\left(\frac{\partial \overline{v}}{\partial x}-\frac{\partial \overline{u}}{\partial y}\right)\right] -\overline{w}^{S}\frac{\partial \overline{u}}{\partial z}+\frac{F_{br,1}}{\rho}+\frac{F_{mx,1}}{\rho}+\frac{F_{fr,1}}{\rho}, \tag{5.86}$$

$$\frac{\partial \overline{v}}{\partial t}+\overline{u}\frac{\partial \overline{v}}{\partial x}+\overline{v}\frac{\partial \overline{v}}{\partial y}+\overline{w}\frac{\partial \overline{v}}{\partial z}+f\overline{u}+\frac{1}{\rho}\frac{\partial \overline{p}^{H}}{\partial y}=-\frac{\partial J}{\partial y}-\overline{u}^{S}\left[f+\left(\frac{\partial \overline{v}}{\partial x}-\frac{\partial \overline{u}}{\partial y}\right)\right] -\overline{w}^{S}\frac{\partial \overline{v}}{\partial z}+\frac{F_{br,2}}{\rho}+\frac{F_{mx,2}}{\rho}+\frac{F_{fr,2}}{\rho}. \tag{5.87}$$

The continuity equation is:

$$\frac{\partial \overline{u}}{\partial x}+\frac{\partial \overline{v}}{\partial y}+\frac{\partial \overline{w}}{\partial z}=0. \tag{5.88}$$

A comparison between the equations of Bennis *et al.* (2011) and the new equations expressed in the Quasi-Eulerian framework in the *x*-direction is presented in Table 6-2. It shows the momentum equations of Bennis *et al.* (2011) and Nguyen *et al.* (2021a) are equivalents. The vertical current shear $K$ is taken into account by Ardhuin *et al.* (2008); however, it is neglected in Bennis *et al.* (2011) to simplify their equations. The current-

induced turbulence and the effect of molecular viscosity are excluded in equation of Bennis *et al.* (2011). These terms can be added to their equations without much effort.

*Table 6-2 Comparison of equations of Bennis et al. (2011) and new equations*

| **Terms** | Bennis *et al.* (2011) | New equations |
|---|---|---|
| Pressure gradient | $-\frac{1}{\rho}\frac{\partial \overline{p}^{H}}{\partial x}$ | $-\frac{1}{\rho}\frac{\partial \overline{p}^{H}}{\partial x}$ |
| Conservative wave forcing | $-\frac{\partial J}{\partial x}+\overline{v}^{S}\left[f+\left(\frac{\partial \hat{v}}{\partial x}-\frac{\partial \hat{u}}{\partial y}\right)\right]$ $-\overline{w}^{S}\frac{\partial \hat{u}}{\partial z}$ | $-\frac{\partial (J+K)}{\partial x}+\overline{v}^{S}\left[f+\left(\frac{\partial \overline{v}}{\partial x}-\frac{\partial \overline{u}}{\partial y}\right)\right]$ $-\overline{w}^{S}\frac{\partial \overline{u}}{\partial z}$ |
| Non-conservative wave forcing | $\frac{F_{br,1}}{\rho}$ : applied as a surface stress<br>$\frac{F_{mx,1}}{\rho}$ : was not specified<br>$\frac{F_{fr,1}}{\rho}$ : applied as a bottom stress | $\frac{F_{br,1}}{\rho}$ : applied as a body force<br>$\frac{F_{mx,1}}{\rho}$ : applied as a body force<br>$\frac{F_{br,1}}{\rho}$ : applied as a bottom stress |
| Turbulence | Excluded | $\frac{1}{\rho}\left(\frac{\partial \overline{\tau}_{11}}{\partial x}+\frac{\partial \overline{\tau}_{12}}{\partial y}+\frac{\partial \overline{\tau}_{13}}{\partial z}\right)$ |
| Mass conservation | $\frac{\partial \overline{u}}{\partial x}+\frac{\partial \overline{v}}{\partial y}+\frac{\partial \overline{w}}{\partial z}=0$ | $\frac{\partial \overline{u}}{\partial x}+\frac{\partial \overline{v}}{\partial y}+\frac{\partial \overline{w}}{\partial z}$ $=\frac{\partial \overline{Z}^{S}}{\partial t}-\left(\frac{\partial \overline{u}^{S}}{\partial x}+\frac{\partial \overline{v}^{S}}{\partial y}+\frac{\partial \overline{w}^{S}}{\partial z}\right)$ |

The non-conservative wave forcing terms including $F_{br}$, $F_{mx}$, and $F_{fr}$ are included in the momentum equations of Bennis *et al.* (2011) and Nguyen *et al.* (2021a). The only difference is the way to calculate breaking wave and roller wave-induced forcing terms $F_{br}$. In Bennis *et al.* (2011), it is assumed as surface stress, whereas it is provided as body force in Nguyen *et al.* (2021a). Therefore, the equations of Bennis *et al.* (2011) are valid in the condition of strong vertical mixing due to breaking waves when the vertical

distribution of breaking wave-induced forcing is not very important. In other conditions, the vertical distribution of breaking wave-induced forcing terms should be considered.

The continuity equation of Bennis *et al.* (2011) shows the convergence of the Quasi-Eulerian mean velocity consistent with the presence of conservative waves. For non-conservative waves, the divergence of the Quasi-Eulerian mean velocity should be compensated by the divergence of the Stokes drift as presented in the new continuity equation.

Finally, the equations of Bennis *et al.* (2011) are expressed in terms of the vortex force representation. As indicated in Section 2, this representation is based on the assumption that the ambient current is small in comparison with orbital velocity, i.e., $|\overline{\mathbf{u}}| \ll \mathbf{u}_{orb}$. This assumption is not present in the wave radiation stress representation and is therefore potentially more suitable in the presence of strong ambient currents.

## 6.3 COMPARISON WITH EQUATIONS OF MOTION OF KUMAR *ET AL.* (2012)

Equations of motion of Kumar *et al.* (2012) are based on the asymptotic theory of McWilliams *et al.* (2004). In their equations, the dynamic pressure $\varphi$ is employed. The relationship between $\varphi$ and $\overline{p}$ is given by (McWilliams *et al.*, 2004):

$$\overline{p} = \rho\varphi + \overline{p}^{w}, \tag{5.89}$$

where, $\overline{p}^{w}$ is wave-induced pressure given by:

$$p^{w} = -\frac{1}{2}\rho\left(\overline{\tilde{u}^2} + \overline{\tilde{v}^2} + \overline{\tilde{w}^2}\right). \tag{5.90}$$

Using the formula (4.3) we obtain the following relationship between $\varphi$ and $\overline{p}^{H}$:

$$\varphi = \frac{\overline{p}^{H}}{\rho} + J, \tag{5.91}$$

where, $J$ is defined by (3.33).

Using this, the momentum equations of Kumar *et al.* (2012) can be rewritten as:

$$\begin{aligned} &\frac{\partial \overline{u}}{\partial t} + \overline{u}\frac{\partial \overline{u}}{\partial x} + \overline{v}\frac{\partial \overline{u}}{\partial y} + \overline{w}\frac{\partial \overline{u}}{\partial z} - f\overline{v} = -\frac{1}{\rho}\frac{\partial \overline{p}^{H}}{\partial x} - \frac{\partial\left(J+\kappa\right)}{\partial x} + \overline{v}^{s}\left(f + \left(\frac{\partial \overline{v}}{\partial x} - \frac{\partial \overline{u}}{\partial y}\right)\right) \\ &-\overline{w}^{s}\frac{\partial \overline{u}}{\partial z} - \frac{\partial}{\partial z}\left(\overline{u'w'} - \upsilon\frac{\partial \overline{u}}{\partial z}\right) + F_1^{bf} + F_1^{sf} + F_1^{br} + D_1 + F_1, \end{aligned} \tag{5.92}$$

$$\frac{\partial \overline{v}}{\partial t}+\overline{u}\frac{\partial \overline{v}}{\partial x}+\overline{v}\frac{\partial \overline{v}}{\partial y}+\overline{w}\frac{\partial \overline{v}}{\partial z}+f\overline{u}=-\frac{1}{\rho}\frac{\partial \overline{p}^{H}}{\partial y}-\frac{\partial\left(J+\kappa\right)}{\partial y}-\overline{u}^{s}\left(f+\left(\frac{\partial \overline{v}}{\partial x}-\frac{\partial \overline{u}}{\partial y}\right)\right)$$
$$-\overline{w}^{s}\frac{\partial \overline{v}}{\partial z}-\frac{\partial}{\partial z}\left(\overline{v'w'}-\upsilon\frac{\partial \overline{v}}{\partial z}\right)+F_{2}^{bf}+F_{2}^{sf}+F_{2}^{br}+D_{2}+F_{2}, \tag{5.93}$$

$$\frac{1}{\rho}\frac{\partial \overline{p}^{H}}{\partial z}+g=-\frac{\partial \kappa}{\partial z}+\left(\overline{u}^{S}\frac{\partial \overline{u}}{\partial z}+\overline{v}^{S}\frac{\partial \overline{v}}{\partial z}\right), \tag{5.94}$$

where, $F_{\alpha}^{bf}$ and $F_{\alpha}^{sf}$ are wave-induced forcing terms due to bottom and surface streaming, respectively, $F_{\alpha}^{br}$ is wave-induced forcing term due to white-capping, breaking wave, and roller, $F_{\alpha}$ is non-wave non-conservative forcing and $D_{\alpha}$ is horizontal mixing term.

The Bernoulli head $\kappa$ is given by:

$$\kappa=\frac{\sigma H_{rms}^{2}}{16k\sinh^{2}\left[k(h+\overline{\zeta})\right]}\int_{-h}^{z}\frac{\partial^{2}\left(\mathbf{k}.\overline{\mathbf{u}}\right)}{\partial z'^{2}}\sinh\left[2k(z-z')\right]dz'. \tag{5.95}$$

If the effect of vertical shear of mean current in the wave forcing term is neglected then $\kappa$ can be neglected.

Continuity equation shows the convergence of Eulerian mean velocity, i.e.:

$$\frac{\partial \overline{u}}{\partial x}+\frac{\partial \overline{v}}{\partial y}+\frac{\partial \overline{w}}{\partial z}=0. \tag{5.96}$$

In adiabatic condition, horizontal momentum equations (5.92) and (5.93) become:

$$\frac{\partial \overline{u}}{\partial t}+\overline{u}\frac{\partial \overline{u}}{\partial x}+\overline{v}\frac{\partial \overline{u}}{\partial y}+\overline{w}\frac{\partial \overline{u}}{\partial z}-f\overline{v}=-\frac{1}{\rho}\frac{\partial \overline{p}^{H}}{\partial x}-\frac{\partial J}{\partial x}$$
$$+\overline{v}^{s}\left(f+\left(\frac{\partial \overline{v}}{\partial x}-\frac{\partial \overline{u}}{\partial y}\right)\right)-\overline{w}^{s}\frac{\partial \overline{u}}{\partial z}, \tag{5.97}$$

$$\frac{\partial \overline{v}}{\partial t}+\overline{u}\frac{\partial \overline{v}}{\partial x}+\overline{v}\frac{\partial \overline{v}}{\partial y}+\overline{w}\frac{\partial \overline{v}}{\partial z}+f\overline{u}=-\frac{1}{\rho}\frac{\partial \overline{p}^{H}}{\partial y}-\frac{\partial J}{\partial y}$$
$$-\overline{u}^{s}\left(f+\left(\frac{\partial \overline{v}}{\partial x}-\frac{\partial \overline{u}}{\partial y}\right)\right)-\overline{w}^{s}\frac{\partial \overline{v}}{\partial z}. \tag{5.98}$$

Equations (5.97) and (5.98) are similar to horizontal momentums equations of Bennis *et al.* (2011) in adiabatic condition. Therefore, similar to the equations of Bennis *et al.* (2011), equations of Kumar *et al.* (2012) pass the adiabatic test.

A comparison between the set of equations of Kumar *et al.* (2012) and the new set of equations for the *x*-direction is given in Table 6-3. It shows that hydrostatic pressure and

conservative wave forcing terms in momentum equations of Kumar *et al.* (2012), and new momentum equations are equivalent.

In Kumar *et al.* (2012), the wave forcing is provided as a body force or bottom stress. These two approaches are implemented in their model to calculate the effect of bottom streaming on the current. The first approach (body force) is applied for the resolving bottom boundary layer condition, and the second approach (bottom stress) is suitable for non-resolving bottom boundary layer conditions. In new momentum equations, the bottom boundary layer is assumed non-resolved then the bottom stress approach is employed. The surface streaming is not considered by new momentum equations. This term could be significant outside the surfzone (Lentz *et al.*, 2008).

*Table 6-3 Comparison between equations Kumar et al. (2012) and new equations*

| **Terms** | Kumar *et al.* (2012) | New equations |
|---|---|---|
| Pressure gradient | $-\frac{1}{\rho}\frac{\partial \overline{p}^{H}}{\partial x}$ | $-\frac{1}{\rho}\frac{\partial \overline{p}^{H}}{\partial x}$ |
| Conservative wave forcing | $-\frac{\partial J}{\partial x}+\overline{v}^{s}\left[f+\left(\frac{\partial \overline{v}}{\partial x}-\frac{\partial \overline{u}}{\partial y}\right)\right]$ $-\overline{w}^{s}\frac{\partial \overline{u}}{\partial z}$ | $-\frac{\partial\left(J+K\right)}{\partial x}+\overline{v}^{s}\left[f+\left(\frac{\partial \overline{v}}{\partial x}-\frac{\partial \overline{u}}{\partial y}\right)\right]$ $-\overline{w}^{s}\frac{\partial \overline{u}}{\partial z}$ |
| Non-conservative wave forcing | $F_1^{br}$ : applied as a body force<br>$F_1^{sf}$ : surface streaming<br>$F_1^{bf}$ : bottom streaming | $\frac{F_{br,1}}{\rho}$ : applied as a body force<br>$\frac{F_{br,1}}{\rho}$ : applied as a bottom stress<br>$\frac{F_{mx,1}}{\rho}$ : applied as a body force |
| Turbulence | $-\frac{\partial}{\partial z}\left(\overline{u'w'}-\upsilon\frac{\partial \overline{u}}{\partial z}\right)+D_1$ | $\frac{1}{\rho}\left(\frac{\partial \overline{\tau}_{11}}{\partial x}+\frac{\partial \overline{\tau}_{12}}{\partial y}+\frac{\partial \overline{\tau}_{13}}{\partial z}\right)+\upsilon\Delta\overline{u}$ |
| Mass conservation | $\frac{\partial \overline{u}}{\partial x}+\frac{\partial \overline{v}}{\partial y}+\frac{\partial \overline{w}}{\partial z}=0$ | $\frac{\partial \overline{u}}{\partial x}+\frac{\partial \overline{v}}{\partial y}+\frac{\partial \overline{w}}{\partial z}$ $=\frac{\partial \overline{Z}^{S}}{\partial t}-\left(\frac{\partial \overline{u}^{S}}{\partial x}+\frac{\partial \overline{v}^{S}}{\partial y}+\frac{\partial \overline{w}^{S}}{\partial z}\right)$ |

The mass conservation equation of Kumar *et al.* (2012) shows a divergence-free Eulerian mean velocity field. It is thus representative of conservative surface waves. For non-

conservative wave conditions, the divergence of Eulerian mean velocity is compensated by the divergence of wave-induced current (Stokes drift) included in new momentum equations.

The equations of Kumar *et al.* (2012) are expressed in terms of vortex force representation, thus assuming that the mean current is weak in comparison with orbital velocity.

Finally, with the use of the classical Eulerian mean method, the momentum equations of Kumar *et al.* (2012) are only valid below the wave trough. This implies that mean velocity has to be extrapolated from the trough to obtain the velocity profile up to the mean water level.

## 6.4 CONCLUSIONS

New equations were expressed in both radiation stress and vortex force representations. This set of equations was used to compare with recent well-known equations of mean motion. It showed that:

- In Walstra *et al.* (2001), terms of second-order of wave amplitude, i.e., $\overline{p}^{S}$ and $T_{\alpha}$, are neglected in conservative wave forcing terms. This causes spurious oscillations and as a result, their set of equations did not pass the adiabatic test.
- The effect of strong ambient currents on the wave-induced forcing term is not considered in the work of Walstra *et al.* (2001); Bennis *et al.* (2011); and Kumar *et al.* (2012). Therefore, it is a problem when applying their sets of equations for nearshore applications, where the current is usually comparable to the orbital velocity.
- In Walstra *et al.* (2001); and Bennis *et al.* (2011) the wave forcing term caused by breaking wave and roller wave is applied as surface stress. This is only suitable in cases of strong vertical mixing due to breaking waves. In general, the vertical distribution of breaking wave and roller wave-induced forcing term is more appropriate.
- Sets of equations of Bennis *et al.* (2011); and Kumar *et al.* (2012) are expressed in terms of vortex force representation. This is only suitable if the ambient current is small in comparison with orbital velocity, i.e., $|\overline{\mathbf{u}}| \ll \mathbf{u}_{orb}$. When the ambient current is comparable to the orbital velocity, the wave radiation stress representation is preferred.
- Mass conservation equation in Bennis *et al.* (2011); and Kumar, Voulgaris [21 shows a divergence-free Eulerian mean velocity field. This is suitable for conservative waves. In general, the divergence of Quasi-Eulerian mean velocity should be compensated by the divergence of Stokes drift.

# 7

# CONCLUSIONS

## 7.1 CONCLUSIONS

In this study, a new set of equations of motion written in terms of Quasi-Eulerian mean velocity was developed based on the GLM method. The new equations were valid from the bottom to the mean water surface even in the presence of finite-amplitude waves. These equations are practical for a wide range of applications from deep water to shallow water areas. All terms in these equations are expressed to the second-order of the wave amplitude. Both non-wave forcing and wave-induced forcing terms are under consideration. When the wave height is infinitesimal, the Quasi-Eulerian mean equations of motion reduce to the classical Eulerian mean equations of motion. In cases of density stratification, the buoyancy effect should be included as external forcing.

In this study, a three-dimensional wave radiation stress formulation was introduced. The effects of surface waves on the mean current are specified at any level of the water column. With the use of an empirical coefficient $C_{WR}$, the 3D wave radiation stress is suitable for the presence of a strong ambient current. The vertical integration of the new three-dimensional wave radiation stress coincides with the traditional radiation stress. Besides, the comparison between three-dimensional radiation stress and vortex force representations was studied in detail. Those representations are equivalent if the irrotational part of the waves is dominated, and the mean current is weak in comparison with orbital velocity.

A 2DV numerical model was developed to validate new Quasi-Eulerian mean equations of motion. The 2DV model passed the well-known adiabatic condition suggested by Ardhuin *et al.* (2008). It does not produce spurious velocities when the waves propagate on a sloping bottom. As a result, vertical uniform distribution of Quasi-Eulerian mean horizontal velocity was obtained even on the slope.

Subsequently, the experiment of Klopman (1994) for random waves was employed to validate the 2DV model in the condition of non-breaking waves combined with a strong current. The comparison between experimental data and numerical results showed very good agreement in the whole vertical sections even in areas that were very close to the bed. In the condition of breaking waves, two experiments presented in the dissertation of Boers (2005) were employed. It showed that new equations performed very well for the experiment of smaller wave height (test 1C). In the experiment of bigger wave height (test 1B), the vertical distribution of the mean velocity near the breaking point gave qualitatively correct results. In the comparison of longshore current in the LSTF test (Hamilton and Ebersole, 2001), a good agreement was found not only for depth-averaged longshore current but also for depth varying longshore current. For cross-shore currents, there was a difference between model results and experimental data in the wave-breaking zone. The difference between the experimental data and model results in tests 1B and LSTF was likely to be due to the empirical formulas for wave breaking that were strong simplifications of the complex breaking process. Further tuning of such formulations

against a large number of datasets on wave decay and generated longshore and cross-shore currents was recommended.

The comparisons with other well-known sets of equations of motion show that new set of equations of motion is more suitable in the presence of a strong ambient current, and finite amplitude nonconservative waves. New set of equations of motion can be applied in a wide range of applications from offshore to coastal zones, estuaries, and outflow areas.

Finally, with the use of Quasi-Eulerian mean variables, new set of equations of motion can be easily implemented to existing 3D models developed based on the classical Eulerian mean method. The implementation is straightforward and does not require much effort. It can improve significantly the results of simulating coastal processes such as coastal sediment transport, transport of plastic, and other pollutants such as oil slicks.

## 7.2 ANSWER TO RESEARCH QUESTIONS

*1. How to simulate three-dimensional mean current from the deep ocean to the coastal, estuary, and outflow areas in the presence of finite-amplitude non-conservative waves?*

The Eulerian mean method is usually applied to simulate the mean current. However, in the presence of finite-amplitude surface waves, the region between wave crest to wave trough is not always filled by water. Therefore, the use of the Eulerian mean method is not suitable to apply in this area. In the GLM method, the hydrodynamic quantities are averaged over disturbance positions of a fluid particle. Then, this method is valid from the bottom to the mean water surface even in the presence of finite-amplitude non-conservative waves. This method provides a physical interpretation of definitions of mean properties from the wave trough to the mean water level.

*2. How to express the effects of surface waves on three-dimensional mean currents, especially under the condition of non-conservative waves and strong ambient currents?*

When the mean current is small in comparison with orbital velocity, the effect of surface waves on the currents can be expressed in terms of either radiation stress or vortex force representations. The wave radiation stress forcing is the total vortex force, Bernoulli head, and dissipative wave forcing. In the presence of a strong ambient current, the three-dimensional wave radiation stress representation is recommended.

*3. Specify the relationship between vortex force and radiation stress representations in different conditions of surface waves combined with mean currents?*

In this study, the relationship between three-dimensional wave radiation stress and vortex force representations is investigated in detail. The results showed that:

i) In conservative waves and weak ambient current: wave radiation stress and vortex force representations are equivalent.

ii) In non-conservative wave and weak ambient current: wave radiation stress representation is the sum of vortex force representation and wave-induced dissipative forcing terms.

# REFERENCES


Andrews, D., McIntyre, M., 1978. An exact theory of nonlinear waves on a Lagrangian-mean flow. Journal of Fluid Mechanics 89, 609-646.

Ardhuin, F., Rascle, N., Belibassakis, K.A., 2008. Explicit wave-averaged primitive equations using a generalized Lagrangian mean. Ocean Modelling 20, 35-60.

Ardhuin, F., Suzuki, N., McWilliams, J.C., Aiki, H., 2017. Comments on "A Combined Derivation of the Integrated and Vertically Resolved, Coupled Wave–Current Equations". Journal of Physical Oceanography 47, 2377-2385.

Battjes, J., Stive, M., 1985. Calibration and verification of a dissipation model for random breaking waves. Journal of Geophysical Research: Oceans 90, 9159-9167.

Battjes, J.A., Janssen, J., 1978. Energy loss and set-up due to breaking of random waves. Coastal Engineering 1978, pp. 569-587.

Belibassakis, K., Athanassoulis, G., 2002. Extension of second-order Stokes theory to variable bathymetry. Journal of Fluid Mechanics 464, 35-80.

Bennis, A.-C., Ardhuin, F., Dumas, F., 2011. On the coupling of wave and three-dimensional circulation models: Choice of theoretical framework, practical implementation and adiabatic tests. Ocean Modelling 40, 260-272.

Boers, M., 2005. Surf zone turbulence. PhD Thesis, TU Delft, the Netherlands.

Bowen, A.J., 1969. The generation of longshore currents on a plane beach. J. Mar. Res. 27, 206-215.

Craik, A., Leibovich, S., 1976. A rational model for Langmuir circulations. Journal of Fluid Mechanics 73, 401-426.

Deigaard, R., 1992. Mechanics of coastal sediment transport. World scientific publishing company.

Deigaard, R., Fredsøe, J., 1989. Shear stress distribution in dissipative water waves. Coastal Engineering 13, 357-378.

Deltares, 2014. Delft3D-FLOW: Simulation of multi-dimensional hydrodynamic flows and transport phenomena, including sediments. User Manual, the Netherlands 690.

Dingemans, M.W., 1997. Water wave propagation over uneven bottoms: Linear wave propagation. World Scientific.

Feddersen, F., Guza, R., Elgar, S., Herbers, T., 2000. Velocity moments in alongshore bottom stress parameterizations. Journal of Geophysical Research: Oceans 105, 8673-8686.

Groeneweg, J., 1999. Wave-current interactions in a generalized Lagrangian mean formulation. Ph.D. Thesis, Delft University of Technology, Delft, The Netherland.

Guza, R., Thornton, E., 1985. Velocity moments in nearshore. Journal of waterway, port, coastal, and ocean engineering 111, 235-256.

Hamilton, D.G., Ebersole, B.A., 2001. Establishing uniform longshore currents in a large-scale sediment transport facility. Coastal Engineering 42, 199-218.

Jonsson, I.G., Carlsen, N.A., 1976. Experimental and theoretical investigations in an oscillatory turbulent boundary layer. Journal of Hydraulic Research 14, 45-60.

Klopman, G., 1994. Vertical structure of the flow due to waves and currents: Laser-Doppler flow measurements for waves following or opposing a current. Delft Hydraulics, Report no. H840.32, Part 2.

Kumar, N., Voulgaris, G., Warner, J.C., Olabarrieta, M., 2012. Implementation of the vortex force formalism in the coupled ocean-atmosphere-wave-sediment transport (COAWST) modeling system for inner shelf and surf zone applications. Ocean Modelling 47, 65-95.

Lane, E.M., Restrepo, J.M., McWilliams, J.C., 2007. Wave–current interaction: A comparison of radiation-stress and vortex-force representations. Journal of physical oceanography 37, 1122-1141.

Leibovich, S., 1977. On the evolution of the system of wind drift currents and Langmuir circulations in the ocean. Part 1. Theory and averaged current. Journal of Fluid Mechanics 79, 715-743.

Leibovich, S., 1980. On wave-current interaction theories of Langmuir circulations. Journal of Fluid Mechanics 99, 715-724.

Lentz, S.J., Fewings, M., Howd, P., Fredericks, J., Hathaway, K., 2008. Observations and a model of undertow over the inner continental shelf. Journal of Physical Oceanography 38, 2341-2357.

Longuet-Higgins, M.S., 1970. Longshore currents generated by obliquely incident sea waves: 1. Journal of geophysical research 75, 6778-6789.

Longuet-Higgins, M.S., Stewart, R., 1962. Radiation stress and mass transport in gravity waves, with application to 'surf beats'. Journal of Fluid Mechanics 13, 481-504.

Longuet-Higgins, M.S., Stewart, R., 1964. Radiation stresses in water waves; a physical discussion, with applications. Deep Sea Research and Oceanographic Abstracts. Elsevier, pp. 529-562.

Longuet-Higgins, M.S., Stewart, R.W., 1960. Changes in the form of short gravity waves on long waves and tidal currents. Journal of Fluid Mechanics 8, 565-583.

McWilliams, J.C., Restrepo, J.M., 1999. The wave-driven ocean circulation. Journal of Physical Oceanography 29, 2523-2540.

McWilliams, J.C., Restrepo, J.M., Lane, E.M., 2004. An asymptotic theory for the interaction of waves and currents in coastal waters. Journal of Fluid Mechanics 511, 135-178.

Mellor, G., 2003. The three-dimensional current and surface wave equations. Journal of Physical Oceanography 33, 1978-1989.

Mellor, G., 2015. A combined derivation of the integrated and vertically resolved, coupled wave–current equations. Journal of Physical Oceanography 45, 1453-1463.

Mellor, G., 2016. On theories dealing with the interaction of surface waves and ocean circulation. Journal of Geophysical Research: Oceans 121, 4474-4486.

Mellor, G.L., 2008. The depth-dependent current and wave interaction equations: a revision. Journal of Physical Oceanography 38, 2587-2596.

Michaud, H., Marsaleix, P., Leredde, Y., Estournel, C., Bourrin, F., Lyard, F., Mayet, C., Ardhuin, F., 2011. Threedimensional modelling of wave-induced current from the surf zone to the inner shelf. Ocean Science Discussions 8, 2417-2478.

Nairn, R.B., Roelvink, J., Southgate, H.N., 1991. Transition zone width and implications for modelling surfzone hydrodynamics. Coastal Engineering 1990, pp. 68-81.

Newberger, P., Allen, J.S., 2007. Forcing a three-dimensional, hydrostatic, primitive-equation model for application in the surf zone: 1. Formulation. Journal of Geophysical Research: Oceans 112.

Nguyen, D.T., Jacobsen, N.G., Roelvink, D., 2021a. Development and Validation of Quasi-Eulerian Mean Three-Dimensional Equations of Motion Using the Generalized Lagrangian Mean Method. Journal of Marine Science and Engineering 9, 76.

Nguyen, D.T., Reniers, A.J.H.M., Roelvink, D., 2021b. Relationship between Three-Dimensional Radiation Stress and Vortex-Force Representations. Journal of Marine Science and Engineering 9, 791.

Nielsen, P., You, Z.-J., 1997. Eulerian mean velocities under non-breaking waves on horizontal bottoms. Coastal Engineering 1996, pp. 4066-4078.

Ockenden, M., Soulsby, R., 1994. Sediment transport by currents plus irregular waves.

Putnam, J., Johson, J., 1949. The dissipation of wave energy by bottom friction. Eos, Transactions American Geophysical Union 30, 67-74.

Rascle, N., Ardhuin, F., Terray, E.A., 2006. Drift and mixing under the ocean surface: A coherent one-dimensional description with application to unstratified conditions. Journal of Geophysical Research: Oceans 111.

Roelvink, J., Reniers, A., 2011. A guide to modeling coastal morphology. World Scientific.

Soulsby, R., 1997. Dynamics of marine sands: a manual for practical applications. Thomas Telford.

Stelling, G.S., Busnelli, M.M., 2001. Numerical simulation of the vertical structure of discontinuous flows. International Journal for Numerical Methods in Fluids 37, 23-43.

Supharatid, S., Tanaka, H., Shuto, N., 1992. Interactions of waves and current (Part I: Experimental investigation). Coastal Engineering in Japan 35, 167-186.

Svendsen, I.A., 1984. Mass flux and undertow in a surf zone. Coastal Engineering 8, 347-365.

Tamura, H., Miyazawa, Y., Oey, L.Y., 2012. The Stokes drift and wave induced-mass flux in the North Pacific. Journal of Geophysical Research: Oceans 117.

Teles, M.J., Pires-Silva, A.A., Benoit, M., 2013. Three dimensional modelling of wave-current interactions in the coastal zone with a fully coupled system. Geography.

Thornton, E.B., 1970. Variation of longshore current across the suft zone. Coastal Engineering Proceedings 1, 18.

Uchiyama, Y., McWilliams, J.C., Shchepetkin, A.F., 2010. Wave–current interaction in an oceanic circulation model with a vortex-force formalism: Application to the surf zone. Ocean Modelling 34, 16-35.

Van Rijn, L.C., 2011. Principles of fluid flow and surface waves in rivers, estuaries, seas and oceans. Aqua Publications Amsterdam, The Netherlands.

Walstra, D., Roelvink, J., Groeneweg, J., 2001. Calculation of wave-driven currents in a 3D mean flow model. Coastal Engineering 2000, pp. 1050-1063.

Xia, H., Xia, Z., Zhu, L., 2004. Vertical variation in radiation stress and wave-induced current. Coastal engineering 51, 309-321.

Xie, L., Wu, K., Pietrafesa, L., Zhang, C., 2001. A numerical study of wave-current interaction through surface and bottom stresses: Wind-driven circulation in the South Atlantic Bight under uniform winds. Journal of Geophysical Research: Oceans (1978–2012) 106, 16841-16855.

You, Z.-J., 1997. On the vertical distribution of <ũw̃> by FJ Rivero and AS Arcilla: comments. Coastal engineering 30, 305-310.

# LIST OF ACRONYMS

| | |
|---|---|
| 2D | Two Dimensional |
| 3D | Three-dimensional |
| GLM | Generalized Lagrangian Mean |
| RANS | Reynolds-averaged Navier–Stokes |
| LSTF | Large-scale sediment transport facility |
| CO | Current-only |
| WO | Wave-only |
| WFC | Wave following current |
| WOC | Wave opposing current |

# LIST OF TABLES

Table 5-1 Wave properties at the paddle ..... 52

Table 5-2 Bottom boundary thickness $\delta$ in different waves and current condition ..... 54

Table 5-3 Wave energy dissipation ..... 55

Table 5-4 Characteristics of the near-bed mean flow ..... 55

Table 5-5 Wave properties at the offshore boundary. ..... 62

Table 5-6 Incident wave properties at the boundary ..... 69

Table 6-1 Comparison between equations of Walstra et al. (2001) and the new set of equations in the GLM framework ..... 79

Table 6-2 Comparison of equations of Bennis et al. (2011) and new equations ..... 82

Table 6-3 Comparison between equations Kumar et al. (2012) and new equations ..... 85

# LIST OF FIGURES

Figure 5.1 A flowchart of the validation scheme ..... 40
Figure 5.2 Bathymetry of the computational area ..... 49
Figure 5.3 Spatial distribution of Stokes drift ..... 50
Figure 5.4 Distribution of mean water level ..... 50
Figure 5.5 Distribution of $F_{w,1}/\rho$ ($m/s^2$) ..... 50
Figure 5.6 Vertical distribution of horizontal mean velocity ..... 51
Figure 5.7 Vertical distribution of the Eulerian-mean velocity ..... 52
Figure 5.8 Vertical distribution of observed Reynolds shear stress $\overline{-u^t w^t}$ in the CO condition ..... 53
Figure 5.9 Reynolds turbulent viscosity ($\upsilon_v^T$) ..... 56
Figure 5.10 Vertical distribution of the wave radiation stress component $\overline{\tilde{u}\tilde{w}}_{CS}$ ..... 56
Figure 5.11 Vertical distribution of wave-induced forcing terms ..... 57
Figure 5.12 Spatial distribution of Quasi-Eulerian mean velocity in the CO condition 57
Figure 5.13 Spatial distribution of Quasi-Eulerian mean velocity in CO condition ..... 58
Figure 5.14 Vertical distribution of Quasi-Eulerian mean velocity in CO condition..... 58
Figure 5.15 Spatial distribution of mean velocity fields in the WO condition..... 59
Figure 5.16 Vertical distribution of Quasi-Eulerian mean velocity in the WO condition ..... 59
Figure 5.17 Spatial distribution of Quasi-Eulerian mean velocity ..... 60
Figure 5.18 Distribution of Quasi-Eulerian mean velocity in the linear scale ..... 60
Figure 5.19 Distribution of Quasi-Eulerian mean velocity in the semilogarithmic scale ..... 61
Figure 5.20 The bottom profile ..... 62
Figure 5.21 Distribution of significant wave height ..... 63
Figure 5.22 Distribution of wave-induced forcing terms at $x = 22.9\,\mathrm{m}$ ..... 64
Figure 5.23 Distribution of mean water level $\overline{\zeta}$ ..... 64
Figure 5.24 Distribution of Stokes drift (a,b) and Quasi-Eulerian mean velocity (c,d) . 65

Figure 5.25 Vertical distribution of horizontal mean velocity in test 1B ..... 66
Figure 5.26 Vertical distribution of horizontal mean velocity in test 1C ..... 68
Figure 5.27 Distribution of significant wave height ..... 70
Figure 5.28 Distribution of mean water level ..... 71
Figure 5.29 Vertical distribution of wave-induced forcing terms ..... 71
Figure 5.30 Distribution of cross-shore velocity ..... 71
Figure 5.31 Vertical profiles of cross-shore velocity ..... 72
Figure 5.32 Vertical distribution of wave-induced forcing terms ..... 73
Figure 5.33 Distribution of the longshore velocity ..... 73
Figure 5.34 Longshore velocity at $z = -2h/3$ ..... 74
Figure 5.35 Vertical profiles of the longshore velocity at different locations ..... 74
Figure 6.1 Distribution of Quasi-Eulerian mean horizontal velocity ..... 81

# ABOUT THE AUTHOR

Nguyen Tan Duoc was born on 22nd April 1981 in Haiphong, a city in the North of Vietnam. He studied mathematics and physics at Haiphong University from 1998 to 2001. After two years of teaching mathematics and physics, he started studying physical oceanography at the Honour Program of Hanoi University of Science, Hanoi National University from 2003 to 2007. He obtained the degree of Master of Science in Oceanography at Hanoi National University in 2011.

He worked for several national and international organizations including the Vietnam Institute of Meteorology, Hydrology, and Climate Change (IMHEN) from 2007 to 2008; the Vietnam Administration of Seas and Islands (VASI) from 2009 to the present; and the Regional Integrated Multi-Hazard Warning System (RIMES, UNEP, Thailand) from 2012 to 2013. He started his Ph.D. at IHE Delft and Delft University of Technology in March 2014 under the supervision of Prof.dr.ir. J.A. Roelvink and Prof.dr.ir. A.J.H.M. Reniers. His topic is about the development and validation of waves and currents interaction formulation. In this, he developed a new set of equations of motion to simulate the evolution of the mean flow in the presence of finite-amplitude surface waves. The new set of equations is valid in a wide range of applications from deep water to the coastal zone, estuaries, and outflow areas.

## Journal publications

Nguyen, D.T., Jacobsen, N.G., Roelvink, D., 2021a. Development and Validation of Quasi-Eulerian Mean Three-Dimensional Equations of Motion Using the Generalized Lagrangian Mean Method. Journal of Marine Science and Engineering 9, 76.

Nguyen, D.T., Reniers, A.J.H.M., Roelvink, D., 2021b. Relationship between Three-Dimensional Radiation Stress and Vortex-Force Representations. Journal of Marine Science and Engineering 9, 791.

## Conference proceedings

Nguyen, D.T., Jacobsen, N.G., Roelvink, D., 2017. Development and validation of a three-dimensional wave-current interaction formulation. IHE Delft Ph.D Symposium.

Nguyen, D.T., Jacobsen, N.G., Roelvink, D., 2018. Development of a 3D wave-current interaction formulation. European Geosciences Union, General Assembly.

*Netherlands Research School for the*
*Socio-Economic and Natural Sciences of the Environment*

# D I P L O M A

## *For specialised PhD training*

The Netherlands Research School for the
Socio-Economic and Natural Sciences of the Environment
(SENSE) declares that

# *Duoc Tan Nguyen*

born on 22 April 1981 in Hai Phong City, Vietnam

has successfully fulfilled all requirements of the
Educational Programme of SENSE.

Delft, 10 June 2022

The Chairman of the SENSE board

Prof. dr. Martin Wassen

the SENSE Director of Education

Dr. Ad van Dommelen

*The SENSE Research School has been accredited by the Royal Netherlands Academy of Arts and Sciences (KNAW)*

KONINKLIJKE NEDERLANDSE
AKADEMIE VAN WETENSCHAPPEN

The SENSE Research School declares that **Duoc Tan Nguyen** has successfully fulfilled all requirements of the Educational PhD Programme of SENSE with a work load of 32.1 EC, including the following activities:

## SENSE PhD Courses

- Environmental research in context (2014)
- SENSE writing course (2015)
- Research in context activity: 'Taking initiative, preparing and reviewing with colleagues the Wikipedia page on the new concept of "Quasi-Eulerian mean velocity"' (2018)

## Other PhD and Advanced MSc Courses

- Where is little data, IHE Delft – Institute for Water Education (2017)
- Estuary and coastal process in relation to Coastal Zone Management, NCK summer school (2017)
- Scientific text processing with LaTeX, Delft University of Technology (2017)
- Developing your academic skills: critical/analytical thinking and scientific reflection, Delft University of Technology (2017)
- Becoming a creative researcher in academia, Delft University of Technology (2017)
- Career development – Preparing for your next career step in academia, Delft University of Technology (2017)
- Exploring a research career outside academia, Delft University of Technology (2017)
- Time management, Delft University of Technology (2017)
- Time management II – Self-Management to the max, Delft University of Technology (2017)
- Self-Awareness and autonomy in the research, Delft University of Technology (2017)
- Creative tools for scientific writing, Delft University of Technology (2017)
- Popular scientific writing, Delft University of Technology (2017)
- How to become effective in a network conversation, Delft University of Technology (2017)

## External training at a foreign research institute

- MegaPex field campaign, TU Delft and IHE Delft Institute for Water Education, The Netherlands (2014)

## Oral Presentations

- *Development and validation of a three-dimensional wave-current interaction formulation*, IHE Delft – PhD Symposium, 02-03 October 2017, Delft, The Netherlands
- *Development of a 3D wave-current interaction formulation*, EGU general assembly, 08-13 April 2018, Vienna, Austria

SENSE Coordinator PhD Education

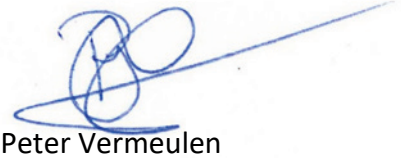

Dr. Peter Vermeulen

A set of three-dimensional equations was developed based on Generalized Lagranrian Mean method to simulate mean motion of fluid particle in the presence of finite amplitude surface waves. In the new equations, effects of waves are included through source terms. Both conservative and non-conservative waves are under consideration. A concept of three-dimensional wave radiation stress is introduced to express the effects of waves on the currents. Moreover, the relationship between three-dimensional wave radiation stress and vortex force representations is investigated in detail. In the book, there are several well-known sets of equations of mean motion were selected to compare with the new set of equations. The results showed that the new set of equations is more suitable for coastal applications, especially in the presence of finite amplitude waves and strong ambient current.

To validate the new set of equations on various conditions of waves and currents, a two-dimensional numerical model was developed using Fortran language. The comparisons showed very good agreements between model results and experimental data. As shown by successful implementation and validations in the tests, the implementation of new equations in three-dimensional model code is straightforward and expected to provide consistent results from deep water to the surf zone.

This book is printed on paper from sustainably managed forests and controlled sources

9 789073 445420